STRUCTURAL, ELECTRICAL AND OPTICAL CHARACTERIZATION OF Ge-IMPLANTED GaSe SINGLE CRYSTAL GROWN BY BRIDGMAN METHOD

A THESIS SUBMITTED TO
THE GRADUATE SCHOOL OF NATURAL AND APPLIED SCIENCES
OF
MIDDLE EAST TECHNICAL UNIVERSITY

By

HAZBULLAH KARAAĞAÇ

IN PARTIAL FULFILLMENT OF THE REQUIREMENTS
FOR
THE DEGREE OF MASTER OF SCIENCE
IN
PHYSICS

SEPTEMBER 2005

Approval of the Graduate School of Natural and Applied Sciences

Prof. Dr. Canan Özgen
Director

I certify that this thesis satisfies all the requirements as a thesis for the degree of Master of Science.

Prof. Dr. Sinan Bilikmen
Head of Department

This is to certify that we have read this thesis and that in our opinion it is fully adequate, in scope and quality, as a thesis for the degree of Master of Science.

Prof. Dr. Mehmet Parlak
Co-Supervisor

Prof. Dr. Bülent Akınoğlu
Supervisor

Examining Committee Members

Prof. Dr. Çiğdem Erçelebi (METU, PHYS)

Prof. Dr. Bülent Akınoğlu (METU, PHYS)

Prof. Dr. Mehmet Parlak (METU, PHYS)

Prof. Dr. Bahtiyar Salamov (Gazi Unv., PHYS)

Dr. Orhan Karabulut (Pamukkale Unv., PHYS)

I hereby declare that all information in this document has been obtained and presented in accordance with academic rules and ethical conduct. I also declare that, as required by these rules and conduct, I have fully cited and referenced all material and results that are not original to this work.

Name, Last name : Hazbullah Karaağaç

Signature :

ABSTRACT

STRUCTURAL, ELECTRICAL AND OPTICAL CHARACTERIZATION OF Ge -IMPLANTED GaSe SINGLE CRYSTAL GROWN BY BRIDGMAN METHOD

Karaağaç, Hazbullah
M.S., Department of Physics
Supervisor: Prof. Dr. Bülent Akınoğlu
Co-Supervisor: Prof. Dr. Mehmet Parlak

September 2005, 97 pages

In this work, structural, electrical and optical characterization of as-grown, Ge-implanted, and annealed GaSe single crystals grown by using 3-zone vertical Bridgman-Stockbarger system, have been studied by carrying out X-ray Diffraction (XRD), electrical conductivity, Hall effect, photoconductivity, and spectral transmission measurements. The temperature dependent electrical conductivity of these samples have been measured between 100 and 400 K. As a result, it was observed that upon implanting GaSe with germanium following annealing process, the resistivity is reduced from 2.1×10^9 to 6.5×10^5 Ω-cm. Also it was found that Ge-implantation followed by annealing at 500 ^oC increases the conductivity in exponential fashion. From the temperature dependent conductivities, the activation energies have been found to be 4, 34 and 314 meV for as-grown, 36 and 472 meV for as-implanted, and 39 and 647 meV for implanted and annealed at 500 ^oC GaSe single crystals.

Using XRD measurements it was observed that there is an increase in peak intensities at specific annealing temperatures (300 and 500 ^{o}C) and a decrease in higher annealing temperatures (700 ^{o}C).

Temperature dependent carrier concentration and Hall mobility measurement were performed in the temperature range of 230 - 410 and 100 - 400 K for as-grown and Ge-implanted and annealed GaSe samples, respectively. All of the samples in this study were found to be p-type with the help Hall measurements. In addition, the density of donor and acceptor atoms are found for each sample and results are compared with each other.

In addition, using photoconductivity measurement the relation between photocurrent and illumination intensity and the character of photoconduction were determined. As a result it was found that while at specific temperature intervals impurity scatterings are dominant, in other intervals phonon scatterings start to dominate.

Finally, in order to determine annealing dependent change of band gap of unimplanted and Ge-implanted GaSe samples at room temperature, the transmission measurement have been carried out as a optical characterization part of our study. As a consequence of this measurement it was observed that there is almost no considerable change in optical band gap of samples with increasing annealing temperatures for as-grown GaSe samples and a slight shift of optical band gap toward to high energy for Ge-implanted samples with annealing process.

Keywords: Crystal growth, Bridgman technique, GaSe, ion implantation, III-VI compounds, electrical characterization, optical characterization.

ÖZ

BRİDGMAN YÖNTEMİ İLE BÜYÜTÜLEN Ge- EKİLMİŞ GaSe TEK KRİSTALLERİN YAPISAL, ELEKTRİKSEL VE OPTİK KARAKTERİZASYONU

Karaağaç, Hazbullah
Yüksek Lisans, Fizik Bölümü
Tez Yöneticisi: Prof. Dr. Bülent Akınoğlu
Ortak-Tez Yöneticisi: Prof. Dr. Mehmet Parlak

Eylül 2005, 97 sayfa

Bu çalışmada, 3-bölgeli dikey Bridgman düzeneği ile büyütülmüş katkılanmamış, Ge-iyonu ekilmiş ve tavlanmış GaSe tek kristal örneklerin yapısal, elektriksel ve optiksel karakterizasyonu X-ışını kırınımı (XRD), elektriksel iletkenlik, Hall etkisi, fotoiletkenlik ve tayfsal geçirgenlik ölçümleri gerçekleştirilerek incelendi. Bu örneklerin sıcaklık bağımlı elektriksel iletkenlikleri 100 ile 400 K aralığında ölçüldü. Bu ölçüm sonucunda GaSe kristaline Ge-iyonu ekildiğinde ve tavlama işlemi gerçekleştirildiğinde özdirenç değerin 2.1×10^{9} den 6.46×10^{5} Ω-cm'ye düştüğü gözlemlendi. Ayrıca 500 ^{o}C de tavlanma ve Ge iyonu ekimi ile birlikte elektriksel iletkenliğin exponansiyel olarak arttığı gözlemlendi. Sıcaklık bağımlı elektriksel iletkenlik ölçümleri sonucu aktivasyon enerjileri; iyon ekilmemiş örnek için 4, 34, ve 314 meV, Ge ekilmiş örnek için 36 ve 472 meV, ve Ge-ekilmiş ve 500 ^{o}C 'de tavlanmış örnek için 39 ve 647 meV olarak bulundu.

XRD ölçümleri sonucu belirli tavlanma sıcaklıklarında (300 ve 500 ^{o}C) örneklerin kırınım pik şiddetlerinde artmalar olduğu gözlemlenirken bir diğer sıcaklık değerinde (700 ^{o}C) tavlanan örnekte azalmalar gözlemlendi.

Sıcaklık bağımlı taşıyıcı yoğunluğu ve Hall mobilite ölçümleri iyon ekilmemiş örnek için 230-410 K, Ge ekilmiş ve tavlanmış örnekler için 100-400 K sıcaklık aralığında gerçekleştirildi. Hall ölçümü sonucu olarak bütün örneklerin p-tipi olduğu saptandı. Ayrıca, her bir örnek için verici ve alıcı atomların yoğunluğu bulundu ve birbiriyle karşılaştırıldı.

Ayrıca, gerçekleştirilen photoiletkenlik ölçümü sonucu photoakım ile aydınlatma şiddeti ilişkisi incelenerek fotoiletkenliğin karakteri belirlendi.

Son olarak, iyon ekilmemiş ve Ge iyonu ekilmiş GaSe örneklerin bant aralıkların oda sıcaklığında tavlanma sıcaklığına bağlı değişimlerini belirlemek için tayfsal geçirgenlik ölçümleri çalışmamızın optiksel karakterizasyonun bir parçası olarak gerçekleştirildi. Ölçüm sonucu olarak ekilmemiş örnekte tavlanma sıcaklığına bağımlı bant aralığı değişimi önemli ölçüde gözlenmezken Ge-iyonu ekilmiş örnekte artan tavlama sıcaklığı ile birlikte bant aralığın daha yüksek enerji değerlerine kaydığı gözlemlendi.

Anahtar Kelimeler: Kristal büyütme, Bridgman tekniği, GaSe, iyon ekme, III-VI bileşikleri, elektriksel karakterizasyon, optik karakterizasyon.

To My Father

ACKNOWLEDGEMENTS

I would like to express my thanks to my supervisor Prof. Dr. Bülent Akınoğlu for his patience, great efforts to encourage and motivate me as a friend and sometimes as a father. In addition, it was a great honor for me to work with my co-supervisor Prof. Dr. Mehmet Parlak. In every step of my study he was with me and never leaves me alone.Without help of him it would be diffucult to complete this work on time. I would also like to present my sincere thanks to Dr.Orhan Karabulut for his endless support during this work. And, thanks to Prof Dr. Raşit Turan and his group members; Uğur Serincan, Mustafa Kulakçı, and Arife Gencer due to laboratory opportunity during implantation and absorption measurements. Also, thanks go to Yücel Eke due to the technical assistance and help I received during every stage of this study.

Special thanks go to my familily's each member. Throughout my life, I have been very lucky to have such a family. They have supported, given me necessary criticism, and taught me a great deal about how to live my life. Without them the life would be meaningless for me.

H. Mehmet Duranoğlu is another important person whom I must thank very much about home mate, friendship, and actually for everything we share during two years.

TABLE OF CONTENTS

LIST OF TABLES

TABLE

LIST OF FIGURES

FIGURES

CHAPTER I

INTRODUCTION

Semiconductors are a class of materials having electrical conductivities between metals and insulators [1]. Semiconductors can be defined by their many properties: (i) they have electrical resistivity in the range between metals and insulators, (ii) the temperature coefficient of resistance is usually negative (i. e., the resistivity decrease with increasing of temperature), and (iii) the conductivity of semiconductors can be changed by external agents such as impurities (doping), temperature, excess charge carrier injection, and optical excitation. These external agents have a great influence on semiconductors properties. For instance, they can change the conductivity of a semiconductor by several orders of magnitude. The capability of changing the electrical conductivity offers unique applications of semiconductors in various electronic devices, like transistors, and many optoelectronic devices [2].

Semiconductors are found in column IV and neighboring columns of the periodic table. The column IV materials are called *elemental* semiconductors, such as silicon and germanium. There are also compound semiconductors which may consist of two different pure elements. The combination of them results in intermetallic or compound semiconductors [1].

There are, of course, quite different semiconductor materials which have wide range of their electrical and optical properties that they can be used in the design of various electronic and optoelectronic devices. Many combinations of pure elements have been carried out so as to produce specific compounds in order to be used for

specific applications so far. The compounds are classified according to the column number of combined pure elements. Ga and Se, for instance, combine and perform III-VI compound, namely GaSe. Similarly, Ga and As combine and make up the compound GaAs belonging to III-V family. In fact, each group may be used for different specific application. For example, III-V compounds, like GaAs and GaP, are produced to be used as Light- Emitting-Diodes (LEDs), and II-VI family are generally used as fluorescent materials [3].

In recent years many investigations have been carried out on compounds of the type III-VI [4]. The layer compounds of this type: GaS, GaSe, GaTe and InSe were of particular interest because of their specific energy bands, crystal structure, electrical and optical properties [4, 5].

In the family of III-VI compounds, the structures consist of multiple layers of ions (slab, packet, sandwich) which consist of four atomic sheets. These atomic sheets are sequenced as X-M-M-X (X = Chalcogenide, M = Metal) [4, 6]. There is an intrinsic property of these layered compounds in wiev of bonding they have. The slabs or multiple layers are bound together by weak Van der Waals forces, while the intralayer bonds are stronger and are of covalent character [4, 7]. Because of this structure the layered crystals have an easy basal cleavage and lubricity [8].

The structure of a slab is made up of prisms of anions; the centers of the prisms are occupied by pairs of cations as shown in Fig.1.1. As the anion sheets at the top and bottom of each slab are close packed, the four- atom-thick layers can be arranged in several different ways. That's why, these different arranging of 4-atom-thick layers can cause various polytypic structures [4].

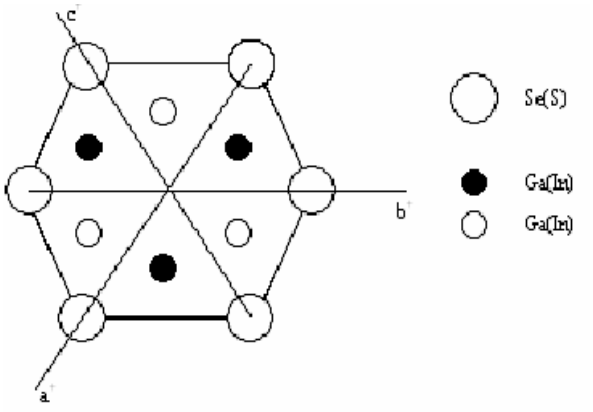

(a)

(b)

Figure 1.1: (a) Projection of the different positions of the ions in the multiple layer in the (001) plane, (b) Model of a multiple layer consisting of two close packed layers of anions and two layer of cations between them.

Each layer's position is fixed by the anion sheets' position. Mostly, these positions are taken as origin. Although the places of anion sheets are fixed, the layers may have different orientations. Assuming that the places of an anion sheet is at (0, 0, 0), then, the cation pairs can be found in either of the positions (1/3, 2/3, z) and (2/3, 1/3, z). Hence, it will give rise to more stacking varieties due to the fact that there are possibilities of cation pairs finding in different positions within slabs [4].

In order to describe the position and structure of layered compounds, there are many notation developed to fulfill this aim. One of these notations is indicating position of anion sheets by the roman letters A, B and C and describing cation pairs' places by the Greek letters α, β, and γ. As a result, it is possible to characterize a

multiple layer by AββA or AγγA; then, by looking at this notation it is said that the anion sheets are chosen in the A-position and the cation pairs are chosen in the position of β or γ. After choosing one of the three possible positions of anion sheets, the other layer which will stack can positioned in two alternative ways. That's, if the first layer is in A-position, the second layer can stack to the first in position of –B or –C. Also, the cation pairs can have the positions of α, β, and γ, respectively. As a result of possible variations in both anion sheets positions and cation pairs, with increasing numbers of layers by stacking onto each other, the number of different stacking possibilities increases considerably.

Another widely known notation of layered compounds is that of Ramsdell's [4]. This notation is consists of a number and a capital letter. The number gives the number of structural layers, while the capital latter indicates the symmetry of the system such as 2T, 4H, 3R, where T, H, and R stand for trigonal, hexagonal and rhombohedral, respectively [4].

In Roman-Greek letter notation, there are also signs, "+" and "-", which indicates the sequence of these letters. In the "+" layer, the sequence is Aβ, Bγ or Cα, while in the "-"layer, the sequence is Aγ, Bα or Cβ [4].

The Nabarro-Frank notation is another method which specifies the relationship between successive layers. In this notation, the passages $A \rightarrow B$, $B \rightarrow C$, $C \rightarrow A$ is denoted by an operator "∇" and a passage $B \rightarrow A$, $C \rightarrow B$, $A \rightarrow C$, is denoted by an operator "Δ" [4].

1.1 Structural Properties of GaSe

In the family of III-IV compounds some of members have layered structure. One member of this family is Gallium Selenide .The structure of GaSe consist of multiple layers of ions which consist of four-monoatomic sheets in the sequence of Se-Ga-Ga-Se as shown in Fig 1.1. In another words, each four-fould slab contains a double layer of Ga atoms packed between two Se atom sheets [4,9].

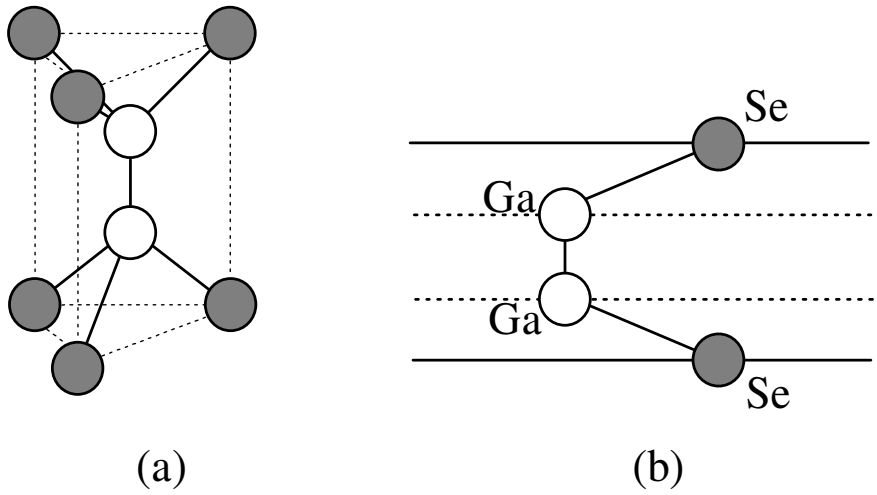

Figure 1.2: GaSe structure; a) indication of the basic unit cell, and b) a section through a single layer.

The slabs are bound together by weak Van der Waals forces, while the intralayer forces are of strong covalent forces [7]. Due to having a strong covalent bonds within the slabs and the all available valance electrons being used in the formation of these bonds, only Van der Waals forces can act between slabs [10]. The influence of these combined bonds in different character gives rise to creation of a material with anisotropic property [11].

Although in slabs each atomic sheet is close-packed, within a multiple layer these are not stacked so [10]. Hence, since the anion sheets (selenium atom's sheets) at the top and the bottom of each multiple layer are close packed, the four-atom-thick layers can be stacked in different ways. Thus, as a result of stacking of different positioned anion layer and the different positions of cation pairs occupying positions within the multilayer slabs, a GaSe crystal can be grown in form of many polytypes under specific growth conditions and methods [4]. That is, different ways of stacking of the four-monoatomic sheet layers give rise to various polytypes of GaSe single crystal as shown in Fig. 1.3.

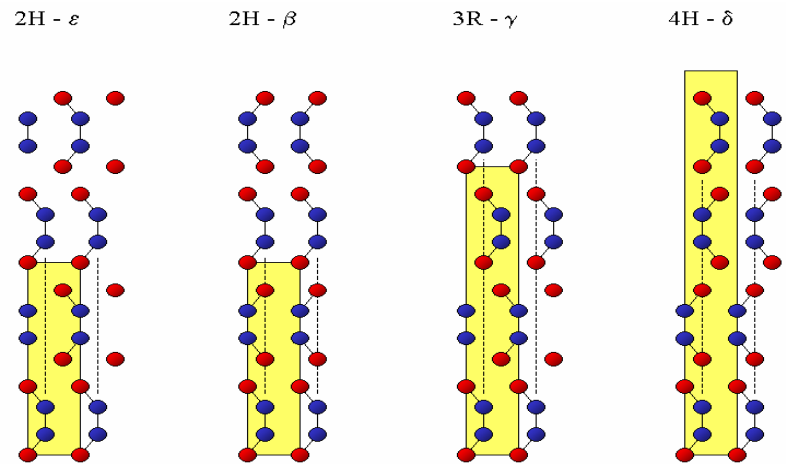

Figure 1.3: Polytypes of GaSe [6-8] ;(a) 2H-ε polytype, (b) 2H-β polytype, (c) 3R-γ polytype, (d) 4H-δ polytype

There are four polytypes of GaSe, which are β, δ, γ, and ε [12-14]. At each poltypes the interatomic distances can be different. As it is mentioned by Schubert et al [15] and A. Kuhn [12], in their study on determination of the distances between the atoms in the layers, they have calculated the interatomic distances in the GaSe polytypes ε (2T), γ (3R), and δ (4H) as shown in the Table 1.1.

Table 1.1: The interatomic distances in the GaSe polytypes

Type	Ref	Se-Ga intralayer	Ga-Ga intralayer	Se-Se intralayer	Se-Se interlayer
ε(2T)	(15)	2.485 (A^o)	2.383 (A^o)	4.766 (A^o)	3.840 (A^o)
γ(3R)	(15)	2.467 (A^o)	2.386 (A^o)	4.722 (A^o)	3.847 (A^o)
δ(4H)	(12)	2.463 (A^o)	2.457 (A^o)	4.784 (A^o)	3.880 (A^o)

There are many theoretically and experimentally studies performed in order to investigate the structure of GaSe single Crystals. Mc Canny *et al* [9] have reported that the GaSe is a member of layered compounds with a direct band gap of 2 eV at room temperature. In the references [12-14], it is observed that GaSe has anisotropy in its structure. Kuhn *et al* [12] has reported that the GaSe single crystals grown by Bridgman method have generally ε-type and the lattice parameters *a* and *c* are 3.75

and 15.95 A^o, respectively. Moreover, it was reported that while *a* parameter's value is almost the same for all polytypes, the *c* parameter's value is changing according to the form of polytype, and the values are found to be 15.95, 23.86, and 31.99 A^o for β, γ, and δ polytypes, respectively. The interatomic distances between the atoms, Ga-Se, Ga-Ga and Se-Se within layer of ε-type GaSe are found to be 2.48, 2.38, and 4.77, respectively [11,12]. Another study on structure of GaSe has been carried out by. Anis *et al* [6] and Sanchez-Ruyo *et al* [16]. They have reported that the structure of GaSe contains layers consist of atoms arranged in either hexagonal or rhombohedral and the c-axis is perpendicular to the layer planes.

In 1981, M.K. Anis [11] studied the structure of GaSe and found that the undoped GaSe is p-type with a direct band gap of 2 eV. In addition, M. Schluter [17] have studied band structure of GaSe and observed that GaSe single crystal has also indirect band gap and its value is very close to direct band gap. Then, in 1974, Voitchovsky *et al* [17] found these values to be 2.127 and 2.106, for direct and indirect band gap, respectively.

1.2 Previous Studies

As it is mentioned in introduction part, in recent years, many researches on III-VI layered family have been carried out to deduce their structural, electrical and optical properties.

GaSe has been the subject of investigation of several research groups; and numerous publications on its structural, electrical and optical properties have presented in the literature. In Switzerland (E. Mooser), Italy (C. Manfredotti, A. Rizzo), Holland (R. M. A. Lieth, J. C. J. M Terhell), England (A. A. Bachin), Japan (Y. Sasaki, S. Shigetomi, T. Ikari, H. Nakashima) have studied the properties like electrical conductivity, Hall effect, photoconductivity, electroluminescence, optical absorption, magneto-optical absorption, refractive indices [4]. As it was possible to grow large pure single crystals of GaSe by various techniques such as Bridgman-Stockbarger (B-S), transport reactions and vacuum sublimation, the investigators were able to perform such measurements. Of all these growth techniques, Bridgman-Stockbarger method was used most commonly due to many advantages it provides as

it will be seen in Chapter 2 in details.

It is reported that [4] GaSe single crystals were synthesed firstly by Klemm in 1934. From the investigation of GaSe till now researchers have grown GaSe single crystals and carried out measurements in order to reveal the properties of this new promising material in many aspects by using several growth techniques.

In 1959, Richard H. Bube and Edward L. Lind [19] grew p-type GaSe by reaction of the elements, followed by gradient freeze crystallization, and studied photoconductivity of Gallium Selenide crystals. As a yield of their study they found hole mobility, hole concentration, and acceptor ionization energy to be 15 cm^2/volt sec, 10^{16} cm^{-3}, and 0.12 eV, respectively. In addition, it was observed that in many ways the properties of GaSe crystals were very similar to those of ZnTe crystals. The other results they found as a consequence of this study were that the absorption edge of GaSe is at 6310 A^o, corresponding to a band gap of 1.97 eV; thermal quenching of photoconductivity corresponds to ionization energy of 0.5 eV, whereas optical quenching corresponds to ionization energy of about 1.0 eV.

In 1967, Fivaz and Mooser [20] measured the electrical resistivities and Hall constants of the compound semiconductors GaSe, MoS_2, $MoSe_2$, and WSe_2 at temperatures ranging from 100 to 700K. The measured Hall mobilities were all of the order of 100 cm^2/volt at room temperature. It was also observed that the mobilities exhibit a temperature dependence of the form $\mu \alpha (T/T_0)^{-n}$, where $n=2.1$ for GaSe, $n=2.6$ for MoS_2, and $n=2.4$ for $MoSe_2$ and WSe_2. In addition, measurements of Hall effect and resistivity carried out on a series of semiconducting layer structure showed that in these materials the charge carriers have rather low but strongly temperature-dependent mobilities. These were interpreted in terms of a short range interaction coupling the carriers to those optical modes of lattice which modulate the layer thickness. The interaction is thus specific of layer structures and reflects the tendency in these structures of the charge carriers to become localized within individual layers.

In 1969, Tredgold and Clark [7] studied hopping conduction in GaSe single crystals. The grown crystals were obtained by using three different methods; the halogen vapour transport method, the stockbarger method, and pulling from the melt using an encapsulation technique. In the both c-direction and at right angle the

electrical conductivity of this material are measured and it was seen that in n-type crystals the hopping process were inferred in the c direction and in p-type material a normal mobility associated with this direction is observed.

Using a different growth technique, sublimation process in closed quartz ampoules, Terhell and Lieth [13] grew needle crystals of GaSe in 1972. Using X-ray and phase contrast microscopy techniques, each part of the grown needle crystal's structure and polytypes were observed. Their study on the crystal grown by sublimation showed pure γ-type ordered stacking on the top parts while a disordered ε-type stacking exist at the bottom. Moreover, they observed that while γ-type has an ordered stacking sequence, the ε-type was a disordered stacking. In the same year, Kuhn *et al* [21] prepared GaSe crystals by vapour transport using iodine.

In 1972, Cardetta *et al* [22] have studied many system parameters effective in the growth of GaSe by using Bridgman method, such as ampoule's diameter, shape of the ampoule bottom, lowering rate and ampoule's position in the furnace. The main results they obtained were that for large ampoule diameters (diameter>10 mm) and high lowering rates (v> 1, 5 mm/h) polycrystalline ingots were obtained and for small ampoule dimeters (diameter<10 mm) and low lowering rates (v<1.5 mm/h) monocrystalline ingots were obtained. In addition, the crystals obtained were p-type with average resistivity and mobility values of 1.8 x10 ^{8} Ω cm and about 100 cm^2/volt sec respectively as measured by the Van der Pauw method. The conclusion of this study was that very good crystals of GaSe can be grown by B-S method using pointed and flat bottom ampoules with a dimeter not larger than 10 mm and a lowering rate range of about 0.2 to 1mm/h.

In 1974, PH. Schmid et al [23] studied the effect of impurity on low temperature photoluminescence of GaSe. The measurement have been carried out on a series of single crystals doped with different elements such as tin, copper, zinc, iodine and cadmium. Concentrations and activation energies of the impurities have been determined by electrical measurements. Prior to this study there were few works on the spectra of GaSe at 4.2 K and there were discrepancies between the experimental findings of the different authors. This was attributed to the difficulties encountered in growing pure and perfect crystals, and it was also partially due to the fact that the impurity and their effect on the luminescence spectra were hitherto unknown. The Hall mobilities of crystals, each of which are doped with different

amounts of impurities were found as a function of temperature. The crystal was containing small impurity concentrations and the results they obtained were in agreement with those of Fivaz and Mooser [20]. The tendency of mobility on temperature was T^{-2} at temperature higher than 300 K. This result was attributed to the predominance of optical phonons scattering in GaSe. In the sample containing more impurity they observed that in low temperatures the mobility decreases and was attributed to scattering by ionized impurities. At higher temperatures optical phonon scattering remained predominant. In the sample of the most heavily doped crystal the predominant scattering was due to the ionized impurities. In addition, different activation energy levels obtained by doping crystal with different elements. For cadmium doped GaSe an acceptor level appeared about 115 meV above the valance band, which was also observed in photovoltaic experiments. And, for zinc doped GaSe an acceptor level associated with Zn was about 140 meV above the valance band. For tin doped GaSe an acceptor level laid some 100 meV above the valance band. It was also observed that small addition of Sn increases the resistivity of the material by several orders of magnitude. For the sample grown by chemical transport with iodine an impurity level appeared at 350 meV below the conduction band. The result of PL at 4. 2 K for the three different crystals was reported to be different. For the purest crystal the spectrum was dominated by a group of lines of energy E>2.1 eV, lying in the energy range of the free exciton, and it was referred to group as FE. In the spectrum of crystals highly doped one a set of lines was visible at E<2.1 eV. These lines were thought to arise from recombinations involving traps and were referred to as TR. Another important result obtained in the study was that although different impurities, with widely varying ionization energies, have been introduced in the crystals, no lines specific of these impurities appeared in the emission spectra.

The charge transport in layered semiconductors has been studied by Minder *et al* [24]. In this study the electron and hole-drift velocity of layered semiconductors such as HgI_2, GaSe, PbI_2 and GaS was measured in the direction parallel to the c-axis between 80 and 400 K. It was observed that electron and hole – drift velocity is proportional to the field applied except in the case of GaS. For GaS a superohmic behaviour was observed. The maximum value of hole mobility was observed in GaS, which was μ_h = 80 cm^2/volt sec. Moreover, for HgI_2 and GaSe they found no evidence for the large anisotropy of charge carrier transport properties that's usually

attributed to layered compounds.

In 1976, Arancia *et al* [25] studied electron diffraction of melt- and vapour – grown $GaSe_{1-x}S_x$ single crystals. By using both Bridgman-Stockbarger and chemical transport method single crystals of $GaSe1_{-x}S_x$ solid solutions have been obtained. To see the variation of lattice parameters *a* and *c* with respect to *x*, the electron diffraction were carried out for both types of crystals. From the analysis of their results they have reached:(i) it is possible to grow high quality single crystals of $GaSe_{1-x}S_x$ solid solution throughout the complete composition range $0 \leq x \leq 1$ by using both Bridgman - Stockbarger and chemical transport method; (ii) between the composition range of $0 \leq x \leq 0.45$, it was seen that the growth method has an important effect on crystals both physical and structural properties; (iii) for the composition value x=0.45 it was observed that there is a sharp discontinuity in the lattice parameter varying with composition for melt-grown crystals, and it was estimated to be due to the transition from a pure parallel structure (ε or ε+ γ) to an antiparallel one (β). In the mixed crystals grown by chemical transport method, for x ranging from 0 to about 0.25, the ε –and β- modifications probably occur simultaneously.

Levy [26] has reviewed the classical method used frequently to prepare crystalline samples of layered materials. In this review, the most important basic concepts of crystal growth kinetics were explained in detail. The methods of growing thin flakes and bulk crystals were also presented.

Augelli *et al* [27] have measured the Hall mobility in a layered compound both along and perpendicular to the layer for the first time. The mobility of GaSe has been measured as a function of both temperature and electric field. And, it was observed that both mobilities are limited by homopolar optical-phonon scattering. Another result was that the hall mobility along the c-axis is evidently field dependent. The difference between the low-field and high –field mobilities was attributed to stacking faults.

Mc Canny and Murray [9] have studied the band structure of both GaSe and InSe. The method they used to investigate the band structure was a semi emprical tight-binding. In this study most of the discrepancies between their experimental work and previous calculations for GaSe have been resolved.

In 1983, M.K.Anis [28] carried out a study to investigate the effect of

physical parameters on quality of grown GaSe single crystals. Especially, he has studied the relation between temperature gradient and translation rate of crucible in the Bridgman system. To fulfil this, two different furnaces have been used; one of them was two-zoned, the other one was three-zoned. For each furnace, different temperature profiles were used. The profile of two-zoned furnace was like that the upper zone at T_1 =1050 ^oC and lower zone at T_2=725 ^oC. The crucible has been translated with velocity of 2 mm/h. On the other hand, in three-zoned furnace upper zone was at T_1=1000 ^oC, middle zone at T_2=850 ^oC, and the lower at T_3=720 ^oC. One of the important results they obtained from this temperature profile was that when the bottom zone was set lower than 700 ^oC the ampoule was breaking. Using these temperature gradients they were able to get samples in dimensions up to 10 mm^2 in area and 300μm in thickness. As a result of study, their conclusions were: (i) it was seen that there is usually a small amount of impurities at the top of the ingot and it causes polycrystalline structure. This shows that the purity degree of the starting material has a considerable effect on the growth of single crystals; (ii) during the growth process non-stability of the crucible can result in a crystal which has more than one specific form or polycrystalline form; (iii) the size and shape of crucible have an important effect on grown crystals. Especially, sharpness of the pointed end is very important to form initially only one nucleus; (iv) upon using argon gas pressure around $5x10^{-4}$ torr in the ampoule, it was observed that it reduces the possibility of formation of voids in the ingot.

Cappozi [29] has studied the photoluminescence spectra of undoped crystals of the layer semiconductor GaSe. This study was based on a detailed study of PL spectra, recorded at different temperatures and excitation levels. In addition, the PL of GaSe doped by Cu by using implantation technique has been studied by Capozzi and Minafra [30]. It was observed that Cu- doped GaSe crystals by implantation are similar to spectra of Cu-doped GaSe by chemical method. Crystals were doped with different concentration of Cu and the analysis of spectra versus temperature and excitation intensity has been carried out.

In 1983, X-ray and electron diffraction analysis of GaSe crystals studied by Anis and Nazar [6]. Analyzing x-ray reflections, they have indexed the planes and relative intensities have been recorded. For comparison, θ (angle) and I (intensity) values obtained by other researchers were also given in the results. The lattice

parameters, *a* and *c*, were derived from the diffractogram. In spite of taking samples from different region of the same ingot, the same structure of crystal was observed. As a result of this study, it was seen that by using B-S technique ε-GaSe hexagonal single crystals are obtained. One another study on structural analysis of GaSe and other form of it was carried out by Anis [31] and Whitehouse [32]. In their study they have grown non-stoichiometric material with selenium content, $50 \leq x \leq 52, 5$ at % that gave rhombohedral γ-modification, while crystal with a selenium content of $48 \leq x \leq 50$ at % gave the hexagonal ε- modification. It was also reported that in Ga–rich GaSe there was a possibility of obtaining Ga_2Se and Ga_3Se_2 [31, 32, 33].

Although there are many studies on the optical and electrical properties of GaSe crystals grown from melt, a few studies have been carried out with vapour-phase grown crystals. In 1986, Ishii and Kambe [34] grew GaSe single crystal by iodine vapour transport aiming to improve the crystalline quality after examining the GaSe grown by vapour transport. Growing high quality crystals, they have carried out systematic characterization of the structure and impurity analysis of samples by X-Ray diffraction, photoluminescence, I-V, and secondary ion mass spectrometry (SIMS) for the first time. In the same year, the optical properties of Mn-doped GaSe were studied by Soo-II Lee [35]. Using photoconductivity and photoluminescence spectra, some donor and acceptor energy levels have been calculated. In the photoconductivity spectra introduced by Mn related defects were observed at 1.916 and 1.724 eV, and in the photoluminescence spectra at 80 K another peak was observed at 1.804 eV. Making use of these results, three energy levels have been investigated, one of them was a donor level (D) which is laying 0.112 eV below the conduction band, and others were acceptor levels A_1 and A_2 which are lying at 348 and 156 meV above the valance band, respectively. Another important result they have obtained was that the energy gap and the defect photoconductivity peaks have the same temperature coefficient. This resulted in pinning of Mn–related defect levels within the conduction band of the GaSe.

Many studies have been carried out on optical properties of layered compound GaSe single crystals. One of them deals with investigation anisotropy of GaSe by photoluminescence [36]. Especially, most of researchers have made use of photoluminescence measurements to investigate complex structure of luminescence spectra of this material. The PL spectrum of GaSe is rather complex at low

temperatures, and, it was reported to be containing either intrinsic sharp lines because of the excitonic recombinations [18, 37] or extrinsic bands at lower energy which are attributed to lattice defects or impurities [38]. Due to special band structure of GaSe, which contains both direct and indirect band gap, the conduction band has an indirect minimum which is only 25 meV lower than the direct minimum [39, 40]. Since these two minima can be occupied by the photoexcited carriers, radiative recombinations from levels associated with them can occure simultaneously [37, 41, 42]. That's why, the spectra obtained is very sensitive to temperature [43, 44], excitation intensity [18, 45], and excitation energy [46, 47]. The excitonic luminescence of GaSe between 580 and 620 nm has been studied by several groups [18, 37, 48, 49]. Although there is no exact agreement on energies of the indirect excitonic recombinations, the different researchers agree with the interpretation of these intrinsic lines owing to free, as well as bound, direct and indirect excitonic emissions [37, 42, 48, 49]. If it is compared with studies on excitonic luminescence of GaSe, it is seen that very little information is available about the emissions related defect levels localized in the forbidden energy gap at energies lower than 2 eV [38].

According to the growth conditions and dopant elements GaSe single crystals can be both n-type and p-type. It was reported that while the undoped crystals grown by B-S technique is p-type, the crystals grown by transport method is n-type [39, 40]. Of course, it is possible to dope a material with different element and study electrical, optical and structural modifications to see the effect of doping element on target material. There are many studies which have been carried out to observe the influence of chemical doping of different element on properties of GaSe single crystals; such as Cl [50], Sn [16, 51], Ge [52], As [52], Cd [53, 54, 55], Sb [56], Cu [57], Tm [58], Li [59], Ag [60], Zn [61], Gd [62], and Mg [63].

Only a few studies appeared in the literature on the implantation up to now [30, 64, 65]. In reference [64], the annealing effect on electrical and photoconductive properties of Si – implanted GaSe single crystal were studied and found that there is four order decrease in resistivity following implantation and annealing process. In addition, in reference [65], electrical properties of N – implanted GaSe single crystal was studied and observed that N – implantation decreases the resistivity values down to 10^3 Ω-cm depending on the annealing temperature. Moreover, temperature dependence of conductivity revealed two distinct regions with the activation energies

of 234-267 meV and 26-74 meV for the samples of GaSe annealed at 500 ^{o} C and 700 ^{o} C, respectively.

1.3 Present Study

The crystals used in this work were obtained in the Crystal Growth Laboratory of Physic Department of METU by the Bridgman- Stockbarger method. GaSe single crystals were implanted by Ge ion- beam with about 100 keV energy and $1X10^{15}$ ions/cm^2 doses at room temperature. In order to investigate the structural, electrical, and optical properties of as-grown, Ge- implanted and annealed at 500 ^{0}C following implantation GaSe, X-ray diffraction (XRD), conductivity, Hall, absorption and phototoconductivity measurements were performed. From electrical characterization, the room temperature and temperature dependent values of conductivity, carrier density, and mobility parameters are calculated in the temperature range of 100 - 480 K. XRD measurements were carried out for different annealing temperatures and results were compared with both unimplanted and implanted GaSe samples. And, finally, as an optical characterization part of our study photoconductivity and transmission measurements were carried out.

The topics covered in this thesis are organized in chapters as follows: chapter 2 present theoretical considerations of crystal growth, doping process, structural, electrical and optical characterization techniques. This is followed, in chapter 3, by describing (i) stages of crystal growth procedure, such as crucible cleaning, material preparation, and synthesis and sample preparation for measurements, and (ii) the experimental set up and explanation of measurement techniques. Chapter 4 includes the results and discussion, and in last chapter (chapter 5), the conclusions are presented.

CHAPTER II

THEORETICAL CONSIDERATIONS

2.1 Introduction

In this chapter, the structural, electrical, and optical characterization techniques are described; i.e., the theoretical basis of general conduction mechanisms, Hall Effect, X-ray diffraction (XRD), absorption and photoconductivity for semiconductors are introduced in detail.

2.2 Crystal Growth

The development of solid state device technology is dependent on many factors which affect the progressing in this field. One of the important factors is the availability of convenient material for the fabrication of desired devices [1]. The first step in the fabrication of modern integrated circuits is the preparation of a single crystal of semiconductor materials. Most crystallizable substances occur in nature in polycrystalline forms. However, for many applications, high quality single crystals are required. In crystalline solids, the elements are stacked in a periodic pattern. When the periodicity extends through the solid, one speak of a single crystal, or monocrystal, as opposed to a polycrystal, which consist of small crystals, called grains, arranged in random directions and adhering together at their boundaries.

It is not easy to produce high quality crystals since special conditions are required for their formations. Today, they are produced in laboratories for many scientific investigations and technical applications. Production of single crystals can be achieved in three ways [66]:

1. By crystallization from the solid. In another word, solid to solid process involving solid – solid phase transitions.

2. By crystallization from melt. That is, liquid to solid process involving liquid – solid phase transitions.

3. By crystallization from vapour. That is, vapour to solid process involving gas–solid phase transformations.

Solid to solid processes are generally used for production of metals or in certain cases where a crystal structure change occurs between the melting point and room temperature. The growth from melt to solid is most commonly used process. Normal freezing is most straightforward technique. Moreover, zone refining is included in this category. Vapour to solid processes contains sublimation and vapour phase reactions, such as used in the epitaxial growth of materials [66].

The most convenient method for the production of single crystals of a particular substance depends on not only the nature of the substance, but also on the intended application, desired quality and available laboratory equipment.

The production of single crystals from melt is carried out by passing the melt through a temperature gradient. That is, it is carried out by controlled freezing. The ingot is frozen slowly from one end to the other end by passing from hot zone to the cold zone. One of the important and most commonly used techniques of the growth from melt is the Bridgman-Stockbarger method. This method involves a crucible which is lowered through a furnace so that freezing start at the lowest point in the crucible and the solidification face moves slowly up to crucible. Almost 40 % fabricated materials are produced by this technique. The advantages can be explained as follow [67]:

1. It produces crystals with good dimensional tolerances quickly;
2. It employs relatively simple technology;
3. It requires neither control system nor many hours of supervision.

Since our crystal has been grown by B-S method, the explanation of technique will be presented in detail. Mostly used other techniques of the growth from melt are Czochralski (CZ) and the zone refining methods. In fact, as it is mentioned before, according to requirement of a specific single crystal, the most convenient method is chosen. That's why, each method has its own advantages and disadvantages. The most important advantage of this technique is that it is possible to grow a crystal in large diameters and as a consequence, large wafers can be fabricated and large wafer means giving opportunity to perform many circuits on the

same chip. Today, by using Czochralski method it is possible to grow crystals 30 cm in diameter and 1m in length.

Another commonly used method is the zone refining method. The most important advantage of this method is that it is possible to produce a crystal with high purity. Since it is very important to control many physical properties of semiconductors in specific applications, such as electrical, optical and structural, the purity of materials give us more chance to fulfill this. Hence, crystals with high purity are desired for many applications. For example, for high resistivity material applications, this method is most convenient one to use [1, 67].

The techniques which are explained above belong to bulk growth methods. In addition, there is epitaxial growth technique used to growth a single crystalline film on the surface of the same material or another substrate. In this process, since the growing thin layer takes the same orientation and structure of substrate under it, substrate is serving as seed crystal. So, by using this technique different materials can be produced to be used in electronic and optoelectronic devices [1].

2.3 Structural Analysis

The structural characterization includes investigation of the three-dimensional arrangement of the atoms in solids. That's, the main objective is the measuring the lengths and angles in the unit cell (i.e., the lattice parameters), and determining the arrangement of the atoms in the unit cell. There are some standard methods to fulfill structural characterization of materials such as X-ray diffraction, neutron diffraction analysis, electron microscopy and electron diffraction. By carrying out structural measurement many structural properties of materials can be revealed, such as crystalline state (i.e., whether the material is crystalline, polycrystalline, or amorphous), defects, and stresses present in the material. In order to investigate the structure of our material, we have used X-ray diffraction technique, which will be examined theoretically in detail below.

2.3.1 X-ray Diffraction (XRD) Technique

X-ray diffraction is a nondestructive technique used to investigate an unknown crystal structure [68]. X-rays can interact with a solid in several ways; it can be absorbed, emitted, reflected or transmitted. In the case of diffraction of rays from a periodic structure, the diffraction peaks can give us much valuable information about the crystal structure. In order to make use of this technique, the crystal must be composed of regularly spaced atoms acting as scattering centers for X-rays. Another condition required to be satisfied is that the wavelength of the X-rays and the inter space between atoms must be in the same order. The conditions of diffraction are as follows [69]:

1. the angle made by the diffracting planes (h k l) with the incident and diffracted beams are equal;
2. the directions of the incident and diffracted beams and the normal to the diffracting planes are coplanar;
3. the waves emitted by individual atoms in the direction of a diffracted beams are in phase.

The diffraction condition is given by Bragg's law:

$$n\lambda = 2d \sin\theta \tag{2.1}$$

derived by the English physicist sir W. H. Bragg and his son Sir W. L. Bragg in 1933 so as to explain why the cleavage faces of crystals appear to reflect X-ray beam at certain angle of incidence (θ). n is the order of the diffracted beam and is numerically equal to the path difference in wavelengths for successive planes; d is the inter planar spacing of the diffracting planes and λ is the wavelength of incident X-ray. θ, the Bragg angle, is the angle between the incident X-rays and diffracting planes as shown in Fig. 2.1.

X-ray spectrometers are usually calibrated in terms of 2θ, the angle between the diffracted beam and the undeflected incident beam. Hence, when the Bragg's law is satisfied the diffraction can be observed. Moreover, the parameter included in equation must be appropriate in order to give rise to a diffraction peak.

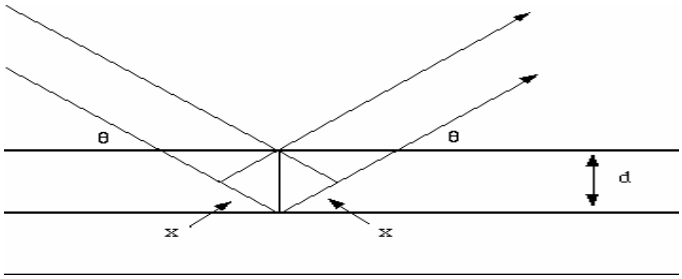

Figure 2.1: X-ray diffraction.

By changing the Bragg's equation parameters such as λ or θ during the experiment, the conditions for diffracting beams can be satisfied [69].

According to the varied parameter, X-ray techniques take a special name in the existing methods, such as Laue, rotating – crystal or powder method. Each method's varied and fixed parameters can be summarized in the Table 2.1 as follow:

Table 2.1: Structural analysis methods

Method	λ	θ
Laue	variable	fixed
Rotating Crystal	fixed	variable
Powder	fixed	variable

In our study, we have used the powder method. In this technique, the crystals are reduced to a very fine powders and it is exposed to a beam of monochromatic X-rays. For every set of crystal planes, by chance, one or more crystal will be in the correct orientation to give the correct Bragg angle in order to satisfy Bragg's relation. Hence, every crystal plane is capable of diffraction. By using powder method we can determine the unknown structure by finding structural parameters such as interatomic spacing d for each peak and considering relative intensities trying to match with known components. The general procedure to investigate the unknown structure is as follows [69];

1. From the angular positions of the diffraction lines the shape and size of the

unit cell can be deduced. After determining the structure, the obtained data is compared with the existed ones in literature, which are grouped according to its belonging one of the seven crystal system. Following specifying the system it belongs, the miller indices are assigned to each reflection, which is called indexing the pattern. When the matching is established, the unit cell and its size is found.

2. From the size and the shape of the unit cell the number of atoms per unit cell is found.

3. And, finally, from the relative intensities of the diffraction lines, the positions of the atoms within the unit cell are deduced. For each system there is a formula to calculate the value of d. These are given in eqn. 2.2 (a-d) as follow:

Cubic	$1/d^2 = (h^2 + k^2 + l^2)/a^2$	(2.2.a)
Tetragonal	$1/d^2 = (h^2 + k^2)/a^2 + l^2/a^2$	(2.2.b)
Hexagonal	$1/d^2 = 4/3(h^2 + hk + k^2)/a^2 + l^2/c^2$	(2.2.c)
Orthorhombic	$1/d^2 = h^2/a^2 + k^2/b^2 + l^2/c^2$	(2.2.d)

And ,after obtaining lattice parameters, the volume of each unit cell can be calculated by making use of formulas given in eqn. 2.3 (a-d) [69];

Cubic	$V = a^3$	(2.3.a)
Tetragonal	$V = a^2c$	(2.3.b)
Hexagonal	$V = \sqrt{3}/2\ a^2/c$	(2.3.c)
Orthorhombic	$V = abc$	(2.3.d)

2.4 Electrical Characterization

In order to analyze a wide range of semiconductor properties, electrical measurements are routinely performed on semiconductors and semiconductor devices. By means of electrical measurements one can derive the followings: (i) the electrical resistivity (or conductivity), (ii) the energy gap and separation of an

impurity from the conduction or valance band, (iii) the majority carrier concentration, (iv) the mobility of electrons and holes, (v) lifetime and diffusion of length of minority carriers, (vi) deep – impurity level, as well as device parameters such as , barrier height, contact resistance, interface densities, junction depth, and channel length and width.

Electrical characterization generally involves conductivity and Hall effect measurement. From the combination of two measurements the properties as mentioned above are investigated. For the electrical characterization of our samples, we have carried out both conductivity and Hall effect measurements. The experimental stages of these measurements will be explained in Chapter 3 in detail.

2.4.1 Fermi Dirac Distribution Function and Carrier concentration in Semiconductors

In order to determine both the carrier concentrations and the energy distributions, the knowledge of the probability of carrier occupancy of a state of energy E and the density of available states or density of states (DOS) are required [1]. The carrier energy distribution is described by the Fermi – Dirac statistics. The probability of an electron occupying energy level E is described by the Fermi – Dirac distribution function $f(E)$. For electrons, the Fermi-Dirac distribution function is [1],

$$F_n(E) = \frac{1}{\exp\left[\left(E - E_f\right)/k_B T\right] + 1} \tag{2.4}$$

where k_B is the Boltzman's constant, 8.62 x 10^{-5} eV/K. The quantity E_f is called the Fermi energy (also referred to as Fermi level), which is defined as the energy at which $F(E) = ½$, in another words, the energy for which the probability of occupation is ½. In addition, the hole distribution function is,

$$F_p(E) = \frac{1}{\exp\left[\left(E_f - E\right)/k_B T\right] + 1} \tag{2.5}$$

In the analysis of many properties of semiconductors, it is essential to know

the carrier concentration of material. In order to calculate the carrier concentration: (1) the number of states per unit volume and per energy (DOS, $g(E)$), over the energy interval between E and $E+dE$, (2) the probability of a carrier occupying an energy level at E, i.e., $f(E)$ must be known [1]. Hence, by knowing the density of available states in the valance and conduction band, the electron concentration in conduction band is:

$$n_o = \int_{E_c}^{\infty} f_n(E)N(E)dE \quad . \tag{2.6}$$

and the hole concentration in the valance band is [1]:

$$p_o = \int_{-\infty}^{E_v} f_p(E)N(E)dE \tag{2.7}$$

If we represent all of the distributed electron states in the conduction band by an effective density of states N_c located at the conduction band edge, the result of integral of eqn. 2.6 is:

$$n_o = N_c f(E_c) \tag{2.8}$$

where N_c is the effective density of states at E_c and $f(E_c)$ is the probability of occupancy at E_c. The density of states for the edge of the conduction and valance band can be obtained to be:

$$N_c = 2(2\pi m_n^* kT/h^2)^{3/2} \tag{2.9a}$$

$$N_v = 2\,(2\pi m_p^* kT/h^2)^{3/2} \tag{2.9b}$$

Moreover, the effective densities of states of many materials at specific temperatures are found in many catalogs [1].

At this point, it will be useful to define intrinsic and extrinsic semiconductors. A crystal that contains only one type of atom is called *intrinsic* material. If its lattice

structure is perfect and the temperature is kept at absolute zero kelvin, the intrinsic material will behave as a good insulator because at this temperature there will be no free charge carriers. However, when the temperature provides enough energy to raise many valance electrons into the conduction band, there will be free carriers for current flow. When an electron is raised from valance band to conduction band in an intrinsic material, it will leave a vacancy (hole) behind in the structure. The free electron and hole form an *electron-hole pair* (EHP). The number of EHP in an intrinsic material can be controlled by external agents such as optical and temperature excitation. Higher the temperature, greater the activity and more EHP's [1].

In order to change the properties of a semiconductor, it must be doped with certain impurities in very carefully controlled amounts. The impurities create two type of material, one with an excess of electrons in the material and the other with excess of holes in the lattice. If the added impurity atoms donate the crystal excess electrons, it is called *donor impurity.* Material doped with a donor impurity has an excess of electrons in the lattice structure and is known as negative or *n-type* material. On the other hand, if the added impurity accepts electrons from the structure and donates holes to material it is called *acceptor* impurity. The impurity atom becomes negatively ionized when it accepts an electron and become positively ionized when release one electron [1].

After having defined extrinsic and intrinsic material, we can evaluate the carrier concentration in these two types of materials. When we assume that the Fermi level E_f lies at least several kT below the conduction band, then the Fermi function can be reduced to;

$$f(E) = \exp-\left(E_c - E_f\right)/kT\,, \tag{2.10}$$

In this case, the concentration of electrons in the conduction band can be expressed as :

$$n_o = N_c\, exp\text{-}(E_c\text{-}E_f)/kT \tag{2.11}$$

and the concentration of holes in the valance band can be expressed as

$$p_o = Nv\ exp\text{-}(E_f\text{-}E_v)/kT\ , \tag{2.12}$$

By substituting N_c and N_v from eqn 2.9, we get,

$$n_o = 2(2\pi m_n^* kT/h^2)^{3/2}\ \ exp(E_f\text{-}E_c)/kT \tag{2.13}$$

$$p_o = \ 2\ (2\pi m_p^* kT/h^2)^{3/2}\ exp(E_v\text{-}E_f)/kT \qquad . \tag{2.14}$$

Equations (2.11) and (2.12) can be used for both intrinsic and extrinsic materials provided that thermal equilibrium is maintained. The Fermi level in an intrinsic semiconductor is positioned at mid gap. However, in real cases, since m_h^* is different from m_e^*, the Fermi level deviate from mid gap a little. That's why, for intrinsic semiconductors, the carrier concentration can be written as;

$$n_i = \ N_c\ exp(E_i\text{-}E_c)/kT \tag{2.15a}$$

$$n_i = N_v\ exp(E_v\text{-}E_i)/kT \tag{2.15b}$$

where $E_f = E_i$.

The equilibrium density of electrons and holes is constant at a given temperature. The product of the electron and hole density at equilibrium is always equal to the square of the intrinsic carrier density, i.e,

$$n\ p = n_i^2 \qquad . \tag{2.16}$$

Therefore, with help of eqn's (2.11) and (2.12) ,we can write eqn. (2.16) as;

$$n\ p = N_c N_v\ exp[(E_v\text{-}E_c)/kT] = \ \ N_c N_v\ exp[(\text{-}E_g)/kT] \tag{2.17}$$

This equation indicates that for a material in equilibrium, *np* product depends on the effective conduction and valance band densities of states, the energy gap of a semiconductor, and the temperature. Also, as it is seen from eqn. (2.17), it is independent of the Fermi level position and of the individual electron and hole

densities. From this equation, the intrinsic carrier density can be found [1] as:

$$n_i = (N_c N_v)^{1/2} \exp[(-E_g)/2kT] \quad . \tag{2.18}$$

2.4.2 Electrical Conductivity

In semiconductors both electrons and holes contribute to the current. That's why, in general, the conductivity is expressed as;

$$\sigma = n\, e\, \mu_e + p\, e\, \mu_p \tag{2.19}$$

where μ is the mobility and described with electron drift in the material. The mobility can be defined as;

$$\mu_n = -\frac{\langle V_x \rangle}{E_x} \tag{2.20}$$

where V_x is the drift velocity of carriers and E_x is the electric field in the x-direction. The unit of mobility is $cm^2/V.s$ And,. n and μ_e in the eqn 2.19 are the concentration and mobility of electrons, respectively, and p and μ_h are the concentration and mobility of holes, respectively. In the case of an intrinsic semiconductor (i.e., $n = p = n_i$), we can write

$$n = p = (constant)\ x\ T^{3/2} \exp[(-E_g)/2kT] \tag{2.21}$$

by making use of eqns.2.9 and 2.18 . Therefore, the conductivity is expressed as

$$\sigma = costant\ x\ T^{3/2} \exp[(-E_g)/2kT] \ = \ \sigma_o \exp[(-E_g)/2kT] \quad . \tag{2.22}$$

Upon plotting $Ln\sigma$ as a function of $1/T$ (which gives a straight line), the energy gap can be derived from the slope $-E_g/2k_B$ for an intrinsic material. The $T^{3/2}$ variation and the temperature variation of E_g are not considered because it can be neglected when it is compared with the exponential temperature variation term. Although the electron

and hole mobilities are also dependent on temperature as $\mu \alpha T^{3/2}$ dependence, it will not be considered in the calculations [1, 68]

2.4.3 Hall Effect

The Hall Effect analyzes the behavior of the free carriers in a semiconductor upon applying an electric and magnetic field. It is one of the most commonly used measurement techniques. From Hall effect measurement, the carrier concentration, carrier type, and the mobility of a material can be obtained. In 1879, Edwin Hall discovered that when a current-carrying conductor is placed in a magnetic field, a voltage is produced in a direction perpendicular to both the current and the magnetic field.

The basic physical principle underlying the Hall Effect is the Lorentz force. When an electron moves along a direction perpendicular to an applied magnetic field, it experiences a force acting normal to both directions and moves in response to this force and the force affected by the internal electric field. The experimental set up shown in Fig. 2.2 indicates a semiconductor bar with a rectangular cross section. A voltage V_p is applied between two contacts, giving rise to a field along the x-direction. The magnetic field is applied in the z-direction.

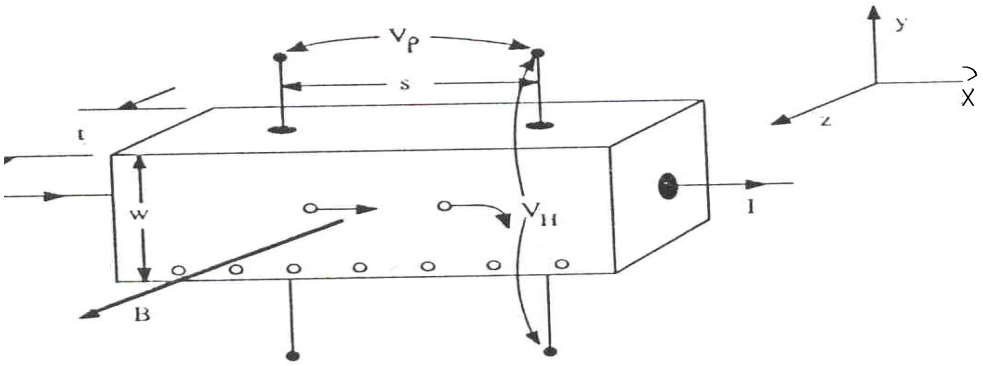

Figure 2.2: Schematic diagram of Hall effect.

The current applied in the x-direction is given by;

$$I = qwtp\upsilon_x \tag{2.23}$$

where p is the hole concentration, V_x is the drift velocity; w and t are the width and

thickness of the material, respectively. The voltage measured along the x-direction is given by;

$$V_P = (\rho\ s\ I) / (w\ t) \tag{2.24}$$

where ρ and s are the resistivity and distance between two contacts, respectively. The resistivity can be drawn from eqn. 2.24 as;

$$\rho = (wt/s)\ (V_P/I) \quad . \tag{2.25}$$

As it is depicted in Fig. 2.2, the holes move in the positive x-direction. The magnetic field causes a force to act on the mobile particles in a direction determined by the right hand rule. As a result there is a force, F_y, along the positive y-direction which is given as

$$\vec{F} = q\left[\vec{E} + \vec{v} x \vec{B}\right] \quad . \tag{2.26}$$

Due to this force some holes are deflected to the bottom of sample and they are accumulated at the bottom. This accumulation of charge at the edges increases until the electrostatic field set up by the charge separation balances the magnetic force on the carriers. When this equilibrium is established, the holes will not be deflected any more downward. And, there will be no current in y-direction. Thus, the force in the y-direction will be zero, that is, $F_y = 0$. By using eqns. 2.23 and 2.26, we can write electric field as;

$$E_y = -Bv_x = \frac{-BI}{qwtp} \quad . \tag{2.27}$$

This electric field is called the Hall field which produces a Hall voltage along the y-direction. The Hall voltage is expressed as;

$$V_H = -\int_0^w E_y dy = \int_0^w \frac{BI}{qwtp} dy = \frac{BI}{qtp} \quad . \tag{2.28}$$

The Hall coefficient, R_H, is defined as the Hall field divided by the applied current density and magnetic field:

$$R_H = \frac{tV_H}{BI} \ (m^3/C) \tag{2.29}$$

Once the Hall coefficient is obtained, one can easily find the hole density through relation:

$$p = \frac{1}{qR_H} \quad . \tag{2.30}$$

By similar derivations, the electron concentration is also found as:

$$n = -\frac{1}{qR_H} \quad . \tag{2.31}$$

Since all quantities appearing in eqn. 2.28 can be measured, a value for the Hall coefficient is easily obtained. The sign and magnitude of R_H give the sign of the charge carriers and their density. When Hall coefficient is combined with the measured conductivity, the Hall mobility is found to be:

$$\mu_h = \sigma R_H \quad . \tag{2.32}$$

A measurement of the Hall voltage is often used to determine the type of semiconductor (n-type or p-type), the free carrier density and the carrier mobility. In addition, upon repeating the measurement at different temperatures, allows one to measure the free carrier density and Hole mobility as a function of temperature. It is also important to distinguishes between the hole and drift mobility, since in the presence of magnetic field the scattering mechanisms may show different behavior; the ratio of μ_H over μ can typically vary in the range between 1 and 2 depending on the scattering mechanisms, which in turn depend on temperature and doping concentration [1, 68, 70].

2.4.4 Single Donor – Single Acceptor (SDSA) Model

As it will be useful to apply, the analysis of typical behavior of hole concentration is carried out by single donor-single acceptor model which is based on assuming that the crystals contain both donor and compensating acceptor levels together. In fact, semiconductors do not contain only either donors or acceptors for n-type and p-type materials, respectively. In real cases, in each type both acceptor in concentration of N_a and donors in concentration of N_d are found. However, the concentration of impurity type is different for n-type and p-type materials. So, the predominance of impurity type makes the material n or p-type. The concentration of donors, for example, in n-type material is dominant, that's why, $N_d > N_a$. If we assume the material contain either donors or acceptors and are ionized, the majority carrier concentrations would be $n_0 = N_d$ or $p_0 = N_a$, respectively, for the n-type and p-type material. However, in real case, since N_a and N_d are found in each type, we must allow for compensation. When an acceptor level is filled with a valance band electron, it leaves behind a hole. Then this hole is filled by recombination with one of the conduction band electrons. When this logic is extended to all the acceptor atoms, it will result in supplying electrons to conduction band in quantity of $N_d - N_a$ instead of N_d. This mechanism is called *compensation* [1].

In semiconductors the space charge neutrality is preserved, the sum of the positive charges (holes and ionized donors) is equal to the sum of the negative charges (electrons and ionized acceptor atoms):

$$P_0 + N_d^+ = n_0 + N_a^- \quad . \tag{2.33}$$

For n-type materials, the relation (2.33) can be reduced to:

$$n_0 = p_0 + (N_d^+ - N_a^-) \quad . \tag{2.34}$$

Upon neglecting p_0 when compared with n_0, we get,

$$n_0 = N_d^+ - N_a \tag{2.35}$$

for n-type material [1].

The following expression may be obtained from the space-charge –neutrality condition given in eqn. (2.33) by writing n_0 explicitly for the partly compensated impurity level:

$$n_0 + N_a = \frac{N_d}{1 + \beta \exp(\mu + E_d / kT)} \tag{2.36}$$

where $\mu = (F\text{-}E_c)/kT$ is the reduced Fermi level energy and β is the spin degeneracy. For a nondegenerate charge carrier, the expression in Eqn. (2.36) can be replaced by $\frac{n}{N_c}$ (where N_c is the effective density of states in the conduction band), and the following relation is found [71]:

$$\frac{n_0(N_a + n_0)}{(N_d - N_a - n_0)N_c'} = \frac{1}{\beta}\left(\frac{m_e^*}{m_0}\right)^{3/2} \exp\left[\frac{-E_d}{kT}\right] \tag{2.37}$$

where $N_c' = 2\left(\frac{\pi m_0 kT}{h^2}\right)^{3/2}$ and m_0 and m_e^* are the free and effective electron mass. In addition, by assuming that crystal contains a single set of acceptor levels of concentration N_a with activation energy E_a from the valance band edge and a set of compensating donors of density N_d, the free-hole density p is given by the relation:

$$\frac{p_0(N_d + p_0)}{(N_a - N_d - p)N_v'} = \frac{1}{\beta}\left(\frac{m_h^*}{m_0}\right)^{3/2} \exp\left[\frac{-E_a}{kT}\right] \tag{2.38}$$

where $N_v' = 4.82 \times 10^{15}\ T^{3/2}\ (cm^{-3})$, β is the degeneracy factor, k is the Boltzman constant, and m_h^* is the hole effective mass [69].

In order to determine the parameters of the acceptor levels from the experimental data, the logarithm of left hand side of eqn. (2.38) versus $1/kT$ is plotted with N_a and N_d as fitting parameters. Then by playing with fitting parameters the best curve is found which resembles to the experimentally obtained hole concentration versus temperature.

2.5 Optical Characterization

2.5.1 Photoconductivity

There are a set of basic concepts which describe many photoelectronic phenomena involving electron activity in semiconductors. These include optical absorption, electrical transport, and the capture of free carriers resulting in either to recombination or trapping. Of course, there are many external agents lead to creation free carriers in semiconductors by excitation. In the case of creation of free carriers in structure, there will be excess electrons and holes which will lead to increase in conductivity. If the excitation is carried out by light, resulting increase in conductivity is called *photoconductivity* [1].

When the surface of a semiconductor is exposed to a radiation with photons, whose energies are higher than the band gap of semiconductors, photogenerated electron – hole pairs give rise to a increase in number of free charge carriers. As the number of free charges is increased, an increase in conductivity is also observed due to the contribution of photogenerated free carriers to current. As it is shown previously, the dark conductivity is given by [72]:

$$\sigma_o = e(n_o\mu_e + p_o\,\mu_h) \quad . \tag{2.39}$$

Then, as a result of photogenerated free carriers, the dark conductivity is increased by:

$$\Delta\sigma = e\,(\Delta n\mu_e + \Delta p\,\mu_h) \quad . \tag{2.40}$$

where Δn and Δp are density of photogenerated electrons and holes, respectively.

The number of free electrons is equal to number of free holes in intrinsic semiconductors due to the fact that upon excitation with light, in an intrinsic semiconductor the electron and holes are created in pairs. Hence, $\Delta n = \Delta p$ in an intrinsic semiconductor. For this reason, the eqn. (2.40) is reduced to:

$$\Delta\sigma = e\Delta n\,(\mu_e + \mu_h) \tag{2.41}$$

There are some parameters which affect the photoconductivity substantionally. One of these parameter is the *photogeneration rate G*. This parameter is defined as the number of carriers collected at the electrodes for each absorbed photon [3].

For one carrier type of transport, the conductivity in dark and in light can be reduced to:

$$\sigma_o = e n_o \mu_o \tag{2.42}$$

and

$$\sigma_o + \Delta\sigma = (n_o + \Delta n) e(\mu_o + \Delta\mu) \quad , \tag{2.43}$$

respectively. Where Δn and $\Delta\mu$ are change in carrier and mobility, respectively. Then, the change in conductivity can be written as [72]:

$$\Delta\sigma = e\, \Delta n\, \mu_o \; + (n_o + \Delta n) e \Delta\mu \tag{2.44}$$

In general, the change in carrier density is expressed as:

$$\Delta n = G\, \tau_n \tag{2.45}$$

where G is the photoexcitation rate ($m^{-3}\ s^{-1}$) and τ_n is the electron lifetime. So, the change in conductivity is written as:

$$\Delta\sigma = e\, \Delta\mu\, n \; + \; eG\, \tau_n\, \mu_o \tag{2.46}$$

Measuring photoexcitation rate, knowing the absorption constant and incident photon flux and the photoconductivity allow the calculation of the electron lifetime [72].

Since the life time can be a function of excitation, it can give rise to a complexity. Therefore, there are three parameter which shows themselves in eqn. (2.46). These are:

1. Increase in carrier density with constant lifetime τ_n, and the contribution is:

$$\Delta\sigma = G\, \tau_n\, e\, \mu_o \tag{2.47}$$

As, it is seen, the photoconductivity is proportional to G and slope of $\Delta\sigma$ versus G is 1.

2. Increasing in carrier density with lifetime τ_n a function of G , so that

$$\Delta\sigma = G\,\tau_n(G)\,e\,\mu_o \qquad (2.48)$$

In addition,

- If τ_n changes as $G^{\gamma-1}$, then $\Delta\sigma$ varies as G^{γ}.
- If $\gamma<1$, the lifetime is decreasing with increasing excitation rate and the behavior is said to be *sublinear*.
- If $\gamma>1$, the lifetime increases with increasing excitation rate and the behavior is said to be *supralinear* .

3. Increase in mobility, so that

$$\Delta\sigma = n\,e\,\Delta\mu \qquad (2.43)$$

There are some possible mechanisms which bring about to observe such behaviors:

- Due to an increase in ionized impurities or a change in cross section of them, scattering by charged impurities may change under photoexcitation.
- An increase in mobility may be due to that photoexcitation is reducing the barrier height of potentials in polycrystalline material with intergrains.
- Excitation of a carrier from a band characterized by one mobility to a band characterized by a different mobility is also possible by photoexcitation.

The value of γ can be found from the measurement of the photoconductivity as a function of photoexcitation intensity which can give background information that can be used in testing a model of the process [72].

1.5.2 Absorption

The absorption measurement is an important technique for determination of band gap of a material. It is based on interaction of the selected photons with the material that gives rise to absorption or transmission according to the energy of photons. If the energy of photons is greater than band gap, it excites an electron from the valance band to conduction band. On the contrary, photons with energy less

than band gap, $h\nu < E_g$, is not absorbed. The optical absorption is described by an absorption coefficient α (cm^{-1}), which can be derived from the transmission measurement [1].

A number of different phenomena may be associated with the incidence of light on a material. In semiconductors the optical process which contribute the total absorption coefficient α (cm^{-1}) [2]: (i) fundamental absorption process, (ii) exciton absorption, (iii) absorption due to dopants and imperfections, (iv) absorption due to intraband transitions, and (v) free carrier absorption. The absorption for excitons occurs when the photon's energy is slightly smaller than the energy gap. Also, in these energies it is possible to see the transitions between impurity and band states. The absorption by free carriers occurs within one of the bands by transition from low to high state.

During the fundamental absorption process, exciting an electron from valance band to conduction band requires preservation of energy and momentum. Basically, there are two types of optical transition, direct and indirect which are shown in Fig. 2.3a and 2.3b, respectively.

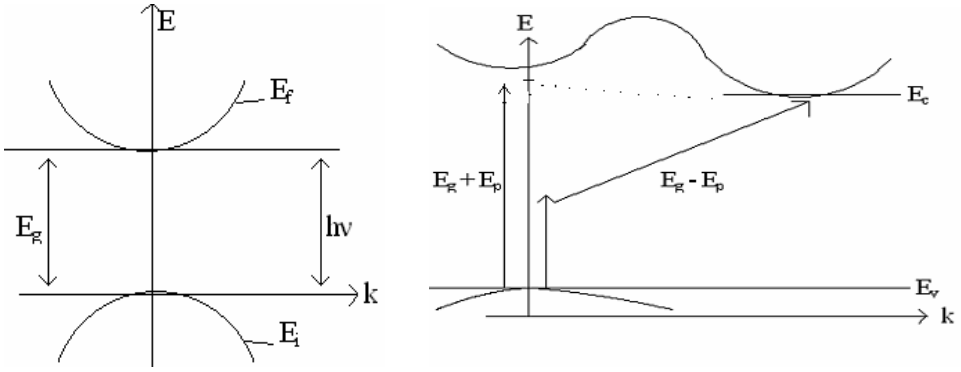

(a) (b)

Figure 2.3: Schematic diagram of (a) the absorption transitions between direct and (b) in indirect parabolic bands [2]

The absorption coefficient can be derived from the absorption transitions between direct parabolic bands as shown in Fig 2.3a:

$$\alpha(h\nu) = A\sum p_{if} n_i n_f \tag{2.44}$$

where p_{if}, n_i, and n_f are the transition probability, density of the electrons in the initial and empty energy levels in the final state, respectively [2, 73]. The energy of a state is given by

$$E = \frac{\hbar^2 k^2}{2m} \quad . \tag{2.45}$$

and the energy of a electron relative to conduction band is

$$E_e = \frac{\hbar^2 k^2}{2m_e^*} \quad . \tag{2.46}$$

Similarly, the hole energy relative to valance band is

$$E_h = \frac{\hbar^2 k^2}{2m_h^*} \quad . \tag{2.47}$$

By using eqns. (2.46) and (2.47) for the direct band gap transitions, the transition energy is expressed as

$$h\nu - E_g = \frac{\hbar^2 k^2}{2m_e^*} + \frac{\hbar^2 k^2}{2m_h^*} = \frac{\hbar^2 k}{2m_r^*} \quad . \tag{2.48}$$

where $m_r^* = \frac{m_e^* m_h^*}{m_e^* + m_h^*}$ is the reduced effective mass. Since the density of states for our case can be written as

$$N(h\nu)d(h\nu) = \left(2\pi^2\hbar^3\right)^{-1}\left(2m_r^*\right)^{3/2}\left(h\nu - E_g\right)^{1/2} d(h\nu) \tag{2.49}$$

then, for direct transitions between parabolic valance and conduction bands, the absorption coefficient is found as:

$$\alpha(h\nu) = A(h\nu - E_g)^{1/2} \tag{2.50}$$

where *A* is a constant.

For indirect band-gap materials as shown in Fig. 2.3b, the minimum of conduction band and maximum of valance band is not at the same wave vector. As it is mentioned before, during the transitions energy and momentum have to be conserved. For indirect band transitions these conditions are satisfied by either emission or absorption of phonons. The absorbtion coefficient for a transition involving phonon absorbtion and emission is given by

$$\alpha_a(h\nu) = \frac{A(h\nu - E_g + E_p)^2}{\exp\left(\frac{e_f}{k_B T}\right) - 1} \quad , \tag{2.51}$$

and

$$\alpha_e(h\nu) = \frac{A(h\nu - E_g - E_p)^2}{1 - \exp\left(\frac{-E_p}{k_B T}\right)} \quad , \tag{2.52}$$

respectively. The term $[\exp(E_p/k_BT)-1]^{-1}$ gives the number of phonons according to Bose- Einstein statistics, and E_p stands for absorbed or emitted phonon energy .

Since both phonon emission and absorption are possible in the case of $h\nu > E_g+E_p$, the absorbtion coefficient for indirect transition is expressed as

$$\alpha(h\nu) = \alpha_a(h\nu) + \alpha_e(h\nu) \tag{2.53}$$

where α_a and α_e are stands for absorption coefficient for transition involving a phonon absorption and emission, respectively [2].

CHAPTER III

EXPERIMENTAL TECHNIQUES

3.1 Introduction

In this chapter, the details of GaSe single crystal growth procedure, electrical, optical and structural characterization measurement and analysis of experimental results are presented. In the growth of GaSe we have used the Bridgman-Stockbarger technique involving a crucible which is lowered through a furnace from the hot zone to cold zone [67]. Using the grown crystal ingots, samples were prepared as as-grown and Ge-implanted single crystals. In order to determine the effect of annealing on both as-grown and Ge-implanted samples, they are annealed at different temperatures and same characterization measurements were performed for them. For electrical characterization measurement, samples were coated with Indium by using Van der Pauw mask geometries by the thermal evaporation technique. The temperature dependent conductivity and Hall effect measurements in between 100-400 K are carried out to investigate the electrical characteristics of the samples as-grown , Ge-implanted and annealed at 500 ^{o}C following Ge implantation. Structural and compositional characterizations of the samples were determined by X-Ray diffraction (XRD) and scanning electron microscopy (SEM) equiped with energy dispersive x-ray analysis (EDXA). In order to reveal the optical characteristic of the material, the temperature dependent photoconductivity measurements under different illumination intensities in the temperature range of 100-400 K and absorption in wavelength range of 450-1000 nm were performed.

3.2 Crystal Growth Process

In this section the crystal growth procedure will be presented step by step, starting from cleaning stage to the growth of crystal ingots.

3.2.1 Preparation of Crucible

As it is mentioned before, Bridgman technique involves a crucible, which has a substantial influence on grown crystal's quality and other physical properties. Hence, choosing of convenient crucible for the planned growing material has a crucial role in getting the crystal at desired quality, shape and size. In order to choose a convenient crucible, there are many physical properties of material required to be considered, such as the thermal expansion coefficient and the melting point. One of the important required properties of a crucible is that it shouldn't contaminate the grown crystal reacting with the crystal melt and will not give opportunity to grow a high purity crystal and a crystal of a compound consisting of specific elements. The chosen crucible's melting point must be substantially higher than the grown crystal's which will be produced in it. Another desired property of a crucible is that it will be better to have a smaller coefficient of thermal expansion to avoid breaking.

Interface shape of the solid-melt contact region for the grown material is a very important parameter to be controlled to grow better crystals. Having smaller thermal conductivity than the grown material inside will be useful in order to have more convenient shape of the solid-liquid interface isotherm to grow crystals with higher quality. Quartz is a suitable crucible material meeting almost all the criteria to grow GaSe crystals [67].

The size and shape of a crucible also has important effects on grown crystal's quality and type. In another words, the dimension and the shape of bottom of the crucible can give rise to grow a single or a polycrystal of GaSe. In addition, it is reported that the crystal orientation depends on the bottom shape and diameter of the crucible [22]. Using several various crucibles with different bottom shape and diameters, it was observed that very good single crystal ingots of GaSe can be grown by using pointed and flat bottom ampoules with a diameter around 10 mm. We have used crucibles of 16 mm in diameter, 100 mm in length, and 1.5 mm in wall

thickness. In addition, our crucible has pointed bottom in order to facilitate the nucleation [22].

As it is mentioned before, cleaning of crucible is a very important in obtaining of high quality crystals. As we chose the quartz crucibles, the cleaning procedure was performed special to this material. We started to the cleaning procedure by removing the grease and dusts, which are possibly stacked to the surface of crucible, by brushing the crucibles with detergent and boiling water. Secondly, in order to remove metallic impurities, we kept the crucibles in a 40 % HNO_3 solution for four hours. Then, it was rinsed with distilled water in an ultrasonic bath for fifteen minute. After distillation with water, the crucible was kept in hot soapy water for 12 hours. Later, the crucible was rinsed with distilled water in ultrasonic cleaner and for an half an hour put in isopropyl alcohol. The crucible was then placed into furnace and heated up to 1050 ^{o}C under the inert argon gas environment for outgasing. After outgasing, the crucibles were cleaned with distilled water and leaved to dry [22, 66, 74].

3.2.2 Synthesis of GaSe

Having obtained clean crucibles, we have prepared the stoichiometric quantity of 4N purity Ga and Se. That is, since the compound is consisted of equal number of atoms of Gallium and Selenium, the condition must be satisfied and the quantities must be adjusted according to this proportion. Then, the prepared stoichiometric quantities of elements were loaded into the cleaned crucible carefully. In order to isolate the crucible and create a vacuum atmosphere, the crucible was connected to a vacuum pump for 2 hours under 10^{-5} torr and then sealed off. Before we put the crucible into the Bridgman system for the elements of Ga and Se to be reacted in the crucible we synthesize GaSe by placing crucible into the constant temperature furnace (Lindberg) and heating the furnace slowly up to 1050 ^{o}C and kept at this stationary temperature for four days in order to complete the reaction. In addition, during the sintering process the shaking of crucible was performed to satisfy the homogeneity.

3.2.3 Bridgman-Stockbarger System

In this study, we have used Crystalox MSD-4000 model three-zone Vertical Bridgman–Stockbarger system in our Crystal Growth Laboratory of Physics Department which is shown in Fig. 3.1 and 3.2. This three zoned-Furnace designed for the growth of crystals by Bridgman-Stockbarger method at temperatures up to 1200 ^{o}C

Figure 3.1: Bridgman-Stockbarger System in the Crystal growth laboratory of Physics Department of METU.

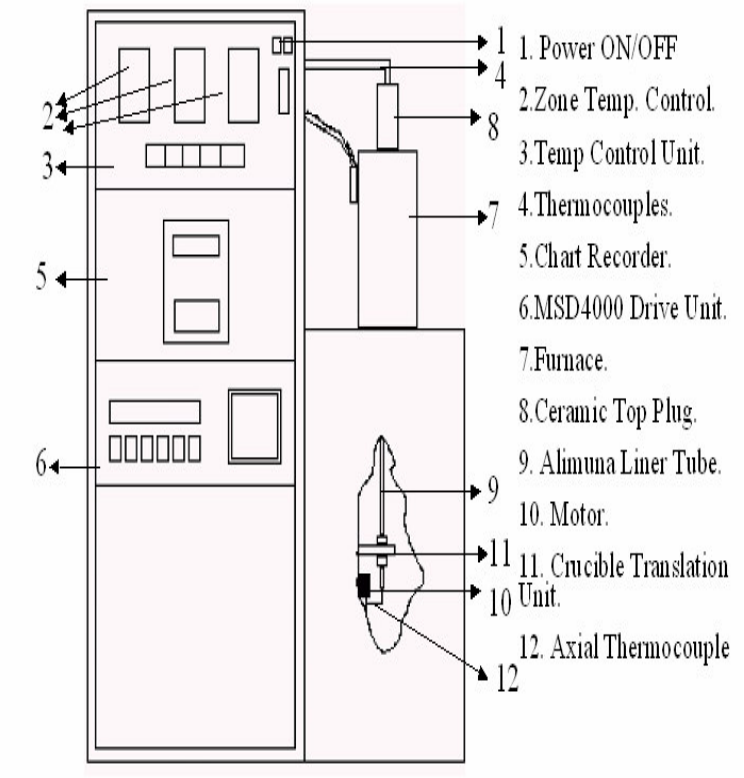

Figure 3.2 Schematic diagram of part of Bridgman-Stockbarger system

The Bridgman-Stockbarger System has four main units which can be seen in Fig. 3.2 [75]:

1. Furnace System,
2. Crucible Translation Unit (CTU),
3. Furnace Temperature Control Unit,
4. Chart Box.

3.2.3.1 Furnace System

The furnace tube has three zones which can be heated independently from each other. Fig. 3.3 shows a schematic diagram of furnace of the Bridgman-Stockbarger system with a pointed bottom crucible and the temperature profile along the furnace. Each one is 150 mm long. There are three thermocouples at the center of each zone which indicates the temperature at that point. There is also two more

thermocouples one of which indicates the temperature of the tip of the crucible and other one is running the alarm system during the over temperature cases in the furnace [75].

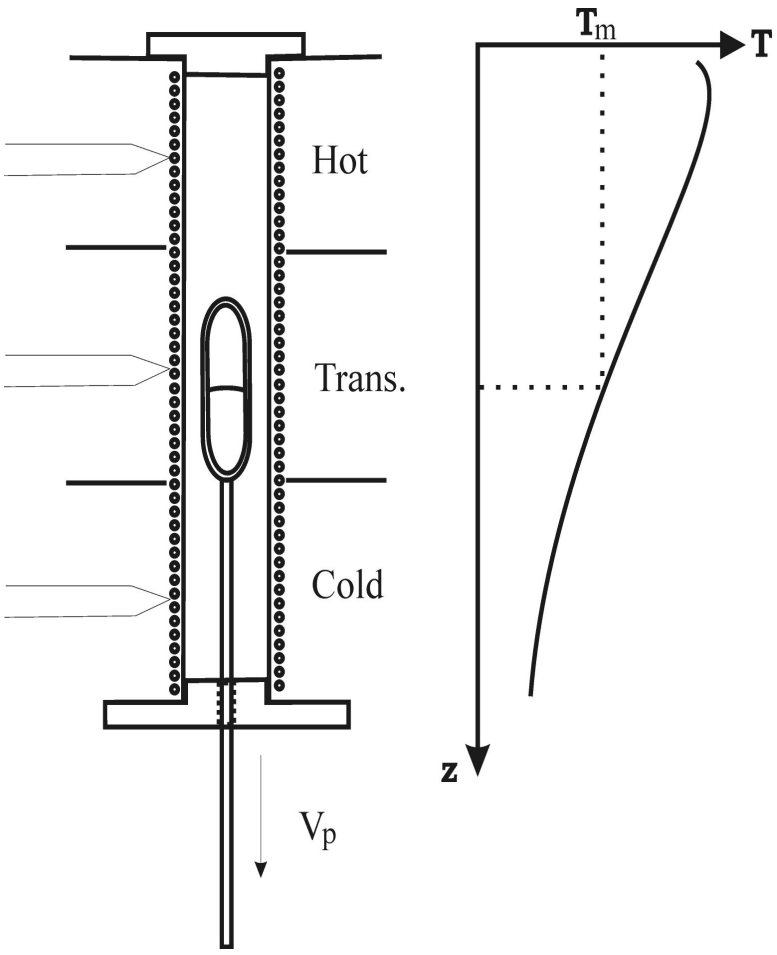

Figure 3.3 The furnace unit and the ideal temperature distribution along the axis of a cylindrical crucible.

3.2.3.2 Crucible Translation Unit

Crucible translation is carried out by means of this unit which is mounted under the worktop. In this unit there is a carriage plate which is raised and lowered by a recirculating ball-leadscerew. This leadscerew is driven by a 5-phase micro stepper motor shown in Fig. 3.2.which operates at 10000 steps/revolution and given a single step increment. This unit is driven by MSD-4000 Drive Unit [75].

3.2.3.3 Furnace Temperature Control Unit

The temperature of each zone of furnace can be heated independently by Eurotherm 902P programmable controller shown in Fig. 3.2. The controllers give full 3-term control accuracy of about 0.1 ºC. 902P operates to maintain the temperature of the relevant zone of the furnace to that of the set point [75].

3.2.3.4 Chart Box

A 4-pen chart recorder is provided in the control consul to indicate the temperature of the three control thermocouple on channel 4 as shown in Fig. 3.4. Each display can be ranged from 0 – 1200 ºC on the chart recorder [75].

3.2.4 Growth Process in Bridgman - Stockbarger System

Having prepared and synthesized the growth crucible, it was ready for the Bridgman's system stage. So, the ampoule was placed into the upper part of the Bridgman furnace, which was 105 mm above the bottom of the translation way in the system. A suitable temperature profile must be used to grow crystals by using this technique. In genaral, each material is produced under different temperature profiles. In our study, the settings of each zone were 1030, 920, and 750 º C for top zone, middle zone and bottom zone, respectively, and we have succesfully grown single crystal of GaSe using this profile before [74] (Fig. 3.4). The translation of crucible was 1.0 mm/h. By making use of the slope of distance dependent temperature graph along the furnace axis, temperature gradient was found to be 10 º C /cm. After about 105 hours of translation from cold zone to hot zone, we were sure that whole length of the crystal has moved below its melting point and solidified. The translation was

stopped and the temperature of tip of the crucible was read as 850º C. Then, we have gradually lowered the tempearture for the system to reach the room temperature. After cooling process, the ampoule was taken from the furnace and broken carefully in order to take off the grown crystal ingot.

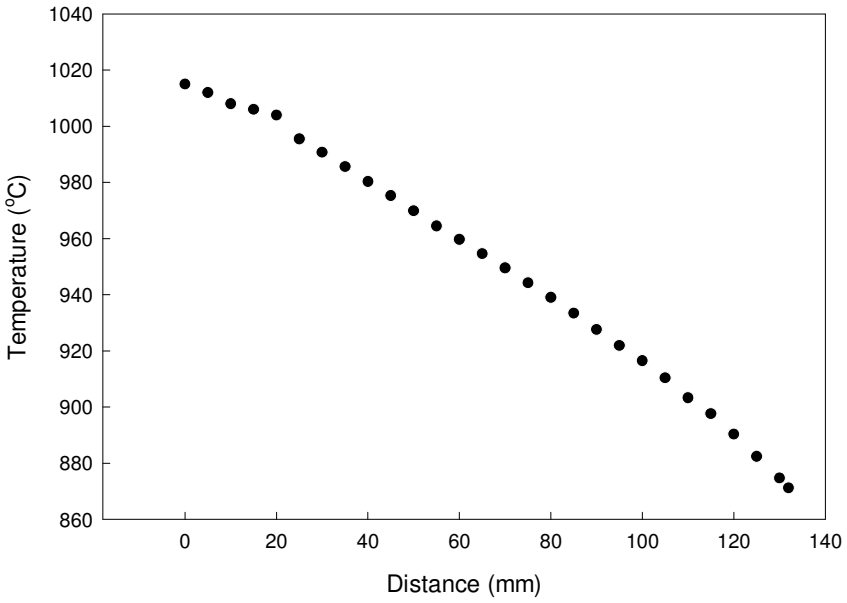

Figure 3.4:Temperature profile for growth of GaSe by using Bridgman-Stockbarger furnace

3.2.5 Sample Preparation For Measurements

After getting the grown crystal ingots from ampoules as, the surface morphology and stoichiometry were investigated with a JSM 6400 scanning electron microscope equipped with EDAX in the Department of Metallurgical and Materials Engineering in METU. As a result of this examination, it was observed that the grown ingot is stoichiometric. In order to carry out both electrical and structural characterization measurements, the samples were prepared by cleaving an ingot parallel to the layer which was perpendicular to the c-axis by using a razor blade.

In order to implant Ge to GaSe single crystals, we have prepared five samples. These samples were assembled on a substrate and placed into implanter. The implanter was a Varian Model 200-DF4 type, which is found in METU Physics Department. Then, the dose and energy of ion beams were adjusted to specific values in room temperature. In our study, these values were $6x10^{15}$ ions/cm^2 and 100 keV,

respectively. Having implanted samples, in order to investigate the ion distribution in target material, GaSe, a programme called the Transport of Ions in Matter (TRIM) was used. This program is based on interaction of the ions sent with target material's atoms and it gives the distribution of ions in material and plots the graph of concentration of ions versus depth in material.

The estimated distribution of ions versus depth showed a Gaussian shape with a projected range, (R_p), about 0.2 μm from the implanted surface. The outcome of these calculations does not exactly correspond to the experimental data. However, the salient features of the ion-solid interactions taking place in material are well presented by the result obtained from these calculations. In calculation of conductivity of material, it is important to know the distribution of ions in target material in order to investigate the depth of conducting layer from the surface of material.

As it was mentioned in previous chapter, during the implantation process there are some events taking place in target material. When an energetic ion enters a solid, it loses its energy either by elastic or nuclear collisions with the matrix of atoms and causing direct atom displacements and disorder or by inelastic or electronic process in which the electrons of solid are excited [76]. Also, it was reported that, in semiconductors, only elastic collisions usually produce lattice damage. However, in insulators both processes can give rise to atomic displacements [77]. During the implantation process, the implanted ions may not be found electrically active states and it may cause ion implantation-induced defects. It is possible to observe these changes from the plot of $Ln(\sigma)$ versus $1/T$. If one can not obtain change in the temperature dependent conduction this means that there is no change in the activation energies [78].

In order to activate ions electrically and reduce implantation – induced defects, we have carried out annealing process. By this process, it is possible to recover the damage partially and make ions electrically active to contribute to conductivity. In our study, in order to see the effect of annealing on Ge-implanted GaSe single crystals, at different temperatures this process was carried out. X-ray diffraction measurements to investigate the influence of annealing on structural recovery in implanted material were performed for the samples after annealing

process in argon gas medium at temperatures 300, 500, and 700 ° C for 20 minutes. To see the change in conductivity in implanted sample after heat treatment, an as-grown sample was annealed at 500 ° C and the result was compared with the as-implanted samples. The obtained results will be discussed in chapter 4 in details.

After implantation and annealing process, three samples were prepared. Typical sample dimensions and the thickness were 4.5 x 4.5 mm^2 and 300 μm, respectively. In order to carry out electrical measurements, an ohmic contact is necessary for attaching electrodes to the semiconductor. As mentioned before, ohmic contacts were formed by evaporation of high – purity indium through an appropriate mask on the samples. For the evaporation procedure, a piece of In was placed in molybdenum boat. Then, GaSe samples with the contact masks placed in a substrate holder. The mechanically controlled shutter was placed such that it performs a barrier between source and material which will be covered with this material for making contacts. Following evacuation of the system to 10^{-6} torr by means of rotary and diffusion pumps as shown in Fig. 3.5, the source was heated slowly by using manually controlled variac. The shutter was opened after a steady evaporation rate was achieved. Having completed the evaporation, the shutter was closed and the system was allowed to cool down to room temperature [79].

After taking out the samples from evaporation system, the copper electrodes were stacked to the contacts by painting the electrode area with silver paste.

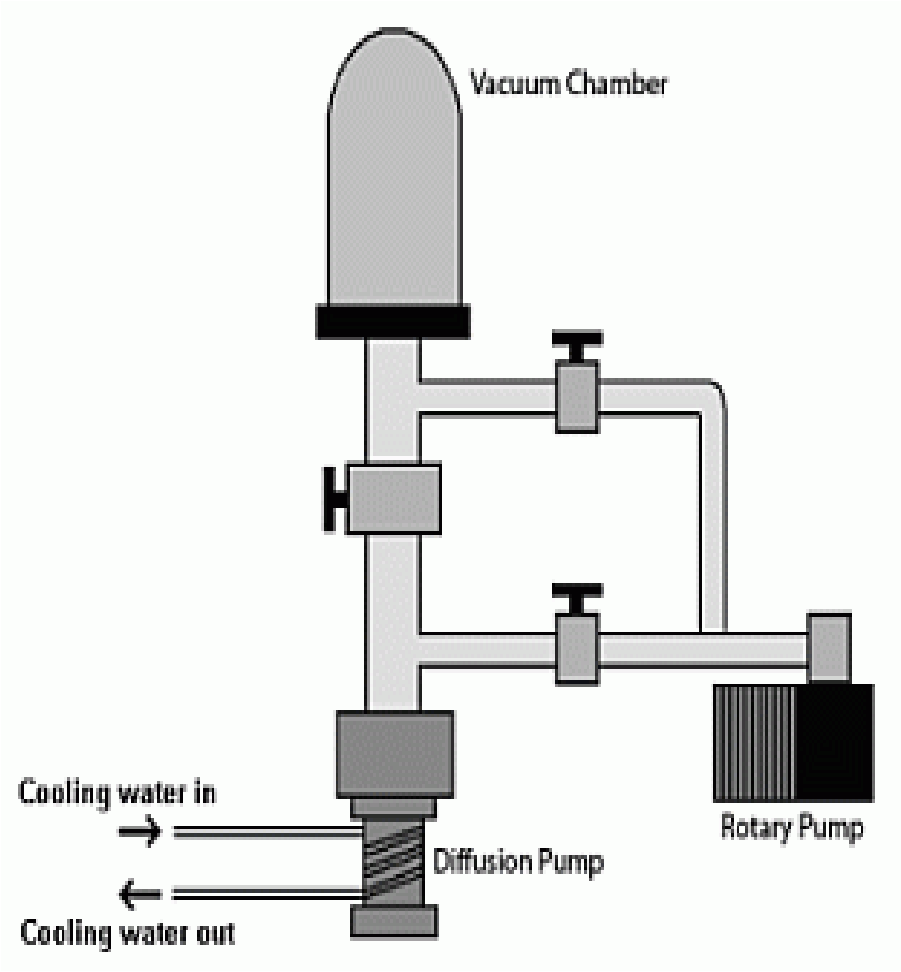

Figure 3.5: Illustration of the metallic evaporation system

3.3 Electrical Measurement

In order to carry out a reliable electrical measurement, it is essential to have ohmic contacts. That's why, firstly, we have checked the ohmicity of the metal contacts to see whether the plotting of *LogI- LogV* gives unity or not. After measurement, it was observed that the I-V characteristics were ohmic and were also found to be independent of the reversal of applied bias. So, the ohmic nature of contacts was confirmed by the I-V characteristic.

In this study, the temperature dependence of the dark conductivity and hall effect measurements of GaSe single crystals have been investigated by using the conventional four-point dc Van der Pauw method. When this method is used, it is essential to measure across different pairs of contacts so as to correct for the

geometry. This can be achieved by interchanging current and voltage leads to the sample as shown schematically for a square sample in Fig. 3.6.

Conductivity measurement was carried out between 100 and 400 K under vacuum in a closed cycle cryogenics helium cryostat using Lake-Shore DRC-91C. A constant current was applied between two ends of contacts by using a Keithley 220 programmable current source which can supply currents in the range between 0.1 nA to 100 mA with a compliance voltage of up to 100 V. In order to measure the voltage drops across the contacts a Keithley 619 electrometer was used.

As shown in Fig. 3.6 (a), firstly, the constant current I is applied through the contacts 1 and 2, and the voltage drop between contacts 3 and 4 is measured (V_{34}). From the known constant value of current (I) and measured value of the voltage drop V_{34}, the resistance is calculated by $R_a = V_{34} / I$. Secondly, the current is applied through the contacts 2 and 3, and the voltage drop between contacts 4 and 1 is measured. The resistance between these contacts are calculated as $R_b = V_{41}/I$ as shown in Fig. 3.6(b). Thirdly, the current is applied between contacts 3 and 4 as shown in Fig. 3.6 (c), and the voltage drop between contacts 1 and 2 is measured. Then, the resistance for these contacts was found from $R_C = V_{12}/I$. Finally, the current is applied between 4 and 1 as shown in Fig .3.6 (d), and voltage drop between 2 and 3 is measured. Then, the resistance between contacts is found from, $R_b = V_{23}/I$.

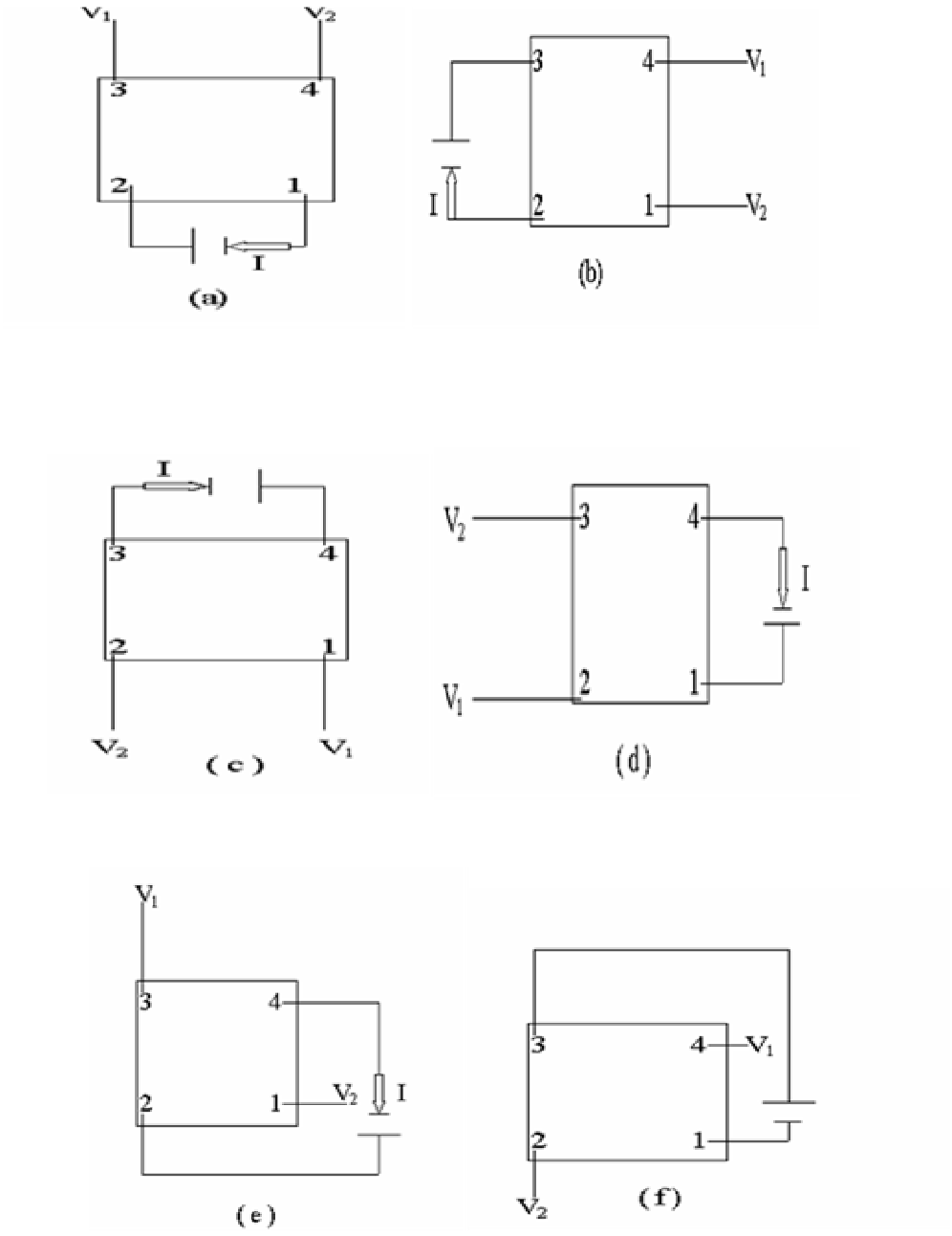

Figure 3.6: Indication of sample connections used for taking Van der Pauw transport data. Configurations (a)-(d) are employed for collecting resistivity data, while (e) and (f) are used with a magnetic field applied perpendicular to the page in order to measure the Hall voltage [80]

Having measured values of R_a, R_b, R_c and R_d , together with the thickness t of the sample , the resistivity is found from the relation,

$$\rho = (\pi t/Ln(2))(R_1 + R_2)/2(f(R_1/R_2) \quad (3.1)$$

where $R_1 = R_a + R_b$, $R_2 = R_c + R_d$, t is the thickness of the sample, and f is a correction factor or Van der Pauw function, which is a function of the potential difference measured [80]. If the contacts are symmetrically, the correction factor is taken to be $f(R_1/R_2) = 1$ [68].

In order to carry out Hall measurement, we have used Van der Pauw samples. The set-up used for Hall measurement is presented in Fig. 3.7. The sample's geometry and connection of contacts are shown in Fig. 3.6 (e) and (f). Firstly, a constant current was applied between 2 and 4 without a magnetic field, and the potential drop between 1 and 3 was measured as shown in Fig. 3.6 (e). Then, from the measured values, the resistance $R_x = (V_3 - V_1)/I$ is found. Secondly, a constant current was applied together with magnetic field B, and the potential drop was measured. Then, the resistance was found from the measured values as $R'_x = (V_3 - V_1)/I$. These measured resistance values with and without magnetic field are subtracted from each other and $\Delta R_x = (R_x - R'_x)$ is found. In the third step, again with no magnetic field, the current was supplied through the contacts 1 and 3 and the voltage drop between 2 and 4 was measured. In this case, $\Delta R_y = (R_y - R'_y)$ is found.

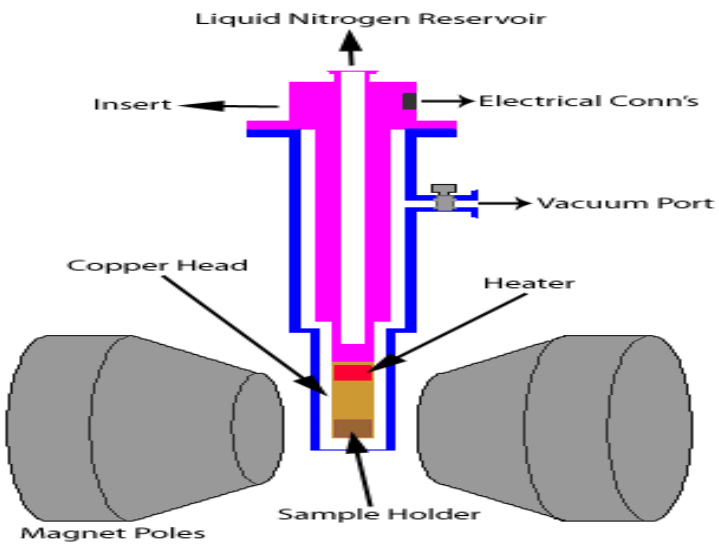

Figure 3.7: Schematic representation of the cryostat and magnet system [81].

Having obtained the changes in the two resistances; ΔR_x and ΔR_y, the Hall coefficient R_H is found from the relation given below:

$$R_H = (\Delta R_x + \Delta R_y)/2(t/B) \quad , \tag{3.2}$$

where t is the thickness, and B is magnetic field [82]. After obtaining Hall coefficient, the carrier density was determined by making use of the relation,

$$p = (r/e\ R_H) \tag{3.3}$$

assuming the Hall factor $r = 1$ [50]. Moreover, as it is mentioned in Chapter 2, from the sign of Hall coefficient, it is possible to determine the type of materials. Lastly, by combining the results of conductivity and the hall measurements, the mobility is found from the relation given below:

$$\mu = \sigma/p\ e \tag{3.4}$$

where σ, p, and e are conductivity, hole concentration, and electron charge, respectively.

3.4 Optical Characterization Measurements

3.4.1 Absorption Measurement

In order to investigate the optical properties of as-grown, Ge-implanted, and Ge-implanted and annealed at 500 ^{o}C GaSe single crystals, absorption and photoconductivity measurements have been carried out. Absorption measurement is a substantially strong tool to determine the band gap energy of the materials. Absorption coefficient is calculated by using relation,

$$\alpha = \frac{1}{d} Ln\left(\frac{I_o}{I}\right) \tag{3.5}$$

where d is the thickness , I is the intensity of transmitted light, and I_o is the incident light which was perpendicular to the crystal plane. According to the theory of interband absorption at the optical absorption edge, the absorption coefficient varies with photon energy $h\nu$ as;

$$\alpha h\nu = A(h\nu - E_g)^n \quad , \tag{3.6}$$

where A is a constant, E_g is the band gap energy, and n is the index, which takes different values according to the type of transition. For instance, it takes ½ value for direct allowed transition, while it is 2 for indirect allowed transition [83]. From the $(\alpha h\nu)^{1/2}$ versus photon energy plot, it is possible to determine the direct or indirect band gap of the material.

In order to determine the band gap of our grown GaSe single crystals, we have used the Bruker Equinox 55 model Fourier Transform Infrared (FT-IR) spectrometer with resolution of 0.5 cm^{-1}.

3.4.2 Photoconductivity Measurement

To determine how photocurrent changes under different illumination intensities and temperatures, we have carried out photoconductivity measurement. The temperature dependence photoconductivity for different intensities were performed inside the Janis Cryostat equipped with a cooling system tanks to liquid nitrogen between the temperature range of 150-480 K. As source of illumination, a 12-Watt halogen lamp was used and located at a convenient place above the sample in order to make certain illumination of the whole surface equally. The schematic diagram of measurement set-up is shown in Fig. 3.8.

To change the intensity of the halogen lamp, we have adjusted the current passing through it between 50 and 100 mA. For the determination of the illumination intensity values for the lamp at different applied currents IL Ford 1700 Radiometer has been used.

After measuring of dark current at a constant voltage difference between electrodes, the photocurrent values were recorded for 5 different applied current, which were 50, 60, 70, 80, and 90 mA. The constant voltage difference was supplied by a Hickok Model 5056 power supply. Having obtained light intensity dependence photocurrent values, the photocurrent versus inverse temperature was plotted for different light intensities. Using the plotted graph, we have determined the type of recombination process inside structure of GaSe single crystals.

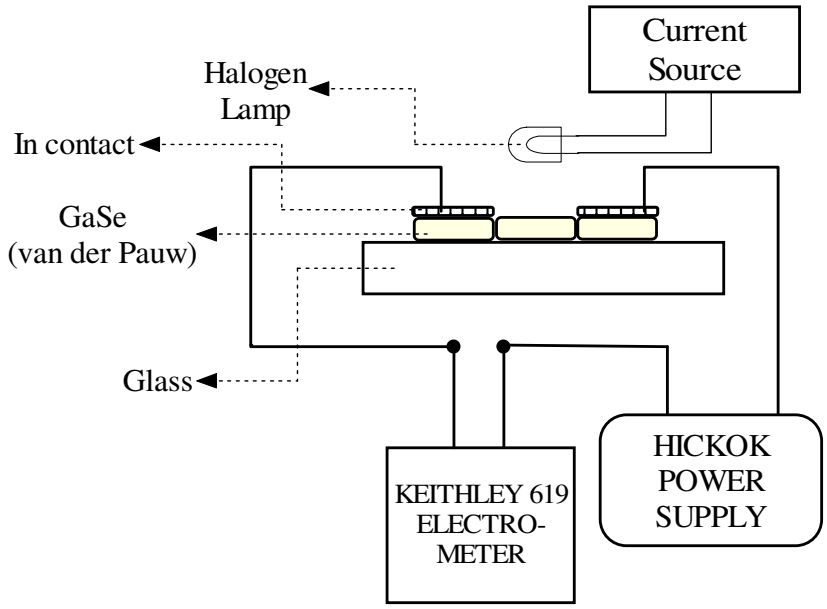

Figure 3.8: Schematic diagram of Photoconductivity measurement set-up.

CHAPTER IV

RESULTS AND DISCUSSIONS

4.1 Introduction

In this chapter, the results of electrical, structural and optical measurements of as-grown, Ge-implanted and annealed GaSe at different temperatures following implantation are presented. Firstly, the structural analysis of samples is discussed. Then, the results of temperature dependence of dark conductivity, carrier concentration and mobility, studied in the temperature range of 100-480 K, are discussed. Finally, the optical absorption measurements results are given.

4.2 Crystal Growth and Structural Characterization

As described in experimental consideration chapter, an ingot of GaSe single crystal 16 mm in diameter and 50 mm in length was obtained. Then, suitable samples for structural, electrical, and optical measurements were obtained by cleaving along plane which is perpendicular to the c-axis. The prepared samples were in dimension of 5x5x0.3 mm^3. Then, in order to determine the composition of grown single crystals, we have performed Scanning Electron Microscope (SEM) analysis. The composition of the crystal was measured by means of the energy dispersive X-ray analysis (EDXA) performed with the SEM measurements. The atomic composition of the grown crystal was approximately 48 % and 52 % for Ga and Se, respectively.

Two of the samples were used for structural analysis and each sample was annealed at different temperatures so as to see the effect of annealing on crystal structure. As- grown samples were annealed at three different temperatures which are 300, 500, and 700 ^oC for 20 minutes. After each annealing process, X-ray diffraction

measurements were carried out (XRD).

X-ray diffraction patterns were obtained by using monochromatic CuK_{α} radiation and a powder diffractometer. The XRD pattern for as-grown samples is given in Fig. 4.1.

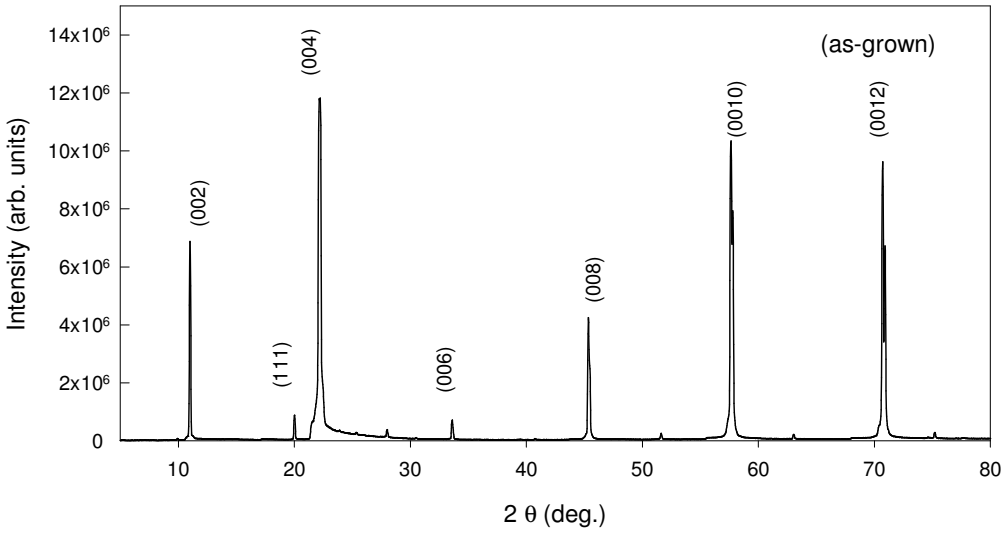

Figure 4.1: X-ray diffraction pattern for as-grown GaSe single crystal.

Then, the same sample is annealed at 300, 500, and 700 ^{o}C and XRD measurement was taken after each annealing. In order to make a comparison between as-grown samples and annealed at three different temperatures obtained XRD patterns are plotted on the same graph shown in Fig. 4.2.

As it is clear from Fig 4.2, the peak positions of the as-grown GaSe samples at different annealing temperatures are the same as as-grown GaSe single crystal sample. In order to specify the planes and interpret the change in intensity of peaks, we have given the miller indices on the peaks in all graphs. As it is illustrated in Fig. 4.2, it is clearly seen that the preferred direction is along (004) plane for as-grown and annealed GaSe samples.

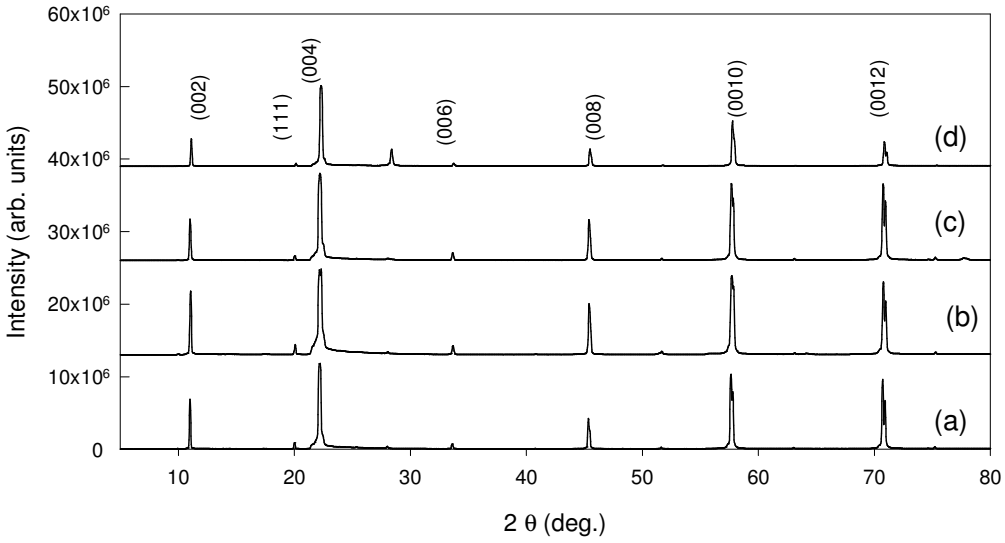

Figure 4.2 X-ray diffraction patterns of (a) as-grown, (b) annealed at 300 ^{o}C, (c) 500, and (d) 700 ^{o}C GaSe samples.

As it is shown in Fig 4.2, although there is no change in peak positions of samples annealed at different temperatures, there is an increase in intensity at specific annealing temperatures and a decrease in other annealing temperatures. At 300 and 500 ^{0}C annealing temperatures, it is observed that the peak intensities along the preferred and other directions are increasing with annealing. However, at 700 ^{0}C annealing temperature a decrease in peak intensities in almost all plane directions were observed. At specific annealing temperatures the increase in peak intensities may be due to that there is a decrease in structural disorder and an increase in crystallinity with annealing [84].

Fig. 4.3 shows the XRD patterns of as-grown and as-implanted GaSe. The peak positions of the implanted GaSe are unchanged and agree with those of the as-grown sample. However, as it is seen clearly from figure, there is a decrease in peak intensities following implantation process. As it is mentioned in experimental section, during the implantation when energetic ions enter a solid, they loses energy either by elastic – nuclear collisions and giving rise to direct atom displacements and disorder or by inelastic-electronic process in which the electrons of the solid are excited. In the first case, upon elastic collisions, it is possible to degenerate lattice. So, this possible damage created in the structure of implanted GaSe single crystal may be the reason of observed decrease in peak intensities [85].

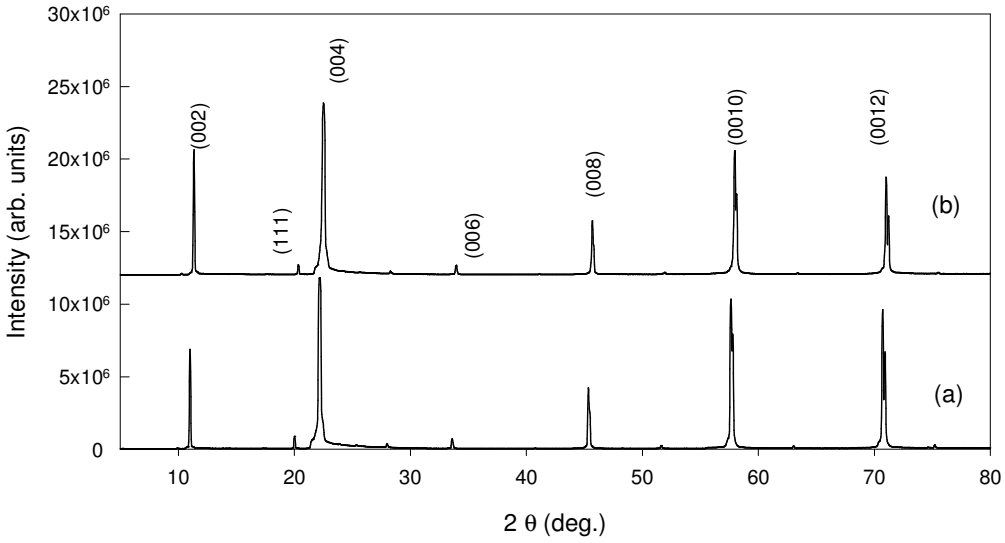

Figure 4.3: X-ray diffraction patterns of (a) as-grown and (b) Ge-implanted GaSe samples.

Fig. 4.4 illustrates the XRD patterns of the sample Ge-implanted and annealed at 500 ^{0}C. This picture indicates that after annealing process the peak intensities are increasing, which is an evidence of improvement of the crystallinity in the sample.

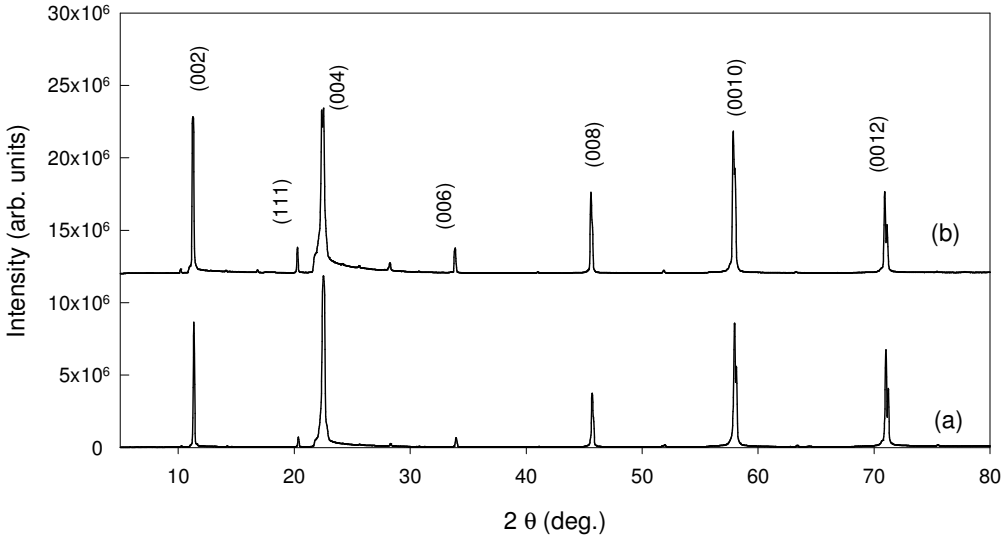

Figure 4.4: X-ray diffraction patterns of (a) Ge-implanted and (b) annealed at 500 ^{0}C GaSe sample.

4.3 Determination of Electrical Properties

4.3.1 Conductivity Measurements Analysis

In order to investigate the general behaviour of the conductivity and determine the existing current transport mechanisms, the temperature dependent conductivity measurements were performed in between 100 and 400 K for the samples as-grown, Ge- implanted, and annealed at 500 ^{0}C.

Having performed conductivity measurement, the room temperature resistivity of as-grown (A0), Ge-implanted (A1), and annealed at 500^{0}C following implantation GaSe samples were found to be 2.1 x 10^9 Ω-cm, 1.09 x 10^6 Ω-cm, and 6.46 x 10^5 Ω-cm, respectively. The obtained room temperature resistivity value of as-grown GaSe single crystal does not differ from the obtained values of the previous studies carried out on GaSe [24, 64, 65].

Fig. 4.5 illustrates the variation of the electrical conductivity of as-grown GaSe single crystal as a function of reciprocal temperature. The values are obtained by using the relation,

$$\sigma = \frac{\sigma_0}{\sqrt{T}} e^{-E_\sigma / kT} \qquad (4.1)$$

where σ_0 is the pre-exponential factor, E_σ is the conductivity activation energy in specific temperature range. As it is clear in Fig. 4.5, there is no considerable increase in conductivity up to a specific temperature, which is 250 K for as-grown sample. However, after this critical temperature, the conductivity is increasing substantially with increasing temperature. Moreover, it is clearly seen that the variation of $Ln\ \sigma$ versus T^{-1} shows three linear regions for as-grown GaSe, with different activation energies (E_σ) describing different conduction mechanisms take part in the conduction at specific temperature intervals. These regions are 100-250, 250-330, and 330-400 K, and, their activation energies are found to be 3.2, 33.5, and 314 meV, respectively.

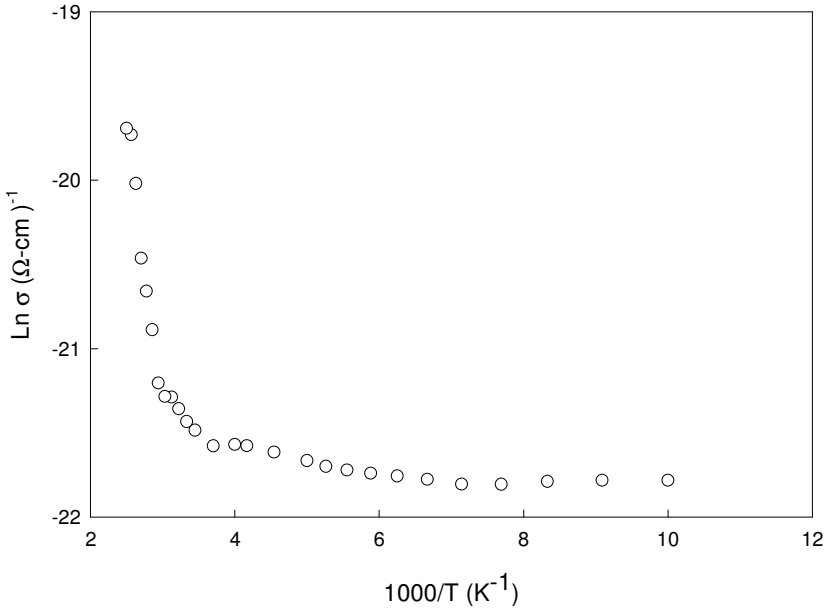

Figure 4.5: The temperature dependent electrical conductivity of as-grown GaSe single crystal.

Below 250 K, the variation of conductivity with temperature is weak which may be attributed to the hopping conduction mechanism. In fact, there are different conduction mechanisms and each of them is dominant at specific temperature intervals. Two of these mechanisms are thermoionic emission and hopping conduction. In thermionic emission mechanism, $\sigma T^{1/2}$ varies exponentially with T^{-1}, and in hopping conduction, $Ln(\sigma T^{1/2})$ varies with $T^{-1/4}$ [83, 86, 87]. So, the weak variation of the conductivity with temperature below 250 K implies that in this temperature interval the hopping conduction mechanism may be dominant mechanism.

The existence of impurities located at different energy levels above valance band can result in different activation energy values at different temperature regions and gives rise to a crystal with extrinsic nature. However, ionization of impurities requires external agents such as temperature in order to satisfy the contribution of free carriers by dopants [1]. At higher temperatures impurity atoms can ionize, and free carriers can contribute to the current and give rise to an increase in conductivity. For other two linear regions in Fig. 4.6, the different conduction mechanism was found to be responsible for increase in conductivity in different temperature intervals and with different activation energies. Upon comparing our calculated activation

energies with previously obtained results for as-grown GaSe single crystal, it was seen that there is a good agreement. As it is was reported previously, the most generally observed activation energies in p-type GaSe are 30 meV, 50-70 meV and particularly 180-210 meV. These levels are generally attributed to intrinsic acceptor centers, generated by structural defects [23, 88, 89]. Therefore, the observed activation energy in our study in interval 250-330 K, which is 33.5 meV, can be attributed to intrinsic acceptor center created by structural defects. It was also reported that a donor state at 280-310 meV below the conduction was observed in as-grown GaSe single crystals which are grown in silica ampoules without carbon coating. It was attributed to the chemical interaction between silica and GaSe, with consequent doping of GaSe with Si which is acting as a donor in GaSe [90, 91]. Therefore, using the results of these studies, we can attribute the third activation energy in interval 330-400 K to a donor level lying 313 meV below the conduction band.

Fig. 4.6 illustrates the variation of the electrical conductivity of as-grown and Ge-implanted GaSe single crystals as a function of reciprocal temperature. As it was seen in as-grown GaSe sample, a similar variation of conductivity with temperature is observed for Ge-implanted GaSe sample. After implantation with Ge, it was observed that the resistivity decreases three orders of magnitudes. At room temperature, the resistivity for Ge-implanted GaSe was found to be 1.09×10^{6} Ω-cm. In the conductivity calculations of implanted samples the thickness is estimated from TRIM (the Transport of Ions in Matter) calculations and found to be 0.2 μm. As it is shown in Fig. 4.6, between 240 and 430 K temperature interval there are two linear regions. One region is in between 240-360 K and other is in 360-430 K. By using the slope of $Ln\ \sigma$ versus T^{-1} plot in each region the activation energies were found to be 35.5 and 471.4 meV, respectively.

Also, the temperature dependent conductivity of the sample annealed at 500 ^{0}C following Ge-implantation of GaSe was performed in between 100-410 K temperature range so as to see the effect of annealing on implanted sample shown in Fig. 4.7. After annealing process, an increase in conductivity was observed. The temperature dependence of conductivity for annealed sample shows a similar behavior as as-implanted sample. However, it has linear regions at different temperature intervals with different activation energies. For the sample annealed at

500 ^{0}C following implantation, from conductivity versus inverse temperature plot two linear regions were observed in between 210-360 K and 360-410 K temperature intervals with activation energies 38.7 and 647.3 meV, respectively. Also, the room

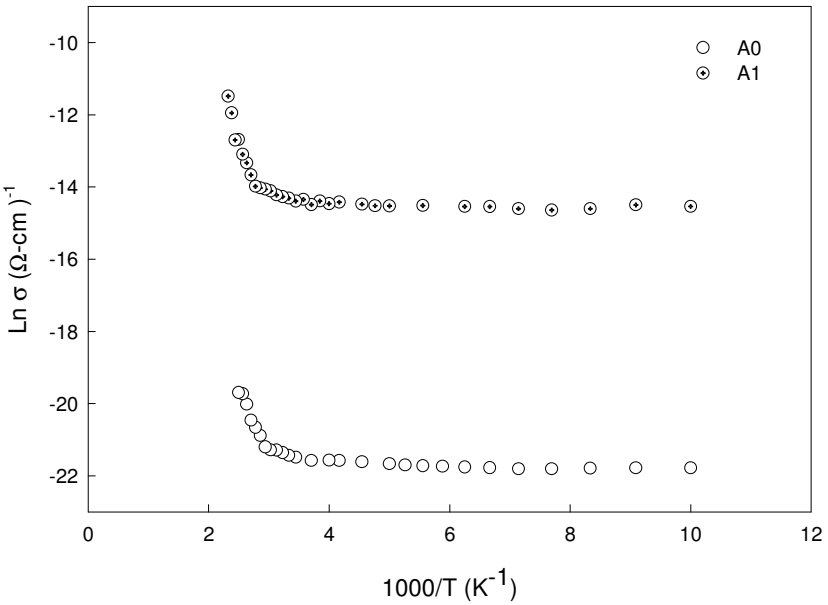

Figure 4.6 The temperature dependent electrical conductivity of as-grown (A0) and Ge-implanted GaSe (A1) single crystals.

temperature resistivity of the sample annealed at 500 ^{0}C following implantation was found to be 6.46 x 10 ^{5} Ω-cm. The rise of conductivity with Ge-implantation and annealing after implantation may be attributed to that upon implanting Ge into the structure, it modifies the structure and adding atoms by implantation process introduce additional structural defects which can result in shallow or deep levels. By thermal ionization of impurity levels, more free carriers are contribute to current and give rise to an increase in conductivity as observed here. After annealing following to the implantation, as it is shown in Fig. 4.7, one order increase in conductivity was observed.

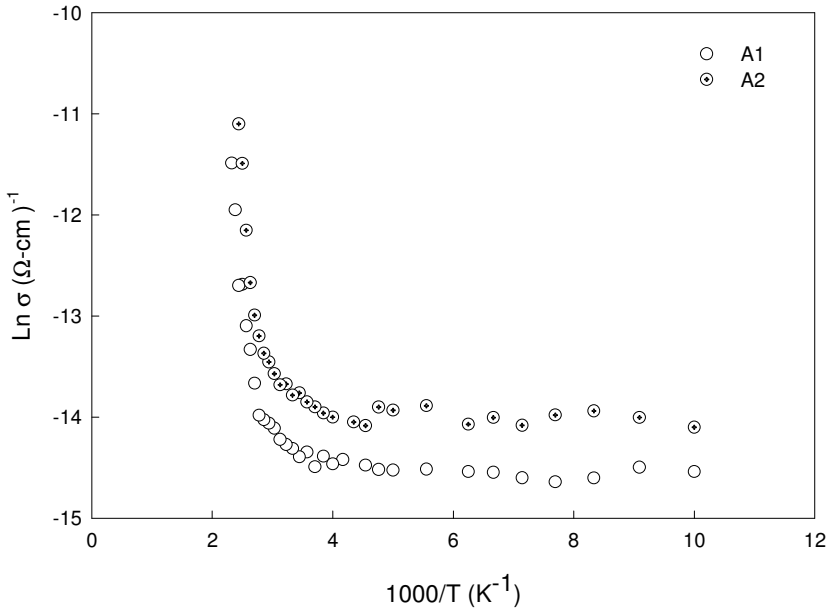

Figure 4.7: The temperature dependent electrical conductivity of Ge-implanted (A1) and annealed at 500 ^{0}C GaSe (A2) single crystals.

Although we have found the activation energies of the samples Ge-implanted and annealed after implantation, it is not easy to speculate about the nature of impurity levels. Calculation of the impurity levels in semiconductors is very complex problem in layered compounds such as GaSe, GaS, and InSe. As it is explained in theoretical consideration part, in layered crystals there is an unusual bonding nature. The weakness of interlayer forces leads to different stacking sequences of the layers, and result in stacking faults parallel to layers where impurity atoms can precipitate and form defects or defect clusters [50]. Therefore, when this structure is doped with different elements it is hard to separate the created impurity levels produced by doping atoms and by defects and defect clusters due to stacking fault which are acting as impurity levels.

In order to compare the change of conductivity with temperature for the as-grown, Ge-implanted and annealed samples at 500 ^{0}C, $Ln(\sigma)$ versus T^{-1} plot of each sample are presented on the same plot shown in Fig. 4.7

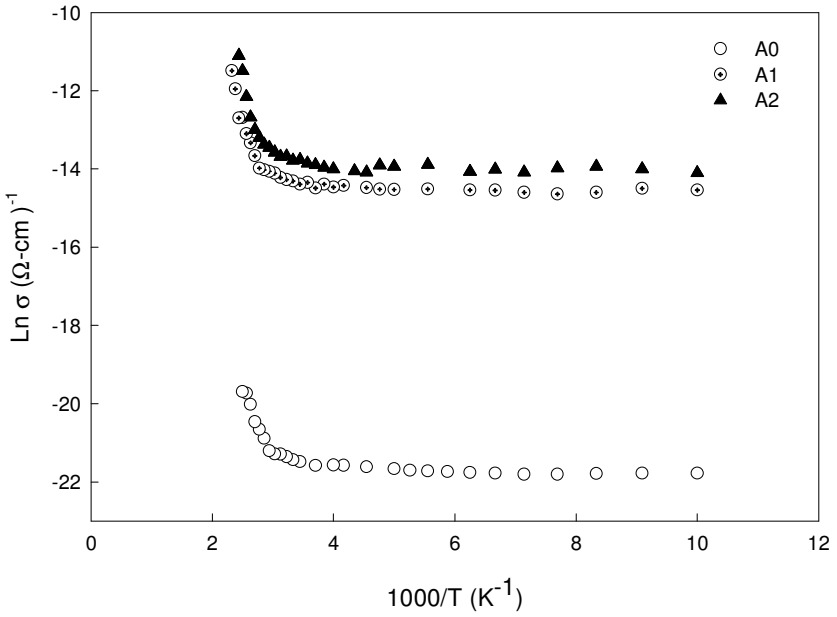

Figure 4.8: The temperature dependent electrical conductivity of as-grown (A0),Ge-implanted (A1) and annealed GaSe samples (A2) at 500 following to the Ge implantation

4.3.2 Determination of Carrier Concentration and Mobility

Temperature dependent carrier concentration and Hall mobility measurement were performed in the temperature range of 230 - 410 and 100 - 400 K for the samples as-grown and Ge-implanted and annealed, respectively. A typical behavior of hole concentration p as a function of $1000/T$ for as-grown GaSe sample is shown in Fig. 4.9.

By using SDSA model in a p-type material the hole concentration is found by eqn. (2.38). We have used the usual three-dimensional expression for the density of states of the valance band which is $N_v = 1.70x10^{15}\ T^{3/2}\ cm^{-3}$ [92]. The hole effective mass ratio of 0.5 [27] and the degeneracy factor for the acceptor level of $\beta = 2$ were taken in calculations. By using eqn. (2.38), we obtained the plot of Fig. 4.10. In order to determine the activation energies of acceptors from the experimentally obtained data, the logarithm of left hand side of eqn. (2.38) was plotted by assigning convenient N_a and N_d fitting parameters in Fig. 4.10, for as-grown GaSe sample. The plot will be resembled to experimentally obtained plot of $p - 1000/T$ only for the correct values of N_a and N_d. Having obtained plot from the slope, the activation

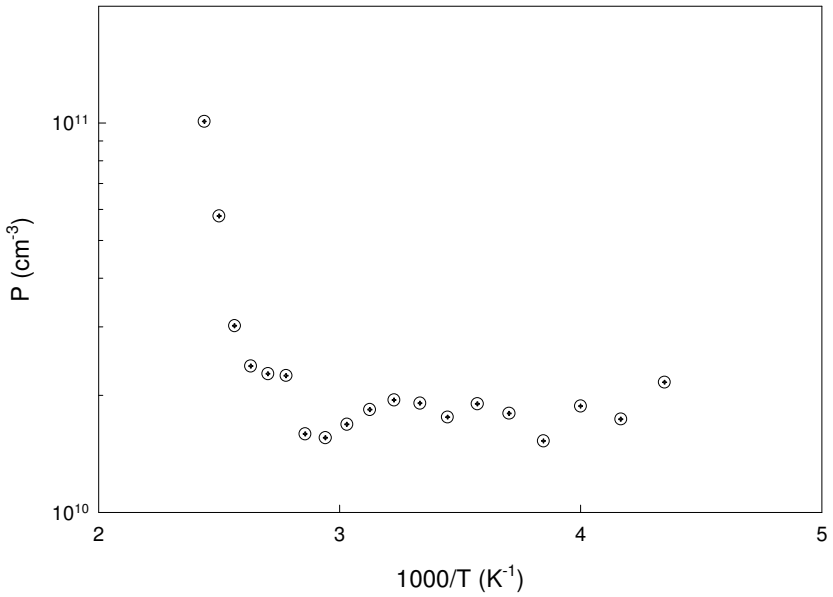

Figure 4.9: The temperature dependent hole density of as-grown GaSe sample.

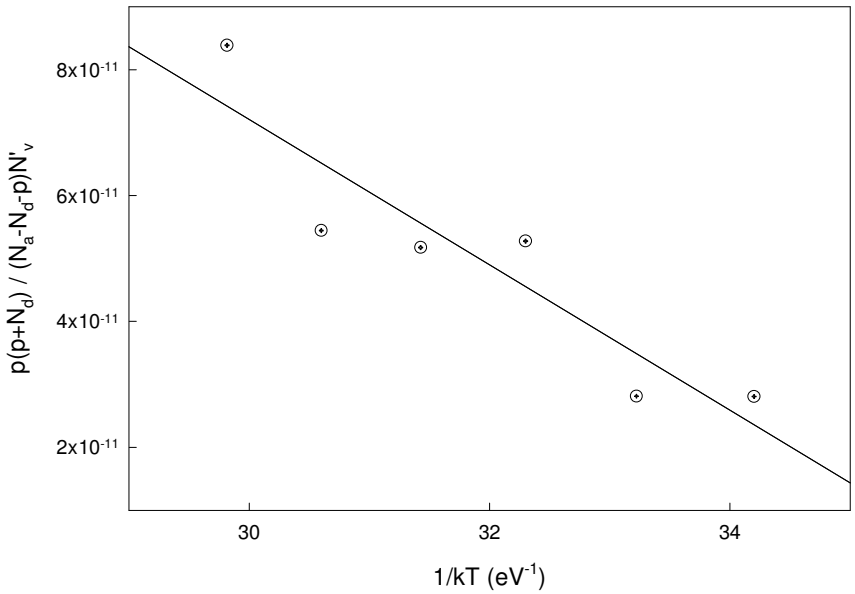

Figure 4.10: Single donor-Single acceptor (SDSA) model analysis of as-grown GaSe sample.

energy of acceptor levels (E_a) *are* determined. The intercept at $1/kT = 0$ gives $\left(m^*_h / m_o\right)^{3/2} \beta^{-1}$ [91]. As it is clearly seen from Fig. 4.9, there is no considerable change of hole concentration with increasing temperature up to a critical point, which

is 340 K. That is, below this temperature, the $p - T$ variation is so weak that almost no change is seen. After this critical value of temperature, the hole concentration is increasing exponentially with increasing temperature up to another critical temperature value, which is 390 K. That is, in between 340 – 390 K, an exponential change of hole concentration with increasing temperature is seen. After this second critical temperature value (390 K), another region starts and a strong increase in hole concentration was observed in the beginning of this region. Due to the used material for contacts, (In), we couldn't take data above a critical temperature value (410 K), which is a starting point of another region of carrier mechanism at high temperature region. It is clear from the data for all samples at 390, 400, and 410 K, a sharp increase in conductivity and hole concentration were recorded. In as-grown GaSe, for temperature range between 230-410, the change in hole concentration was just one order. That is, an increase from 2.16×10^{10} cm $^{-3}$ at 230 K to 1×10^{11} cm $^{-3}$ at 410 K was observed. The room temperature of calculated hole concentration was 1.91×10^{10} cm $^{-3}$, which was lower than the obtained result in literature [27]. This unagreement is not suprising due to intrinsic nature of GaSe crystal. In fact, it is almost impossible to control all growth parameters which have a deep influence on the grown GaSe. The physical parameters such as temperature gradient and others which come from growing in different conditions may be the reason to get such discreapencies. For as-grown GaSe, in temperature range 340-390 K an acceptor level with activation energy of 20 meV was determined from the Hall effect measurement. As it has been reported so far, there are three main groups of acceptor levels observed in crystals grown by Bridgman method, however, comparing our value of 20 meV activation energy with these groups, there seems no match, which were slightly higher than our found result [95]. This slight difference in as-grown GaSe may be due to the nature of our crystal and may stem from defects and stacking faults peculiar to the grown ingot.

In order to analyze the acceptor and donor concentrations, we have used SDSA model as stated earlier. As a consequence of calculations, 9×10^{11}, 1.45×10^{9}, and 8.99×10^{11} cm^{-3} are found for N_a, N_d, and $N_a - N_d$, respectively. By making use of SDSA analysis and using the values for fitting parameters N_a and N_d, the fitting curve was plotted in Fig. 4.10, and using the slope the activation energies were found.

The temperature dependent hole concentration of Ge- doped GaSe sample is

given in Fig. 4.11 in temperature range between 180 and 380 K.

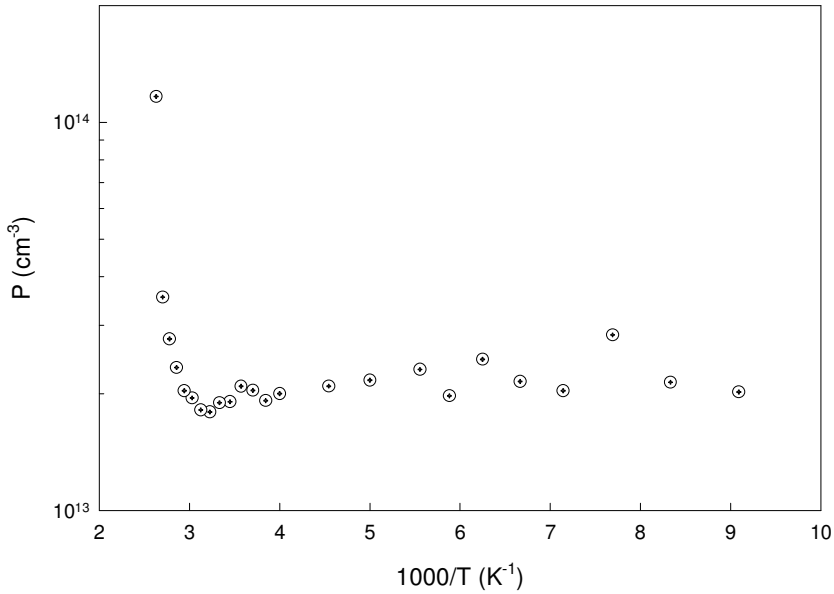

Figure 4.11: The temperature dependent hole concentration of Ge-implanted GaSe sample in the temperature interval of 180-380 K.

The change of hole concentration versus temperature shows a similar behavior as observed for as-grown GaSe. Again there are three regions which are lying between 180-280, 290-360, and 370 K and above which are not recorded due to contacts problems. First region almost remain constant, that is, the hole concentration is not changing with increasing temperature in this region. This behavior may be attributed to that finding of high concentration of shallow impurity states in band gap result in overlapping of states of neighbor atoms which are too close to each other and performing energy state bands which are merging with the edge of conduction or valance band according to the type of material and resulting in a degenerate material at this temperature region. The similar case was reported by reference [96] and they attributed to that if the hole concentration is not changing or weak with increasing temperature, it is a sign that the carrier concentration exhibits the degeneracy of carriers in the samples.

The second region in Fig. 4.11 starts from 280 and ends at 360 K. In this region, an exponential increase in hole concentration is seen with increasing

temperature. The temperature dependent hole concentration is analyzed using SDSA model for the temperature region between 280-360 K. As a result of fitting procedure shown in Fig. 4.12, the calculation of the acceptor and donor concentration were carried out and found to be 8.6×10^{14}, 2.8×10^{12}, and 8.57×10^{14} cm^{-3} for N_a, N_d, and $N_a - N_d$, respectively. The activation energy at this region was calculated to be 29 meV from the slope of fitted curve.

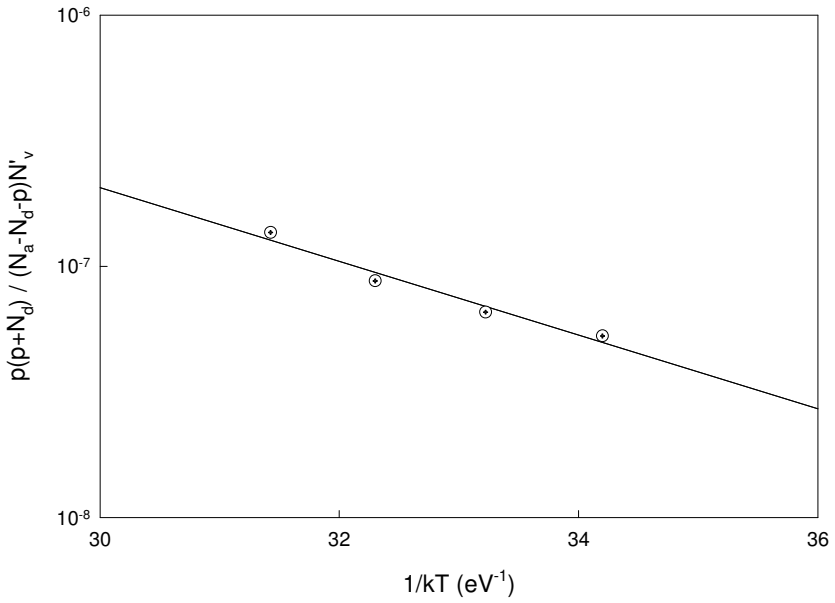

Figure 4.12: Single donor-Single acceptor (SDSA) model analysis of Ge-implanted GaSe sample.

It was clear from a few data points in the high temperature region that there is enormous increase in both conductivity and hole concentration at the start of this region. When the calculated hole concentration is compared with as-grown GaSe, we see that there is three order increase which may stem from the Ge-implantation and its effect on modifying the structure of material by creating defects or other imperfections which give rise to acting as donor or acceptor levels and contributing free carriers to conduction band by thermo ionic emission in the high temperature intervals.

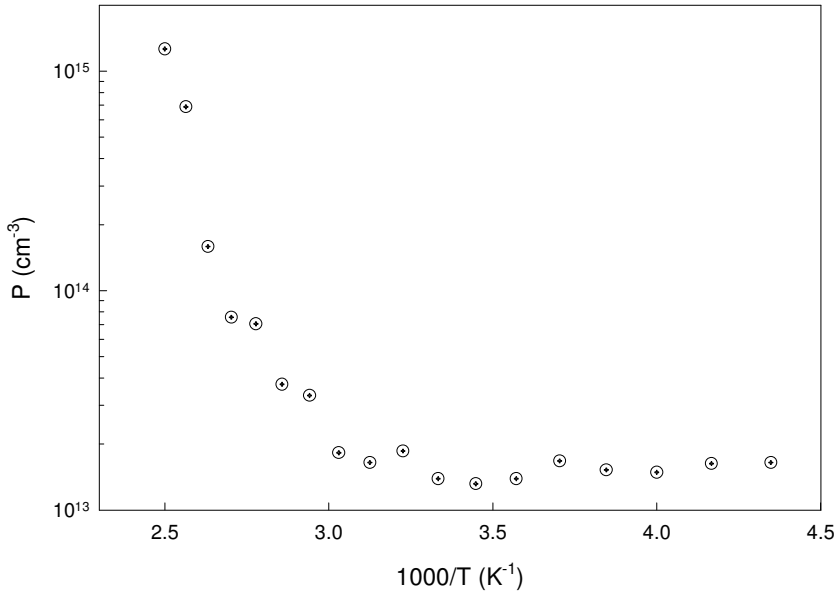

Figure 4.13: The temperature dependent hole density of Ge-implanted and annealed at 500 ^{0}C GaSe sample in the temperature interval of 140-400 K.

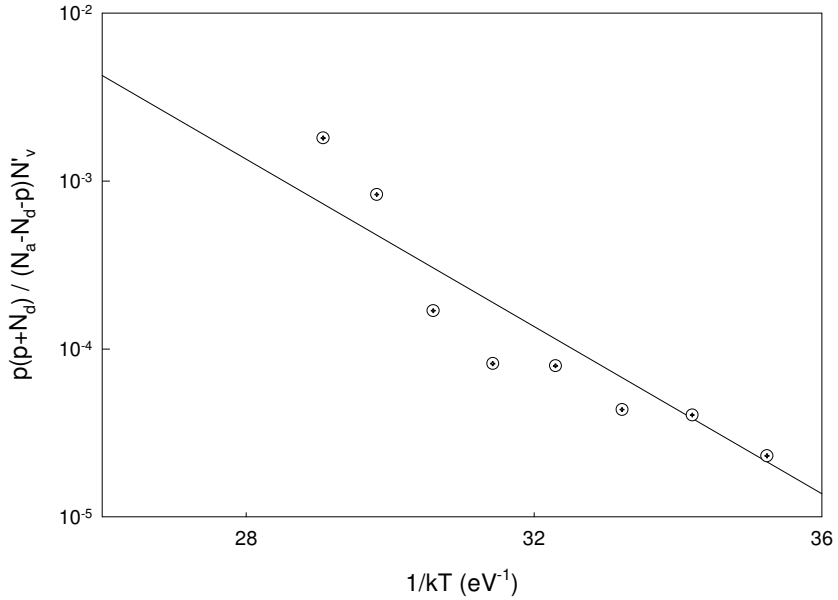

Figure 4.14: Single donor-Single acceptor (SDSA) model analysis of Ge-implanted and annealed at 500 ^{0}C GaSe sample in the temperature range of 310-400 K.

Fig. 4.13 and 4.14 show temperature dependence of hole concentration and fitting curve of Ge-implanted and annealed at 500 ^{0}C GaSe single crystal. As it is seen clearly from the figure, this sample also shows similar behavior as as-grown and

Ge-implanted GaSe crystals except the change one order increase of hole concentration, which is calculated to be 1.38×10^{13} cm^{-3} at 140 K and 1.26×10^{15} cm^{-3} at 400 K. Comparing with as-grown GaSe, the hole concentration of the samples Ge-implanted and annealing following implantation show an increase of about four orders. The hole concentration change with increasing temperature in the temperature range of 100-310 K is very weak as observed in other samples, and, it is seen an exponential increase in hole concentration in the temperature range of 310-400 K. Upon using SDSA model for this region, the fitting curve as shown in Fig. 4.14 give activation energy E_a = 214.8 meV and with $N_a = 5 \times 10^{16}$, $N_d = 3.12 \times 10^{15}$, and $N_a - N_d = 3.9 \times 10^{15}$ cm^{-3} were found. When hole concentration of this sample compared with Ge-implanted GaSe, one order increase is seen which maybe attributed to more electrically activated Ge atoms with annealing.

As it is observed in Gd-doped GaSe [62], the implanted Ge atoms in p-type GaSe may not be electrically active but be responsible for cleaning the impurities between the layers and creating new acceptor or donor states or inactive complexes which may have a deep influence on both free carrier concentration, Hall mobility and activation energies observed in our study.

When the results of conductivity and Hall measurement are combined, it is seen that the new activation energies which are not observed in undoped GaSe single crystals are appeared for Ge-implanted and annealed samples. Although we know these levels are seen upon implanting with Germanium atoms, it is not so clear and we can not be sure to say that these levels are stemming from the electrically activated implanted Ge atoms. These levels may also be created by Ge related defects and other possible defect complex, as it is reported for Cd-doped p-GaSe single crystals [55].

The temperature dependent Hall mobility data were evaluated through the $\mu_H = \sigma R_H$ relation (where σ and R_H are electrical conductivity and Hall coefficient, respectively) and are given in Fig. 4.16 for as-grown GaSe sample.

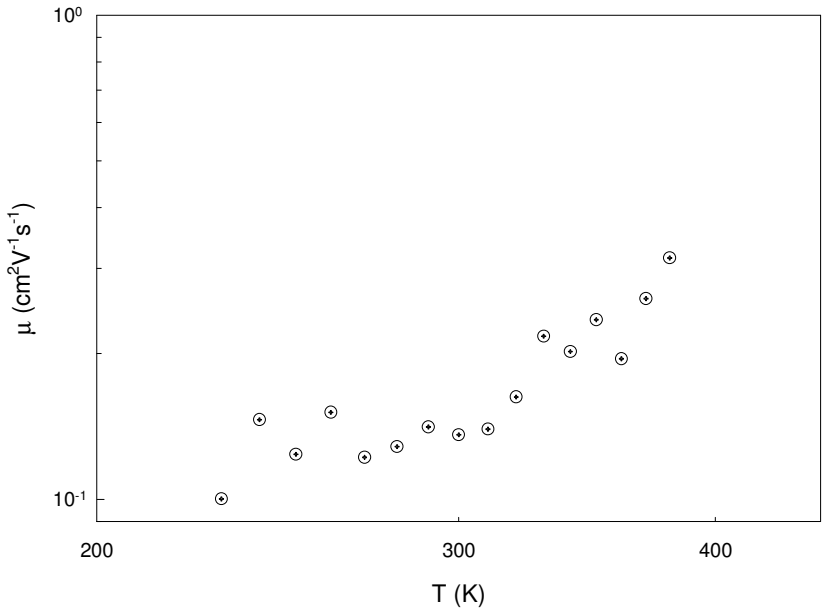

Figure 4.15: Temperature dependent mobility of as-grown GaSe sample.

The room temperature mobility of the as-grown GaSe is calculated to be 0.14 cm^2/V.s which is lower than previously obtained results [20]. For as-grown GaSe, as it is indicated in Fig. 4.15, there is a steady increase in mobility in measured temperature region of 230-400 K. From the plot of *Ln* μ_H versus *Ln T* as illustrated in Fig. 4.16, the slope of straight line was evaluated. This slop gives the temperature exponent (*n*) of the $\mu_H \alpha T^{\pm n}$. The *n* value evaluated from the slope of straight line was found to be $n = 2.37$. A typical Hall mobility curve versus temperature for holes in GaSe was reported by C. Manfredotti *et al* [94]. In this study the temperature dependence of hole mobility between 80-500 K was plotted. They observed from plot that in this temperature interval there is a continuous decrease in mobility with increasing temperature. As it is seen from Fig. 4.15, we also found similar behavior of mobility, however, in reverse direction, that is, in between 230 and 400 K temperature interval there is permanent increase with increasing temperature.

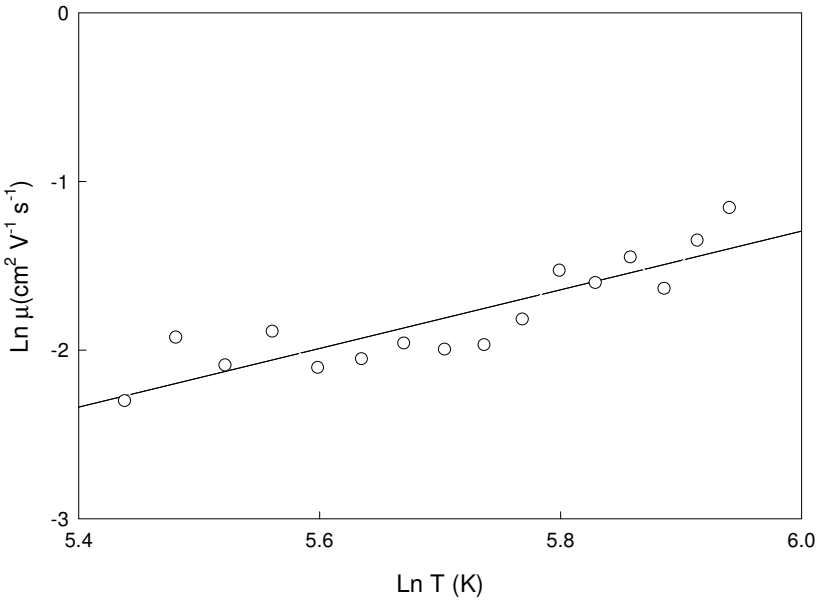

Figure 4.16: Determination of temperature dependent mobility of as-grown GaSe sample.

As it is stated by C. De Blasi [97] for InSe crystals, at low temperature the mobility is increasing with temperature according to the law $\mu \alpha T^n$. The change of mobility with temperature according to this rule is a characteristic of scattering mechanism of charge carriers with ionized impurities which are believed to be found in structure of crystals. In our case, this region extends to high temperatures which may be due to that our p-type GaSe contains high degree of impurity concentration probably contamined during the growing process from medium or crucible which the growth process took place. In another words, for impurities or defects found in structure, there are different temperature values for ionization. Temperature dependent Hall mobility of Ge-implanted GaSe in between 110-400 K is illustrated in Fig. 4.17.

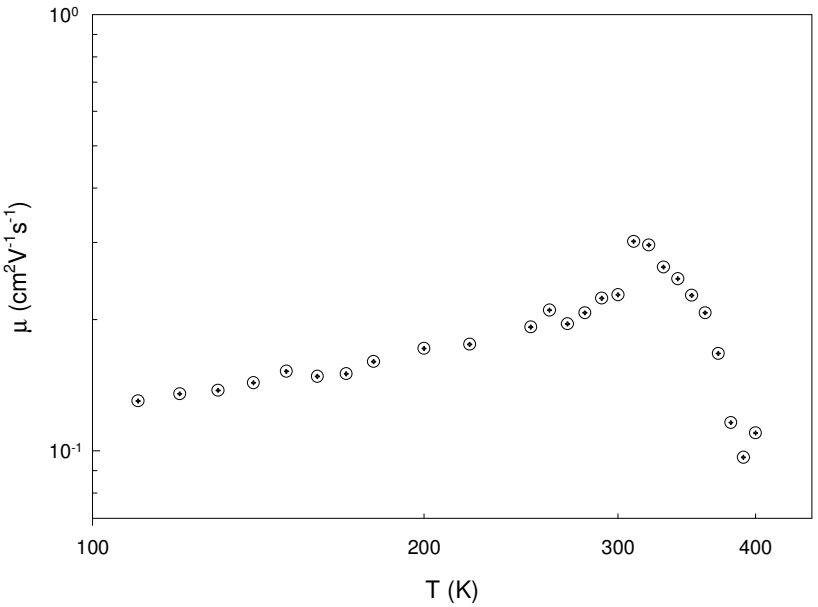

Figure 4.17: Temperature dependent mobility of Ge-implanted GaSe sample.

As it is clearly seen from figure, the Hall mobility increases with increasing temperature in the temperature range 110-310 K and decreases in temperature range of 320-400 K. We have plotted the logarithm of μ_H versus the logarithm of T as shown in Fig. 4.18. This plot result in straight lines in the low and high temperature regions and the slopes give the temperature exponents $n = 0.54$ of the $\mu_H \alpha T^n$ and $n = 5.3$ of the $\mu_H \alpha T^{-n}$ rule, respectively. The temperature dependence of the Hall mobility in the high temperature region which follows the relation $\mu_H \alpha T^{-n}$, with $n = 5.3$ is indication of the domination of the thermal lattice scattering in this temperature region. On the other hand, in low temperature region, the mobility follows $\mu_H \alpha T^n$ with $n = 0.54$, which is indicating that the ionized impurity scattering is dominant in low temperature region [97].

In addition, the calculated mobility of Ge-implanted GaSe at room temperature was found to be 0.23 $cm^2/V.s$ which is greater than obtained for as-grown GaSe sample. This slight increase according to as-grown GaSe is possibly due to the Ge-induced modification in structure after implantation process.

Fig. 4.19 shows temperature dependence of hole mobility of Ge-implanted and annealed at 500 ^{0}C GaSe in the temperature range of 140-400 K:

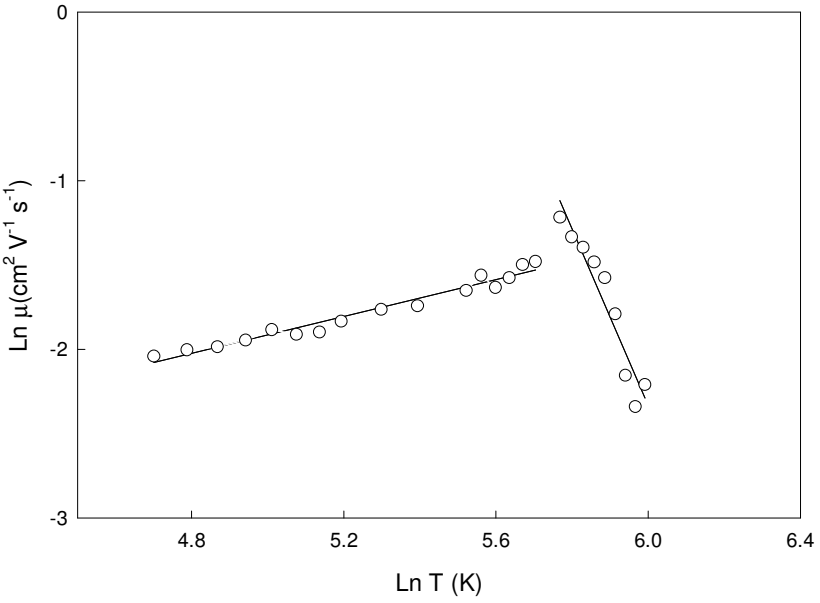

Figure 4.18: Determination of temperature dependent mobility of Ge-implanted GaSe sample.

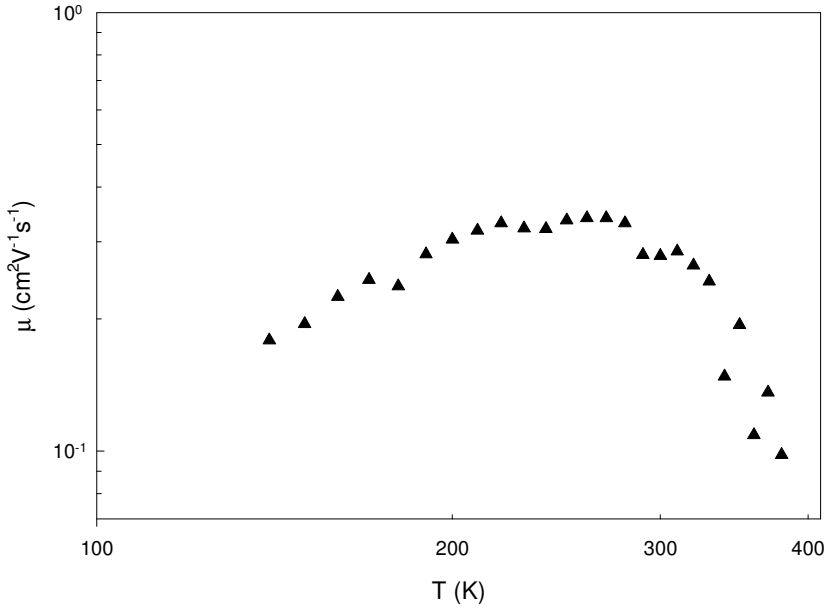

Figure 4.19: Temperature dependent mobility of Ge-implanted and annealed GaSe sample at 500 ^{0}C.

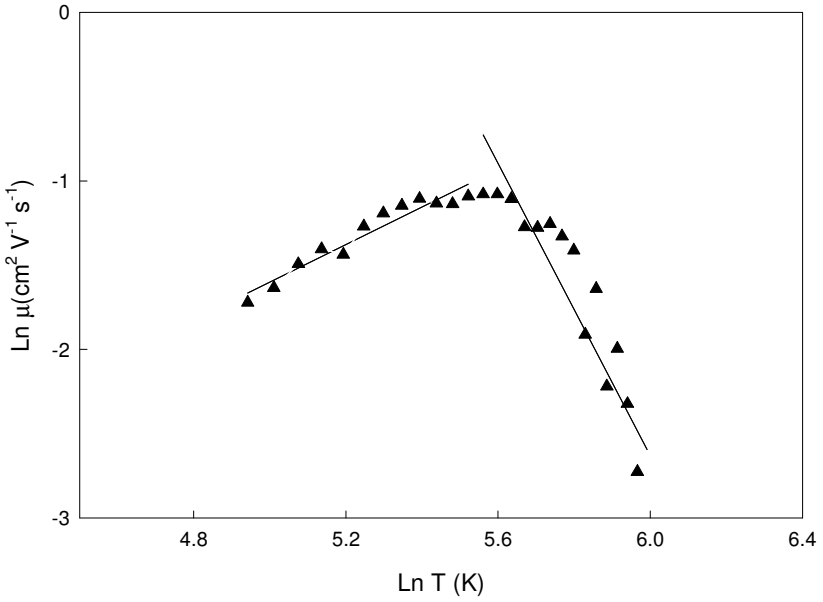

Figure 4.20: Determination of temperature dependent mobility of Ge-implanted and annealed GaSe sample at 500 ^{0}C.

Observing Fig. 4.19 we can say that Hall mobility increases with increasing temperature in the temperature range of 140-250 K and decreases in 260-400 K regions. In order to reveal the temperature dependent change of mobility, the logarithm of μ_H against the *Ln T* for this sample is also plotted in Fig. 4.20. From the slope of plot it was determined that the temperature dependence of Hall mobility follows the relation $\mu_H \ \alpha \ T^{1.11}$ and $\mu_H \ \alpha \ T^{-4.33}$ for 140-250 and 260-400 K temperature regions, respectively. The behavior obtained for low temperature region is attributed to the ionized impurity scattering. For high temperature region, this behavior is interpreted as to be indication of thermal lattice scattering. In addition, the calculated Hall mobility for this sample is found to be 0.28 cm^2/V. s which is higher than both as-grown and Ge-implanted samples. This change may be due to annealing the sample following implantation process, some impurities might enter the structure as interstials acting as defect centers which reduce the charge carrier's life time or cross section related parameters could be possibly swept out. As it is mentioned previously, after Ge-ion implantation, the decrease in intensity of diffraction peaks is observed when compared with as-grown GaSe samples. This was attributed to modifications often encountered after ion implantation which are seen as

origin of the creation of defaults and disorders in the bulk. Then after annealing following the implantation, an increase in peak intensities was observed and attributed to the recovery of crystallinity. Therefore, when we think the results of Hall and conductivity measurements, the idea mentioned for the reason of increase in mobility with annealing following to the Ge implantation seems reasonable explanation of the observed results.

4.4 Photoconductivity Analysis

The photoconductivity measurements of as-grown and Ge-implanted and annealed at 500 ^{0}C GaSe samples were performed as a function of illumination intensity in the temperature range of 150-480 K and 300-480 K, respectively. The measurements were carried out at different light intensities (Φ), which are 20, 35, 55, 80, and 115 mW/cm^2. The electric field was fixed at 20 V/cm. As it is stated in Chapter 3, the illumination was supplied by a halogen lamp, and the light was at normal incidence the surface of sample which was kept approximately 0.5 cm below the lamp in a convenient position to receive light uniformly on the surface.

Fig. 4.21 shows the variation of the photoconductivity as a function of reciprocal temperature for as-grown GaSe single crystal at illumination intensities of 20, 35, 55, 80, 115 mW/cm^2 in temperature range of 150-480 K. As one can easily observe from figure, the photoconductivity varies with temperature and increases with increasing illumination intensities. The variation of photoconductivity versus temperature reveals three distinct regions for each illumination intensities with different activation energies, which are summarized in Table 4.1. Ea1, Ea2, and Ea3 shown in table are the activation energies of the first, second and third region, respectively.

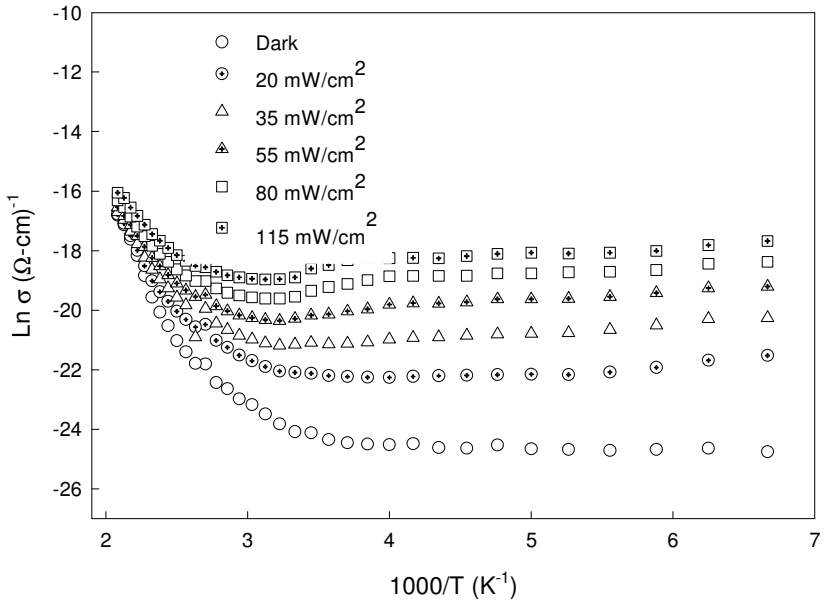

Figure 4.21: The temperature dependent dark conductivity and photoconductivity of as-grown GaSe single crystal.

Table 4.1: Phoconductivity behavior of as-grown GaSe at different illumination intensities.

Φ (mW/cm^2)	Region-1 in K	Region-2 in K	Region-3 in K	E_{a1} meV	E_{a2} meV	E_{a3} meV
20	150-300	310-380	390-480	-	254	664
35	150-300	310-370	380-480	-	186	566
55	150-310	320-380	390-480	-	170	515
80	150-310	320-380	390-480	-	124	468
115	150-310	320-380	390-480	-	92	428

As it is seen from Fig. 4.21, at each illumination intensity the photoconductivity stays almost constant in the temperature range of 150-300 K. Above room temperature, a considerable change in photoconductivity was observed. The photoconductivity varies exponentially with temperature and increase with increasing illumination intensity from 20 to 115 mW/cm^2 with calculated activation energies stated above for the temperature region of 300-380 K and high temperature

region, 390-480 K. It is also seen that with increasing temperature the photocurrent values for each illumination intensity are approaching the dark conductivity value, which is the indication of the saturation of the photoconductivity with temperature at each illumination intensity. In general, the behavior observed here for saturation value of the photoconductivity with temperature for each illumination intensity is seen as the indicator of existing trap levels surpass the photoconduction for as-grown GaSe sample. That is, it shows the existence of deep traps. From the variation of photocurrent as a function of illumination intensity at different temperatures, it is possible to determine the characteristics of these trapping centers.

Fig. 4.22 shows the variation of the photocurrent as a function of illumination intensities of 20, 35, 55, 80, and 115 mW/cm^2 at temperatures of 300, 350, 400, and 450 K for as-grown GaSe sample. As it seen from the plot of *Ln* of I_{PC} vs. *Ln* of Φ, I_{PC} increases with increasing intensity following relation $I_{PC} \alpha \Phi^n$, where n is calculated from the slope of plot of $Ln\ I_{PC}$ vs. $Ln\ \Phi$. According to the model stated in reference [70], a linear dependence of photoconductivity on intensity (n = 1) corresponds to the case of "*monomolecular recombination*" and n = 0.5 to "*bimolecular recombination*". In the case of $I_{PC} \alpha \Phi^n$, $n>1$, the behavior is referred to "*supralinear*" photoconductivity which corresponds to an increase in lifetime with photoexcitation intensity. In other words, when photoexcitation intensity is increasing, the material is becoming more photosensitive.

For as-grown GaSe sample, the n values calculated from the slope of Fig. 4.22 was found to be 1.9, 1.5, 1.3, and 1.4 for constant temperature of 300, 350, 400 and 450 K, respectively. For all temperatures, the values of n changes between 1.4 and 1.9, which is an indication of the supralinear character of the photocurrent. In order to see the change of n versus temperature, the variation is plotted as shown in Fig. 4.23 for as grown GaSe sample.

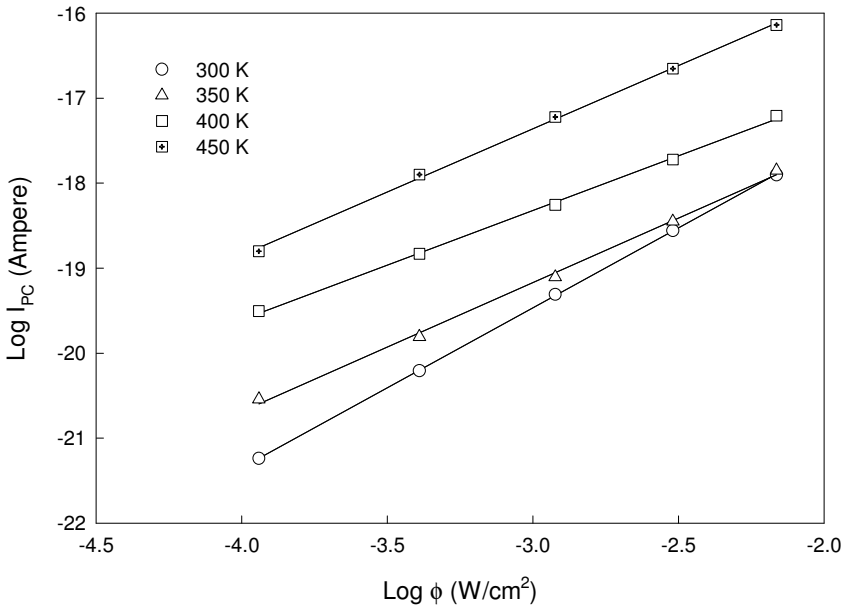

Figure 4.22: Variation of I_{PC} – Φ at several temperatures for as-grown GaSe sample.

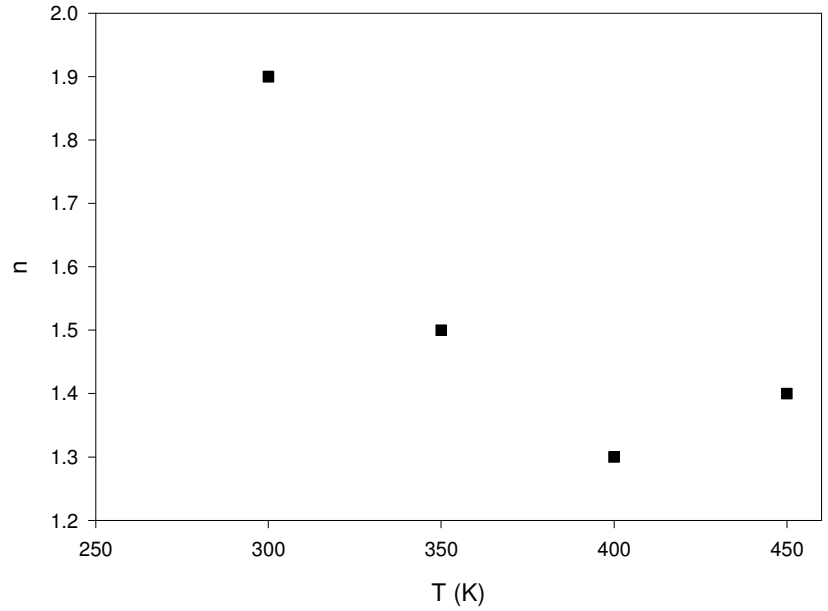

Figure 4.23: Variation of *n* versus temperature for as-grown sample.

As it is seen from Fig. 4.23, *n* decreases with increasing temperature and reach the value of 1.4 at 450 K. The change observed in *n* values is indication of change of recombination mechanisms which are dominant at specific temperature intervals. As

in our case *n* is found to be greater than 1, it is the characteristic of the supralinear at fixed temperature observed when sensitizing centers change their behavior from traps to recombination centers. On the other hand, when sensitizing centers change their behavior from recombination centers to traps at constant illumination intensity, the *thermal quenching* of photocurrent is observed [72]. As it is mentioned in the beginning of discussion during the interpretation of variation of photoconductivity versus inverse temperature, we have observed that approximately above 460 K almost at all intensities photoconductivity value approaches a saturation value. This behavior is generally attributed to that in the case of a material with imperfections an increase in the photoexcitation intensity above a critical limit, which is 460 K in our case, may result in an effective saturation of the photoconductivity. In this situation, the imperfections which are responsible for the long majority carrier lifetimes are totally occupied by minority carriers. Then, by subsequent excitation minority carriers are created, which increase the rate of favorable recombinations.

Fig. 4.24 shows the variation of the photoconductivity as a function of reciprocal temperature for Ge-implanted and annealed at 500 ^{0}C GaSe sample in the temperature range of 300-480 K:

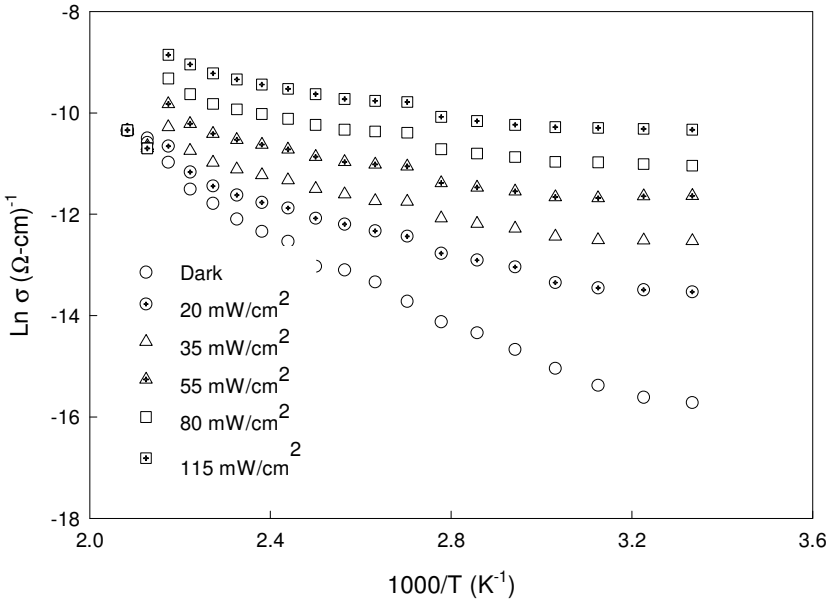

Figure 4.24: The temperature dependent dark conductivity and photoconductivity of Ge-implanted and annealed at 500 ^{0}C GaSe single crystal.

The electric field was fixed at 20 V/cm also for this sample. As it is clearly seen from figure, the photoconductivity varies with temperature and increases with increasing illumination intensities, which are 20, 35, 55, 80, and 115 mW/cm^2 as observed for as-grown GaSe sample. The evaluated activation energies from the slope of Fig. 4.24 reveals two temperature regions in the range of 300-380 K and 390-480 K with ±20 K changes depending on the illumination intensity. From the slope of plot the activation energies were evaluated which are summarized in Table 4.2.

Table 4.2: Phoconductivity behavior of implanted and annealed at 500 ^{o} C GaSe at different illumination intensities

Φ (mW/cm ^{2})	Region-1 in K	Region-2 in K	Ea1 meV	Ea2 meV
20	300-380	390-480	327	160
35	300-380	390-480	103	279
55	300-370	380-480	40	136
80	300-360	370-480	49	128
115	300-360	380-480	60	127

The activation energy of 38 meV was found previously from the conductivity measurement for Ge-implanted and annealed at 500 ^{0}C GaSe sample in the temperature range of 210-360 K, which is almost same as obtained from the photoconductivity measurement at intensity 55 mW/cm^2 in the temperature range of 300-370 K.

As it was done for as-grown GaSe, in order to investigate the characteristics of evaluated trap levels, the photocurrent-illumination intensity (Φ) dependence is analyzed at various temperatures as shown in Fig. 4.25. It. shows the dependence of photocurrent as a function of illumination intensity of 20, 35, 55, 80, and 115 mW/cm^2 at temperature of 300, 350, 370, 400, and 450 K. As it is seen, the photocurrent is increasing with increasing illumination intensities at all temperatures. In order to evaluate the $I_{PC} \alpha \Phi^{n}$ relation, we have calculated the slope of the logarithmic plot of I_{PC} -Φ. For Ge-implanted and annealed sample n is found to be 1.8, 1.7, 1.6, 1.6, and 1.8 for constant temperature of 300, 350, 370, 400, and 450 K, respectively. The change of n versus temperature is drawn in Fig. 4.26

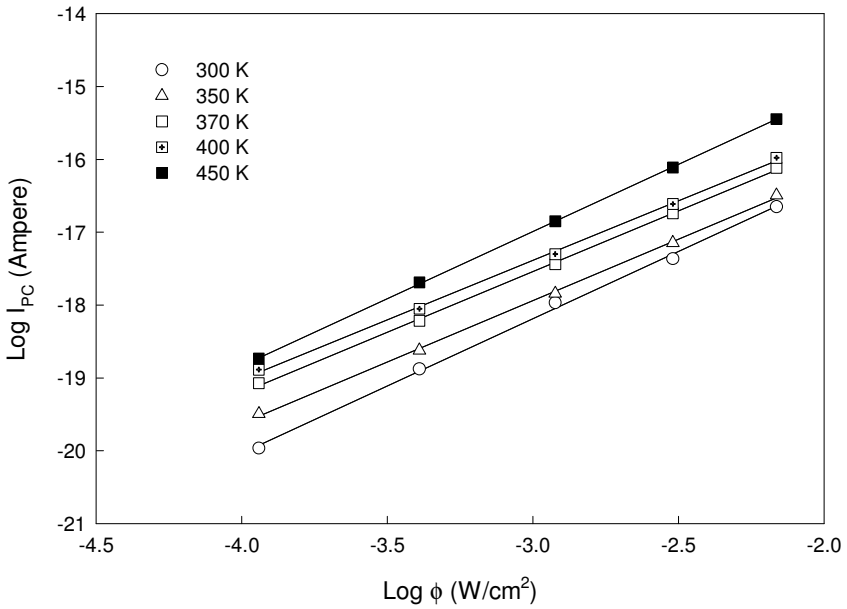

Figure 4.25: Variation of I_{PC} – Φ at several temperatures for Ge-implanted and annealed at 500 ^{0}C GaSe sample.

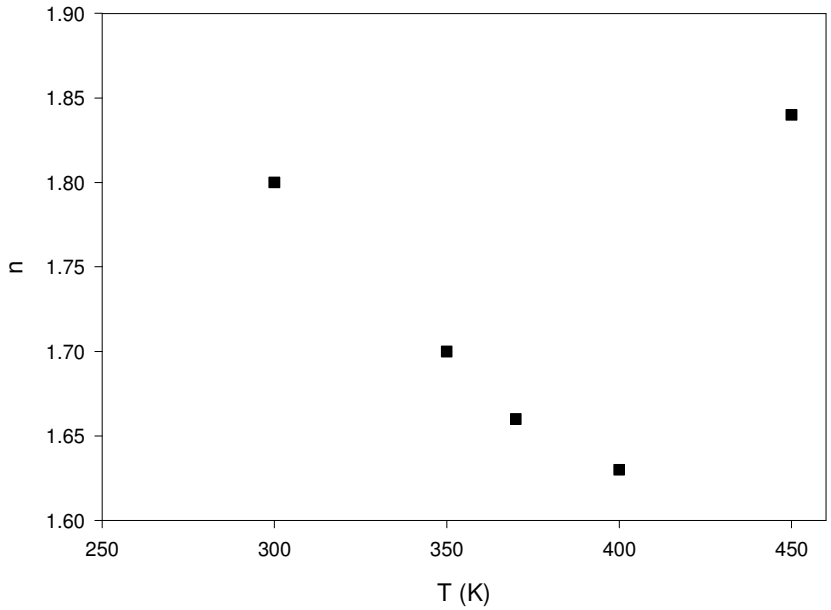

Fig. 4.26: Variation of *n* versus temperature for Ge-implanted and annealed at 500 ^{0}C GaSe sample.

As it is mentioned before, the change of *n* values with temperature is due to the fact

that the change in the recombination mechanism that we stated before and explained according to theory in [72]. In our case, since we have found values ranging from 1.6 to 1.8, that is, $n>1$, it shows the supralinear character of the photocurrent as we observed for as-grown GaSe sample. The supralinear character of the photocurrent observed for Ge-implanted and annealed GaSe sample may be attributed to that as illumination intensity increases, the sample becomes more sensitive due to increase in lifetime with illumination intensity increase owing to the structural defects introduced during the growth process or Ge-induced impurities and modifications.

4.5 Absorption Analysis

As it is mentioned in theoretical consideration part, the absorption measurement is a strong tool to determine the optical energy gap of materials.The optical absorption is described by an absorption coefficient α (cm^{-1}), which can be derived from eqn. (3.5). And, according to the theory of interband absorption at the optical absorption edge, the absorption coeficient varies with photon energy as described through eqn. of (3.6). The exponent n defined in relation is the indicator of type of tarnsition, which takes different values according to the type of transition. The index (n) takes value of 1/2 for direct allowed transition, while it is 1 for indirect allowed transition. It is possible to determine the direct or indirect band gap of the material from the plot of $(\alpha h\nu)^n$ versus photon energy $h\nu$ [83].

In order to determine and reveal the annealing dependent change of band gap of unimplanted and Ge-implanted GaSe samples at room temperature, we have used the Brukermade Equinox 55 model Fourier Transform Infrared (FT-IR) spectrometer with resolution of 0.5 cm^{-1}. Samples with thickness of 31 μm and 0.5 mm for as-grown and Ge-implanted GaSe were prepared, respectively. Then, at two different temperatures, 300 and 500 ^oC, the annealing processes were performed for each sample.

In order to detarmine the direct or indirect optical gap, the change of $(\alpha h\nu)^2$ versus photon energy $h\nu$ was plotted for as-grown, annealed at 300 and 500 ^oC GaSe samples as illustrated in Fig. 4.27. As one can easily see, the general behavior of all plots is almost same except the shifting of absorption edge slightly towards the higher energies with annealing temperatures for unimplanted. GaSe samples.

Although the annealing process was performed for different tempeartures, it was not observed any considerable change in optical band gap of samples with increasing annealing temperatures. In general, the thermal treatment (annealing) has an important effect on physical properties of some materials. It is possible for a semiconductor to contain a short-range disorder and defects like dangling bonds and impurities in the energy gap referred to localized states. The degree of disorder and the density of defects present in the amorphous, for instance, changes owing to performing annealing process. In general, the decrease in the disorder and the defect density in the structural bonding increase the optical gap. It is also known that variation of optical gap with annealing is an indication of the saturation of dangling bonds in the amorphous structure [98]. In our case for GaSe samples with carrying out annealing, as it is seen from Fig. 4.27, there is a neglible effect of heat treatment on the absorbtion and band gap of as-grown GaSe samples. In addition, by extrapolating the linear regions of the obtained plots shown in figure to $(\alpha h\nu)^2 = 0$, the energy gap values were obtained to be approximately same, ≈ 1.98 eV, which was also found by Ismailov at room temperature [99] and in our previous studies below [74], except a slight shift towards high energy region for annealed samples as shown below;

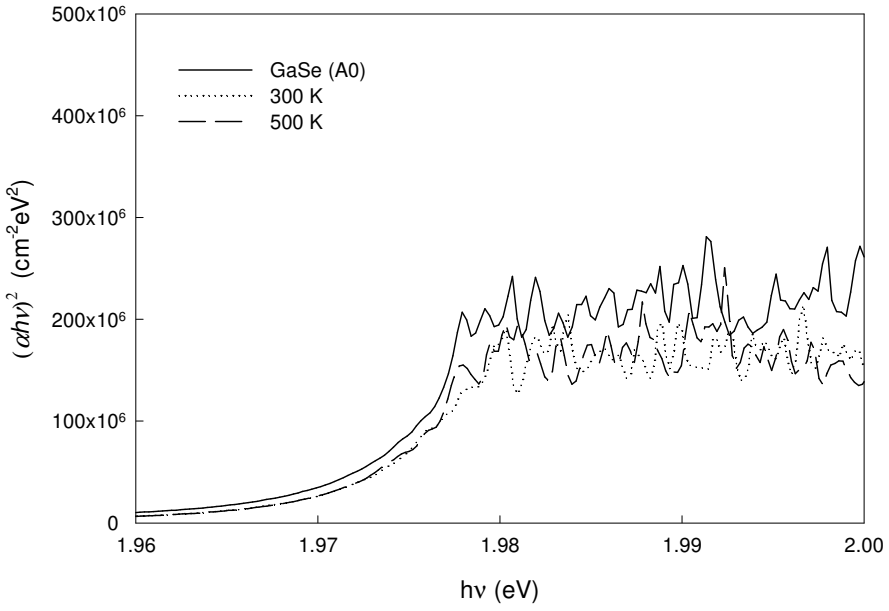

Figure 4.27: Optical absorbtion of as-grown annealed at 300, and 500 ^{o}C GaSe samples at room temperature.

Fig. 4.28 illustrates the optical absorption of Ge-implanted and annealed at 300 and 500 ^{o}C samples. The change in absorption and optical band gap is seen more clearly in this case relative to as-grown GaSe samples. As it is illustarated in figure, after implanting GaSe samples with Ge, a slight decrease in optical band gap is seen when compared with as-grown GaSe samples. In general, when a decrease in band gap is observed in a material, it is attributed to the presence of large number of defects states, which are creating localized states in band gap of semiconductors [98]. In our case, the defects might be due to implantation of Ge resulting in structural moderations, which were also observed in XRD analysis.

As it is illustrated in Fig. 4.28, the behavior of the absorption of Ge-implanted GaSe as a function of annealing is almost same except the magnitude of change in optical band gap for each sample. It is observed that the energy band gap increases with increasing annealing temperature and the most considerable change is seen at annealing temperature of 500 ^{o}C. A similar behavior is reported for InSe thin films, for this material the optical band gap increasing with annealing was attributed to the selenium loss at high temperatures as well as the formation of the different

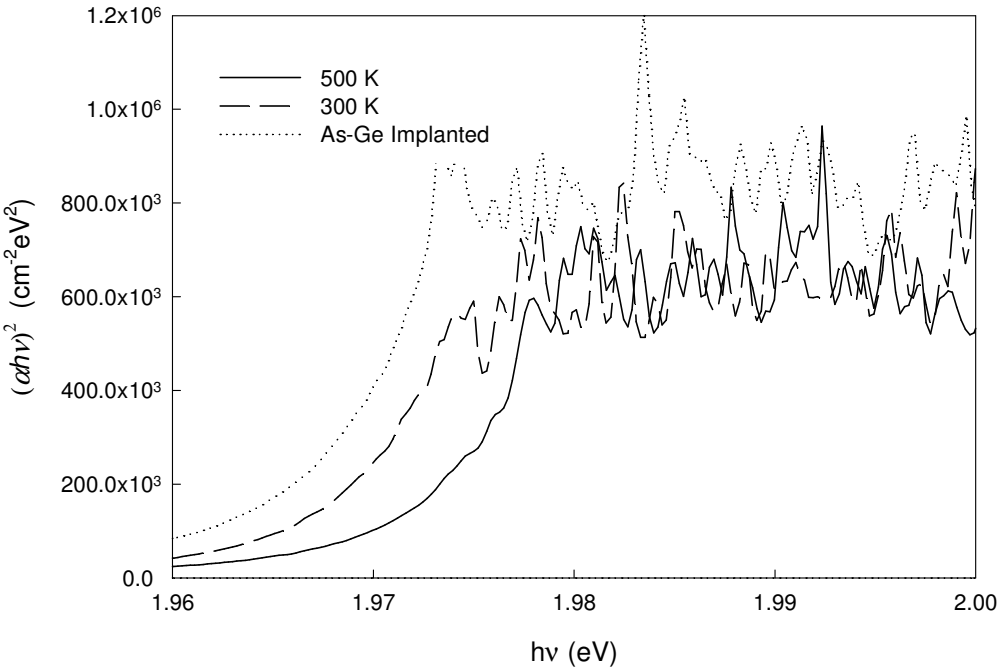

Figure 4.28: Optical absorbtion of Ge-implanted, annealed at 300 and 500 ^{o}C GaSe samples at room temperature.

phases [101, 102]. In our case, as it was stated for as-grown samples, the observed increase in optical band gap with annealing might be due to the decreasing in the disorder and the defect density in the structure.

CHAPTER V

CONCLUSIONS

In this study, following a special procedure as described in experimental part, we have grown an ingot of GaSe single crystal by using 3-zone vertical Bridgman-Stockbarger system in Crystal Growth Laboratory of Department of Physics, METU. In order to see the effect of implanting Ge on the GaSe crystals, the implantation process was performed by accelerating atoms with 100 keV energy and ion dose of $6x10^{15}$ ions/cm ^{2}. Having obtained GaSe single crystals, in order to determine the stoichometry and investigate the structure of material, X-Ray Diffraction (XRD) and Scanning Electronic Measurements (SEM) were carried out. As a consequence of these measurements it was observed that the grown single crystals are nearly stoichometric and have shown crystallographic symmetry which has been reported early.

The structural analysis was performed for unimplanted and implanted GaSe samples. As- grown samples were annealed at three different temperatures which were 300, 500, and 700 ^{o}C for 20 minutes.Upon carrying out XRD measurements for each sample, we observed that although the peak positions of the annealed samples agree with those of the as-grown samples, the intensity of the patterns are changing, that is, there is an increase in peak intensities at specific annealing temperatures (300 and 500 ^{o}C) and a decrease in higher annealing temperature (700 ^{o}C). From the comparison of X-ray patterns of as-grown and as-implanted GaSe samples, it was observed that the intensities of the peaks were decreased for as-implanted samples as compared to as-grown ones. It was clearly seen from X-ray diffraction patterns, the annealling increases the peak intensities both for as-grown and Ge-implanted samples.This increase in peak intensities indicates that there is a

complete recovery of the crystalline nature of the as-implanted sample, which was damaged during the implantation,by annealling process. Similar behaviour was observed for N- and Si-implanted GaSe crystals [103].

In order to investigate the general behavior of the conductivity and determine the existing current transport mechanisms, the temperature dependent conductivity measurements were performed in the range of 100-430 K for as-grown, Ge-implanted, and annealed at 500 ^{o}C (following Ge-implantation) GaSe samples. The room temperature resistivity of as-implanted, Ge-implanted, and annealed at 500 ^{o}C following implantation GaSe samples were found to be $2.1x10^{9}$, $1.09x10^{6}$, and $6.46x10^{5}$ Ω-cm, respectively.

From the temperature dependent conductivity of as-grown GaSe sample in the temparature range of 100-400 K it was observed that the variation of $Ln\ \sigma$ versus T^{-1} shows three linear regions, which are standing for different activation energies describing different conduction mechanisms at specific temperature intervals. These regions were 100-250, 250-330, and 330-400 K, and the activation energies belong to each region was found to be 4, 34, and 314 meV, respectively. Comparing our calculated activation energies with previously obtained results for as-grown GaSe single crystal in literature, it was seen that there is a good agreement.

From the temperature dependent conductivity of Ge-implanted samples, a similar variation of conductivity with temperature was observed for as in as-grown GaSe sample. After implanting with Ge, three order reduction in resistivity was observed for implanted sample. At room temperature the resistivity for Ge-implanted GaSe was found to be $1.09x10^{6}$ Ω-cm and temperature dependent conductivity for this sample revealed two linear regions with different activation energies, which were between 240-360 and 360-430 K with activation energies of 36 and 472 meV, respectively.

The temperature dependent conductivity of annealed at 500 ^{o}C following Ge-implantation of GaSe sample was performed in temperature range of 100-410 K so as to see the effect of annealing on implanted sample. For this sample two linear regions in the 210-360 and 360-410 K tempearture intervals with activation energiers of 39 and 647 meV were found, respectively. The room temperature resistivity of sample annealed at 500 ^{o}C GaSe was found to be $6.46x10^{5}$ Ω-cm.

Temperature dependent carrier concentration and Hall mobility measurement

were performed in the temperature range of 230 - 410 and 100 - 400 K for as-grown and Ge-implanted and annealed GaSe samples, respectively. All of the samples in this study were found to be p-type. We have used Single Donor-Single Acceptor (SDSA) in our analysis. From the temperature dependence of hole concentration for as grown GaSe sample it was observed that there is no considerable change with increasing temperature up to a critical point, which is 340 K. After this critical value of temperature, the hole concentration is increasing exponentially with increasing temperature up to another critical temperature value, which is 390 K for as-grown GaSe, in temperature range between 230-410, the change in hole concentration is just one order. That is, an increase from 2.16×10^{10} cm $^{-3}$ at 230 K to 1×10^{11} cm $^{-3}$ at 410 K was observed. The room temperature of calculated hole concentration was 1.91×10^{10} cm $^{-3}$. For as-grown GaSe, in temperature range 340-390 K an acceptor level with activation energy of 20 meV was determined from the Hall measurement. Using SDSA model, 9×10^{11}, 1.45×10^{9}, and 8.99×10^{11} cm^{-3} are found for N_a, N_d, and $N_a - N_d$, respectively for as-grown GaSe sample.

The temperature dependent hole concentration of Ge- doped GaSe sample was evaluated in temperature range of 180 - 380 K. However, the temperature dependent hole concentration is analyzed using SDSA model in between 280-360 K. As a result of fitting procedure, the acceptor and donor concentration were found to be 8.6×10^{14}, 2.8×10^{12}, and 8.57×10^{14} cm^{-3} for N_a, N_d, and $N_a - N_d$, respectively. The activation energy at this region was calculated to be 29 meV from the slope of fitted curve.

From the temperature dependence of hole concentration and fitting curve of Ge-implanted and annealed at 500 ^{0}C GaSe sample it was observed that this sample also shows similar behavior as as-grown and Ge-implanted GaSe crystals except the change of one order increase of hole concentration, which is calculated to be 1.38×10^{13} cm^{-3} at 140 K and 1.26×10^{15} cm^{-3} at 400 K. Comparing with as-grown GaSe, the hole concentration of Ge-implanted and annealed sample increase about four orders. Using SDSA model for 310-400 K tempearure region, a fitting curve resulted activation energy E_a = 214.82 meV with $N_a = 5 \times 10^{16}$, $N_d = 3.12 \times 10^{15}$, and $N_a - N_d = 3.9 \times 10^{15}$ cm^{-3} .

The temperature dependent mobility of as-grown, as-implanted, and annealed at 500 ^{0} C samples were carried out. The room temperature mobility of the as-grown

GaSe was calculated to be 0.14 cm^2/V.s which was lower than previously obtained results. The n value evaluated from the slope of straight line was found to be n = 2.37 for as-grown GaSe. The change of mobility with temperature according to this rule is a characteristic of scattering mechanism of charge carriers with ionized impurities which are believed to be found in structure of crystals. In our case, this region extends to high temperatures which may be due to that our p-type GaSe contains high degree of impurity concentration probably contamined during the growing process from medium or crucible which the growth process took place.

Temperature dependent Hall mobility of Ge-implanted GaSe in between 110-400 K was carried out. From plot of the logarithm of μ_H versus the logarithm of T it was observed that this plot results in straight lines in the low and high temperature regions and slopes give the temperature exponents n = 0.54 of the $\mu_H \alpha T^n$ and n = 5.2 of the $\mu_H \alpha T^{-n}$ rule, respectively. The temperature dependence of the Hall mobility in the low temperature region which follows the relation $\mu_H \alpha T^{-n}$, with n = 5.2 is indication of the domination of the thermal lattice scattering in this temperature region. On the other hand, in low temperature region, the mobility follows $\mu_H \alpha T^n$ with n = 0.5, which is indicating that the ionized impurity scattering is dominant in low temperature region. In addition, the calculated mobility of Ge-implanted GaSe at room temperature was found to be 0.23 cm^2/V. s which was greater than obtained for as-grown GaSe sample. This slight increase according to as-grown GaSe is possibly due to the Ge-induced related modification in structure after implantation process.

From the temperature dependence of hole mobility of Ge-implanted and annealed at 500 GaSe in the temperature range of 140-400 K it was observed that Hall mobility increases with increasing temperature in the temperature range of 140-250 K and decreases in 260-400 K regions. It was observed that the temperature dependence of Hall mobility follows the relation $\mu_H \alpha T^{1.11}$ and $\mu_H \alpha T^{-4.33}$ for 140-250 and 260-400 K temperature regions, respectively. In addition, the calculated Hall mobility for this sample is found to be 0.28 cm^2/V. s which is higher than both as-grown and Ge-implanted GaSe samples.

The photoconductivity measurements of as-grown and Ge-implanted and annealed at 500 ^{0}C GaSe samples were performed as a function of illumination intensity in the temperature range of 150-480 K and 300-480 K, respectively. The measurements were carried out at different light intensities (Φ), which are 20, 35, 55,

80, and 115 mW/cm^2. The electric field was fixed at 20 V/cm. The variation of photoconductivity versus temperature revealed three distinct regions for each illumination intensities with different activation energies, which were summarized in Table 4.1.

From the variation of the photocurrent as a function of illumination intensities at temperatures of 300, 350, 400, and 450 K for as-grown GaSe sample it was observed that the n in relation $I_{PC} \alpha \Phi^n$ is 1.9, 1.5, 1.3, and 1.4 for these constant temperatures, respectively which is an indication of the supralinear character of the photocurrent according to theory. In addition, it was observed that approximately above 460 K almost at all intensities, photoconductivity value approached a saturation value which is generally attributed to that a material with imperfections an increase in the photoexcitation intensity above a critical limit may result in an effective saturation of the photoconductivity. In this situation, the imperfections which are responsible for the long majority carrier lifetimes are totally occupied by minority carriers. Then, by subsequent excitation minority carriers are created, which are increasing rate of favorable recombinations.

From the variation of the photoconductivity as a function of reciprocal temperature for Ge-implanted and annealed at 500 ^{0}C GaSe sample in the temperature range of 300-480 K it was observed that the photoconductivity varies with temperature and increases with increasing illumination intensities. The evaluated activation energies revealed two temperature regions for each illumination intensity with different activation energies, which are summarized in Table 4.2.

The activation energy of 38 meV was found previously from the conductivity measurement for Ge-implanted and annealed at 500 ^{0}C GaSe sample in the temperature range of 210-360 K, which was almost same as obtained from the photoconductivity measurement at intensity 55 mW/cm^2 in the temperature range of 300-370 K. From the dependence of photocurrent as a function of illumination intensity at temperature of 300, 350, 370, 400, and 450 K, the n is found to be 1.8, 1.6, 1.6, and 1.8 for constant temperature of 300, 350, 370, 400, and 450 K, respectively. It was also observed that all evaluated n values are greater than 1. That is, it shows supralinear character. The supralinear character of the photocurrent observed for Ge-implanted and annealed GaSe sample may be attributed to that as illumination intensity increases, the sample becomes more sensitive due to increase

in lifetime with illumination intensity increase owing to the structural defects introduced during the growth process or Ge-induced impurities and modifications.

Finally, In order to determine and reveal the annealing dependent change of band gap and absorption coefficient of unimplanted and Ge-implanted GaSe samples at room temperature, we have carried out transmission measurement as optical characterization part of our study. At two different temperatures, 300 and 500 ^{o}C, the annealing processes were performed for each sample. From the plot it was observed that the general behavior of all plots are olmost same except the shifting of absorption edge slightly towards the higher energies with annealing for both implanted and unimplanted samples. In general, the decrease in the disorder and the defect density in the structural bonding increase the optical gap. It is also known that variation of optical gap with annealing is an indication of the saturation of dangling bonds in the amorphous structure. A slight change in optical band gap in our implanted and unimplanted samples with annealing may be attributed to the modified crystalline structure after annealing process.

REFERENCES

[1] B. G. Streetman," *Solid State Electronic Devices"*, Prentice-Hall, New Jersey, 1995

[2] B. G. Yacobi, "*Semiconductor Materials"*, Kluwer Academic/Plenum Publishers, Newyork, Boston, Dordrecth, London, Moscow, 2002

[3] Donald A. Neamen, "*Semiconductor Physics and Devices"*, The McGraw-Hill Companies, Inc., second edition, 1997

[4] J. C. J. M Terhell, Prog. Cryst. Growth Charact. Mater., 7, 55-110, 1983

[5] A. Chevy, A. Kuhn and M. S. Martin, J. Crystal Growth, 38,118-122, 1977

[6] M. K. Anis and F. M. Nazar, J. Mater. Sci. Lett., 2, 471, 1983

[7] R. H. Tregold and A. Clark, Sol. Stat. Commun., 7, 1519, 1969

[8] G. Fisger and J. L. Brenber. J. Phys. Chem. Solids, 23, 1363, 1962

[9] J.V. Mc Canny and R. B. Murray, J. Phys. C solid State, 10(8), 1211, 1977

[10] Z. S. Basinski, D. B. Dove, and E. Mooser., J. Appl. Phys., 34 (3), 1963

[11] M. K. Anis, J. Crys. Growth, 55, 465, 1981

[12] A. Kuhn, R. Chevalier, and A. Rimsky, Acta Crystallogr. Sec. B, 31, 2841, 1975

[13] J. C. J. M Terhell and R. M a. Lieth, J. Crystal Growth, 16, 54, 1972

[14] A. Gouskov, J. Camassel and L. Gouskov, Crystal Growth and Charact. 5, 323, 1982

[15] K. Schubert , Z. Metallkunde ,46 , 216, 1955

[16] J. F. Sanchez-Ruyo, D. Errandoned, A. Segura, L. Roa, and A. Chevy, J. Appl. Phys., 83 (9), 4750, 1998

[17] M. Schluter, Nuovo Cimento, 13B, 313, 1973

[18] J. P. Voitchovsky and A. Mercier, II. Nuovo Cimento, 22B, 273,1974

[19] Richard H. Bube and Edward L. Lind, Phys. Rev., 15(5), 1959

[20] R. Fivaz and E. Mooser, Phys. Rev., 163(3), 743, 1967

[21] A.kuhn, A. Chevy, and E. Lendvay, J. Crystal Growth, 13/14, 380-384, 19

[22] V. L. Cardetta, A. M. Mancini and A. Rizzo, J. Crystal Growth, 16, 183-185, 1972

[23] PH. Schmid, J. P. Voitchovsky,and A. Mercier , Phys. Stat. Sol. (a) 21,443,1974

[24] R. Minder, G. Ottaviani and C. Canali, J. Phys. Chem. Solids, 37, 417

[25] G. Arancia ,M. Grandolfo, C. Manfredotti, and A. Rizzo, Phys. Stat. Sol. (a), 33, 563, 1976

[26] F. Levy, II Nuovo Cimento, 38B (2), 359, 1977

[27] V. Augelli, C. Manfredotti,R. Murri, And L.Vasanelli, Phys. Rev. B,17(8),1978.

[28] M. Khalid Anis, J. Crystal Growth, 55, 465-469, 1983

[29] V.Capozzi, Phys. Rev. B, 23, 836, 1981

[30] V. Capozzi and A. Minafra, Sol. Stat. commun., 38, 341-343, 1981

[31] M. K. Anis, PhD Thesis, Bringhton, Polytechine, England, 1977

[32] C. R. Whitehouse, PhD Thesis, Bringhton, Polytechine, England, 1978

[33] H. Suzuki and R. Mori, Jpn. J. Appl. Phys., 13, 417, 1974

[34] T. Ishii, and N. Kambe, J. Crystal Growth, 76, 489-493, 1986

[35] Soo-II Lee, Suk-Ryong Hahn, Choong-Hyun Chung , and Sang-Hyun and Wha-Tek Kim, Sol. Stat. Commun., 60 (5), 453-456, 1986

[36] A. Seyhan, O. Karabulut, B. G. Akınoğlu, B. Aslan, and R. Turan, Cryst. Res. Technol., 40, 893, 2005

[37] V. Capozzi, S. Caneppele, M. Montagna, and F. Levy, Phys. Stat. Sol. B 129, 247, 1985

[38] A. Cingolani, F. Evangelisti, A. Minafra, and A. Rizzo, Phys. Stat. Sol. A 17, 541, 1973

[39] M. Schlüter, Nuovo Cimento 13B, 313, 1973

[40] A. Mercier, E. Mooser, and J. P. Voitchovsky, Phys. Rev. B12, 4307, 1975

[41] N. Kuroda and Y. Nishina, Phys. Stat. Sol. B 72, 81, 1975

[42] Yu. P. Gnatenko, Z. D. Kovalyuk, P. A. Skunenko, and Yu. Zhirko, Phys. Stat. Sol. B 117, 283, 1983

[43] T. Matsumura, M. Sudo, C. Tatsuyama, and S. Ischimura, Phys. Stat. Sol. A 43, 685, 1977

[44] V. Capozzi, and M. Montagna, J. Phys. (paris) Colloq. 46, C7-191, 1985

[45] V. Capozzi and J. L. Staehli, Phys. Rev. B 28, 4461, 1983

[46] V. Capozzi, S. Caneppele, and M. Montagna, J. Lumin. 31/32, 463, 1984

[47] V. Capozzi and K. Maschke, Phys. Rev. B 34, 3924, 1986

[48] G. B. Abdullaev, G. L. Belenkii, E. Yu. Salaev, and R. A. Suleimanov, Nuovo Cimento 38 B, 469, 1977

[49] Y. Sasaki and Y. Nishina, Phys. Rev. B 23, 4089, 1981

[50] G. Micocci, A. Serra, and A. Tepora, J. Appl. Phys., 82 (5), 2365, 1997

[51] G. Micocci, A. Serra, and A. Tepore, Phys. Stat. Sol. (a), 162, 649, 1997

[52] S. Shigetomi, T. Ikari, and H. Nakashima, Jpn. J. Appl. Phys., 39, 5083, 2000

[53] S. Shigetomi, T. Ikari, and H. Nakashima, Jpn. J. Appl. Phys, 35, 4291, 1996

[54] S. Shigetomi, T. Ikari, and H. Nakashima, J. Appl. Phys, 73, 4686, 1993

[55] S. Shigetomi, T. Ikari, and H. Nakashima, J. Appl. Phys, 69 (11), 7936, 1991

[56] S. Shigetomi, T. Ikari, and H. Nakashima, Jpn. J. Appl. Phys, 32, 2731, 1993

[57] S. Shigetomi, T. Ikari, and H. Nakashima, J. Appl. Phys, 80, 4779, 1996

[58] B. G. Tagiev, G. M. Niftiev, and F. S. Aidaev, Phys. Stat. Sol. (b), 128:K65, 1985

[59] S. Shigetomi and T. Ikari, Philosophical Magazine Letters, 79, 575, 1999

[60] S. Shigetomi, T. Ikari, and H. Nakashima, Phys. Stat. Sol. (a), 160, 159, 1997

[61] S. Shigetomi, T. Ikari, and H. Nakashima, J. Appl. Phys., 74(6), 4125, 1993

[62] B. Gurbulak, M. Yıldırım, S. Tuzemen, H. Efeoglu, and Y. K. Yogurtcu, J. Appl. Phys., 83, 2030, 1998

[63] S. Shigetomi, I. Ikari, and H. Nakashima, Phys. Stat. Sol. (a), 156:k21, 1996

[64] O. Karabulut, M. Parlak, K. Yılmaz, R. Turan, and B. G Akınoglu, Cryst. Res. Techn., 38 (12), 1071-1076, 2003

[65] O. Karabulut, M. Parlak, R. Turan, U. Serincan, E. Tasarkuyu, B. G. Akınoglu, Cryst. Res. Techn., 38 (9), 811-816, 2003

[66] B. R. Pumplin, "Crystal *Growth* ", Pergamon Press Ltd., Headington Hill Hall, Oxford, 1975

[67] J. C. Brice," *Crystal Growth Processes"*, NY, 1986

[68] D. K. Schroder," *Semiconductor Material and Device Characterization* ",Jhon Willey and Sons, NY, 1990

[69] B. D. Cullity, "Elements *of X-Ray Diffraction* ", Addison-Wesley, Second Edition, 1978

[70] Raymond A. Serway, John W. Jewett, "*Physics for Scientists and Engineers*",Philadelphia: Saunders College Pub., Third Edition, 1992

[71] G. Micocci, and A.Tepore, R.Rella, and P. Siciliano, J. Appl. Phys, 71(5), 1992

[72] R. H. Bube, "*Photoelectronic Properties of Semiconductors* ", Cambridge University, 1992

[73] S. Pertkowitz, "*Optical Characterization of Semiconductor: Infrared, Raman, and Photoluminescence Spectroscopy* ", Academic Press, London, 1993

[74] O. Karabulut, "*Structural, Electrical and Optical Characterization of N-and Si-Implanted GaSe Single Crystal Grown By Bridgman Method*", Ph. D. Thesis, METU, Ankara, 2003

[75] Crystalox, "*MD4000 Operation Manual*", Crystalox Com., 1994

[76] G. Dearnaley, J. H. Freeman, R. S. Nelson, J. Stephen, "*Ion Implantation* ", North-Holland, Amsterdam,1973

[77] R. Kelly, Nucl. Instrum. Methods, 351,182-183, 1981

[78] Partap Singh, K. Lbhatia, N. Kishore, Mahender Singh, S. K. Malik, D. Kanjilal, Journal of Non-Crystalline solids,191,146-154,1995

[79] M. Parlak, "*Characterization of InSe Thin Films*", Ph.D Thesis, Metu, 1996

[80] Patric M. Hemenger, Rev. Sci. Instrum., 44 (6), 1973

[81] Cryostat, Janis Research Co., Wilmington, MA, USA

[82] L. J. Van der Pauw, Philips Res. Repts. 13, 1-9, 1985

[83] N. F .Mott and E. A. Davis, *"Electronic Process in Noncrystalline materials* ", Clarendon press, Oxford, 1971

[84] S. Shitgetomi, T. Ikari, and N. Nishimura, Phys. Stat. Sol. (a), 185 (2), 341-348, 2001

[85] J. S. Williams, Mater. Sci. Eng., A253, 8-15, 1998

[86] J. Y. W. Seto, J. Appl .Phys, 46(12), 5224, 1975

[87] M. V. Garcia-Cuenca, J. L. Morenza, J. Estevez, J. Appl. Phys., 56(6), 1738, 1984

[88] C. Tatsuyama, C. Hamaguchi, H. Tomita and I. Nakai: Jpn. J. Appl. Phys., 10, 1698, 1971.

[89] C. Manfredotti, A. Rizzo, C. De Blasi, S. Galassini and L. Ruggiero, J. Apply Phys., 46, 4531, 1975

[90] F. I. Ismailov, G. A. Akhundov and O. R.Vermich, Phys. Stat. Sol., 17, k237, 1966

[91] G. B. Abdullaev, E. S. Guseinova and B. G. Tagiev., Phys. Stat. Sol., 16, 205, 1966

[92] R. K. Boncek and D. L. Rode, J. Appl. Phys. 64, 6315, 1988

[93] S. Shigetomi, T. Ikari, H. Nakashima, J. Luminescence 79, 79-84, 1998

[94] V. Capozi, M. Montagna, Phys. Rev. B, 40 (5), 1989

[95] A. F. Q ASravi, N. M. Gasanly, Cryst. Res. Techn., 37, 10, 1104-1112, 2002

[96] C. Manfredotti, A. M. Mancini, R. Murri, A. Rizzo and L.Vasenelli, IL Nuovo Cimento, 39(1) B, 1977

[97] C. De Blasi, G. Micocci, A. Rizzo, and A. Tepore, Phys. Rev. B, 27(4), 1983

[98] C. De Blasi, D. Manno, G. Micocci, and A. Tepore, J. Appl. Phys. , 65 (3), 1989

[99] F. I. Ismailov, E. S. Guseinova and G. A. Akhundov, Sov. Phys. Sol. Stat. 5, 2656-2657, 1963

[100] M. A. Osman, M. A. Elosely, A. A. Gadalla, Physica B, 252, 216-222, 1998

[101] B. Thomas and T. R. N. Kutty, Phys. Stat. Sol. (a), 119, 127, 1990

[102] C. Julien, N. Benramdabe and J. P. Guesdon, Semicond. Sci. Technol. 6, 905, 1990

[103] O. Karabulut, M. Parlak, R. “Turan, U. Serincan and B. G. Akınoğlu, Cryst. Res. Technol., 2005 (in press)